

DOT/FAA/AR-06/11

Office of Aviation Research
and Development
Washington, DC 20591

Statistical Loads Data for the Boeing 777-200ER Aircraft in Commercial Operations

November 2006

Final Report

This document is available to the U.S. public
through the National Technical Information
Service (NTIS), Springfield, Virginia 22161.



U.S. Department of Transportation
Federal Aviation Administration

NOTICE

This document is disseminated under the sponsorship of the U.S. Department of Transportation in the interest of information exchange. The United States Government assumes no liability for the contents or use thereof. The United States Government does not endorse products or manufacturers. Trade or manufacturer's names appear herein solely because they are considered essential to the objective of this report. This document does not constitute FAA certification policy. Consult your local FAA aircraft certification office as to its use.

This report is available at the Federal Aviation Administration William J. Hughes Technical Center's Full-Text Technical Reports page: actlibrary.tc.faa.gov in Adobe Acrobat portable document format (PDF).

1. Report No. DOT/FAA/AR-06/11		2. Government Accession No.		3. Recipient's Catalog No.	
4. Title and Subtitle STATISTICAL LOADS DATA FOR THE BOEING 777-200ER AIRCRAFT IN COMMERCIAL OPERATIONS				5. Report Date November 2006	
				6. Performing Organization Code	
7. Author(s) Daniel O. Tipps, Donald A. Skinn, John W. Rustenburg, Todd Jones, and David A. Harris				8. Performing Organization Report No. UDR-TR-2005-00106	
9. Performing Organization Name and Address University of Dayton Research Institute Structural Integrity Division 300 College Park Dayton, OH 45469-0120				10. Work Unit No. (TRAIS) 065110 RPD-510 RD0300	
				11. Contract or Grant No. Grant No. 2001-G-005	
12. Sponsoring Agency Name and Address U.S. Department of Transportation Federal Aviation Administration Office of Aviation Research and Development Washington, DC 20591				13. Type of Report and Period Covered Final Report	
				14. Sponsoring Agency Code ANM-110	
15. Supplementary Notes The Federal Aviation Administration Airport and Aircraft Safety R&D Division Technical Monitor was Thomas DeFiore.					
16. Abstract <p>The University of Dayton Research Institute supports the Federal Aviation Administration (FAA) by conducting research on the structural integrity requirements for the U.S. commercial transport airplane fleet. The primary objective of this task was to support the FAA's Airborne Data Monitoring Systems Research by developing new and improved methods and criteria for processing and presenting large commercial transport airplane flight and ground loads usage data. The scope of activities included: (1) defining the service-related factors that affect the operational life of commercial aircraft; (2) designing an efficient software system to reduce, store, and process large quantities of optical quick access recorder data; and (3) reducing, analyzing, and providing processed data in statistical formats for the FAA to reassess existing certification criteria. Equally important, these new data also will enable the FAA, the aircraft manufacturers, and the airlines to better understand and control those factors that influence the structural integrity of commercial transport aircraft. Presented herein are Boeing 777-200ER aircraft operational usage data collected from 10,047 flights, representing 67,000 flight hours, recorded by a single international operator. Data are presented that will provide the user with statistical information on aircraft usage, ground and flight loads occurrences, and system operational usage based on actual B-777-200ER operational usage. The aircraft usage data include statistics on aircraft weights, flight distances, altitudes, speeds, and flight attitudes. Flight loads data include statistical information on gust and maneuver load factors, derived gust velocities, and ground-air-ground cycles. Ground loads data include statistics on lateral, longitudinal, and vertical load factors during different ground operational phases. Systems operational data include statistics on flap usage, thrust reverser usage, and engine fan speed.</p> <p>The B-777 airplane sensors, which measure vertical, lateral, and longitudinal acceleration, are located in the cockpit area. The estimates of the center of gravity (c.g.) accelerations are computed in the Air Data Inertial Reference Unit, which converts the measured crew station accelerations to accelerations at the c.g. For some dynamic and ground load conditions, inaccuracies could exist in these filtered c.g. time history measurements. Operators and inspectors who use the recorded B-777 acceleration values as maintenance action triggers or Flight Operational Quality Assurance events should recognize the possibility of recorded Digital Flight Data Recorder acceleration inaccuracies.</p>					
17. Key Words Optical quick access recorder, Flight profiles, Flight loads, Ground loads, Systems operational data, Statistical loads data			18. Distribution Statement This document is available to the public through the National Technical Information Service (NTIS) Springfield, Virginia 22161.		
19. Security Classif. (of this report) Unclassified		20. Security Classif. (of this page) Unclassified		21. No. of Pages 106	
				22. Price	

PREFACE

The Flight Systems Integrity Group of the Structural Integrity Division at the University of Dayton Research Institute (UDRI) performed this work under Federal Aviation Administration (FAA) Grant No. 2001-G-005 entitled “Assessment of Actual Operational Usage on Large Wide Body Transport Aircraft.” The Research Manager for the FAA was Mr. Thomas DeFiore of the Airport and Aircraft Safety Research and Development Division at the FAA William J. Hughes Technical Center, Atlantic City International Airport, New Jersey. The Program Technical Advisor was Mr. John Howford, FAA Chief Scientific and Technical Advisor (CSTA) for Loads/Aeroelasticity. Mr. Daniel Tipps was the principal investigator for the University of Dayton and provided overall technical direction for this effort. Mr. Donald Skinn developed the data reduction algorithms, programmed the data reduction criteria, and performed the data reduction. Mr. David Harris prepared the graphical presentations. Mr. Todd Jones and Mr. John Rustenburg performed the data analysis and compiled the final report.

TABLE OF CONTENTS

	Page
EXECUTIVE SUMMARY	xi
1. INTRODUCTION	1
2. AIRCRAFT DESCRIPTION	1
3. AIRLINE DATA COLLECTION AND EDITING SYSTEMS	3
3.1 Airline Data Collection System	3
3.2 Airline Data Editing System	4
4. UNIVERSITY OF DAYTON RESEARCH INSTITUTE DATA PROCESSING	4
4.1 Recorded Data Parameters	4
4.2 Computed Parameters	5
4.2.1 Atmospheric Density	6
4.2.2 Equivalent Airspeed	6
4.2.3 Dynamic Pressure	6
4.2.4 Derived Gust Velocity	7
4.2.5 Continuous Gust Intensity	7
4.2.6 Lift-Curve Slope	9
4.2.7 Flight Distance	9
4.2.8 Rate of Climb	10
4.3 Data Reduction Operations	10
4.3.1 Initial Quality Screening	10
4.3.2 Time History Files	11
4.3.3 Relational Database	12
4.3.4 Permanent Data Files	12
4.3.5 Loads Data Reduction	12
4.4 Data Reduction Criteria	12
4.4.1 Phases of Flight Profile	12
4.4.2 Specific Events	14
4.4.3 Sign Conventions	17
4.4.4 Peak Selection Technique	17
4.4.5 Separation of Maneuver and Gust Load Factors	18
4.4.6 Flap Detents	19

5.	DATA PRESENTATION	19
5.1	Aircraft Usage Data	23
5.1.1	Weight and Flight Distance Data	23
5.1.2	Altitude and Speed Data	24
5.1.3	Attitude Data	25
5.2	Ground Loads Data	25
5.2.1	Lateral Load Factor Data	26
5.2.2	Longitudinal Load Factor Data	27
5.2.3	Vertical Load Factor Data	28
5.3	Flight Loads Data	29
5.3.1	Gust Vertical Load Factor Data	29
5.3.2	Derived Gust Velocity Data	30
5.3.3	Continuous Gust Intensity Data	30
5.3.4	Maneuver Vertical Load Factor Data	30
5.3.5	Combined Maneuver and Gust Vertical Load Factor Data	31
5.3.6	Combined Maneuver and Gust Lateral Load Factor Data	31
5.3.7	Ground-Air-Ground Cycle Data	32
5.4	Systems Operational Data	32
5.4.1	Flap Usage Data	32
5.4.2	Thrust Reverser Data	32
5.4.3	Propulsion Data	33
6.	CONCLUSIONS	33
7.	REFERENCES	34

APPENDICES

- A—Boeing 777 Center of Gravity Transfer Equations
- B—Great Circle Distance Calculation
- C—Data Presentation

LIST OF FIGURES

Figure		Page
1	B-777-200ER Three-View Drawing	2
2	Airline Recording and Editing System	3
3	Data Processing Flow Chart	10
4	Description of Flight Profile Phases	13
5	Sketch of Ground Phases and Specific Events	15
6	Sign Convention for Airplane Accelerations	17
7	The Peak-Between-Means Classification Criteria	18

LIST OF TABLES

Table		Page
1	B-777-200ER Aircraft Characteristics	2
2	Recorded Parameters Provided to UDRI	4
3	Parameter Editing Values	11
4	Flight Phase Criteria	13
5	Summary of Specific Events Criteria	15
6	Flap Detents (B-777-200ER)	19
7	Statistical Data Formats	20

LIST OF ACRONYMS AND ABBREVIATIONS

ADIRU	Air Data Inertial Reference Unit
CD	Compact disk
DOS	Disk Operating System
c.g.	Center of gravity
DFDAU	Digital Flight Data Acquisition Unit
FAA	Federal Aviation Administration
GAG	Ground-air-ground
MAC	Mean aerodynamic chord
MO	Magneto-optical
nmi	Nautical mile
PSD	Power spectral density
RC	Rate of climb (ft/sec)
rms	Root mean square
URDI	University of Dayton Research Institute

EXECUTIVE SUMMARY

The University of Dayton Research Institute supports the Federal Aviation Administration (FAA) by conducting research on the structural integrity requirements for the U.S. commercial transport airplane fleet. The primary objective of this task was to support the FAA's Airborne Data Monitoring Systems Research Project by developing new and improved methods and criteria for processing and presenting large commercial transport airplane flight and ground loads usage data. The scope of activities included (1) defining the service related factors that affect the operational life of commercial aircraft; (2) designing an efficient software system to reduce, store, and process large quantities of optical quick access recorder data; and (3) reducing, analyzing, and providing processed data in statistical formats for the FAA to reassess existing certification criteria. Equally important, these new data also will enable the FAA, the aircraft manufacturers, and the airlines to better understand and control those factors that influence the structural integrity of commercial transport aircraft. Presented herein are Boeing 777-200ER aircraft operational usage data collected from 10,047 flights, representing 67,000 flight hours, recorded by a single international operator. Data are presented that will provide the user with statistical information on aircraft usage, ground and flight loads occurrences, and system operational usage based on actual B-777-200ER operational usage. The aircraft usage data include statistics on aircraft weights, flight distances, altitudes, speeds, and flight attitudes. Flight loads data include statistical information on gust and maneuver load factors, derived gust velocities, and ground-air-ground cycles. Ground loads data include statistics on lateral, longitudinal, and vertical load factors during different ground operational phases. Systems operational data include statistics on flap usage, thrust reverser usage, and engine fan speed.

The B-777 airplane sensors, which measure vertical, lateral, and longitudinal acceleration, are located in the cockpit area. The estimates of the center of gravity (c.g.) accelerations are computed in the Air Data Inertial Reference Unit, which converts the measured crew station accelerations to accelerations at the c.g. For some dynamic and ground load conditions, inaccuracies could exist in these filtered c.g. time history measurements. Operators and inspectors who use the recorded B-777 acceleration values as maintenance action triggers or flight operational quality assurance events should recognize the possibility of recorded digital flight data recorder acceleration inaccuracies.

1. INTRODUCTION.

The Federal Aviation Administration (FAA) has an ongoing airborne data monitoring systems research program to collect, process, and evaluate statistical flight and ground loads data from transport aircraft used in normal commercial airline operations. The objectives of this program were (1) to acquire, evaluate, and use typical, operational, in-service data for comparison with the prior data used in the design and qualification testing of civil transport aircraft and (2) to provide a basis to improve the structural criteria and methods of design, evaluation, and substantiation of future airplanes. The University of Dayton Research Institute (UDRI) supports the FAA efforts by developing the technology for reducing, processing, analyzing, and reporting on the operational flight and ground loads data received from the airlines participating in the FAA program and by conducting research studies.

Since the inception of the FAA Airborne Data Monitoring Systems Research Program, the scope of the Flight Loads Program has steadily expanded to include research on data collected from several aircraft operators and on aircraft models such as the Boeing 737, B-767, B-747, MD-82/83, A320, CRJ100, and BE-1900D. While current program research efforts are tailored primarily to support the FAA and the aircraft structural design community in evaluating design criteria related to the strength, durability, and damage tolerance of the basic airframe structure, much of the available data, when provided in meaningful statistical formats, can provide the aircraft operator with some valuable insight into how the aircraft and aircraft systems are used during normal flight and ground operations. In an effort to improve the data content and to disseminate meaningful data to the larger community of designers, regulators, and aircraft operators, UDRI has made changes, deletions, and additions to the statistical data formats as presented in past reports. These changes occur throughout the data presentation in appendix C of this report.

This report presents flight and ground loads data obtained from B-777-200ER aircraft representing 10,047 flights and 67,000 hours of airline operations from one carrier.

2. AIRCRAFT DESCRIPTION.

The B-777-200ER airplane is the extended range version of the B-777-200 aircraft. The extended range aircraft is available in three versions, with a range from 5960 nautical miles (nmi) to 7730 nmi compared to 5210 nm for the basic version. The aircraft also has various engine options from three engine manufacturers. The aircraft gross weights are different for each version of the aircraft. The B-777s advanced wing enhances the airplane's ability to climb quickly, cruise at higher altitudes, and allows the airplane to cruise at 0.84 Mach. The aircraft has a fly-by-wire system with fully powered control surface actuators. In terms of gross weight and size, the B-777-200ER is situated approximately midway between the B-767-200ER and the B-747-400, and approximates the Airbus A340-300.

Table 1 presents certain operational characteristics and major physical dimensions of the B-777-200ER aircraft. The table shows the gross weight ranges covering the different aircraft extended range versions. Figure 1 presents a three-view drawing, showing front, top, and side views of the aircraft.

Table 1. B-777-200ER Aircraft Characteristics

Parameter	Measurement
Maximum taxi weight	582,000-658,000 lb
Maximum takeoff weight	580,000-656,000 lb
Maximum landing weight	460,000-470,000 lb
Maximum zero-fuel weight	430,000-440,000 lb
Fuel capacity	43,300-45220 U.S. gallons
2 General Electric GE90-85B/92B/94B	85,000/92,000/93,400 lb maximum thrust each
2 Pratt & Whitney PW4084/4090	84,000/90,000 lb maximum thrust each
2 Rolls Royce TRENT884/892/895	84,000/92,000/93,400 lb maximum thrust each
Wing span reference	199 ft 11 in.
Wing reference area	4604.8 ft ²
Wing mean aerodynamic chord	276.4 in.
Wing sweep	31.66 degrees
Length	209 ft 1 in.
Height	60 ft 9 in.
Tread	36 ft
Wheel base	84 ft 11 in.

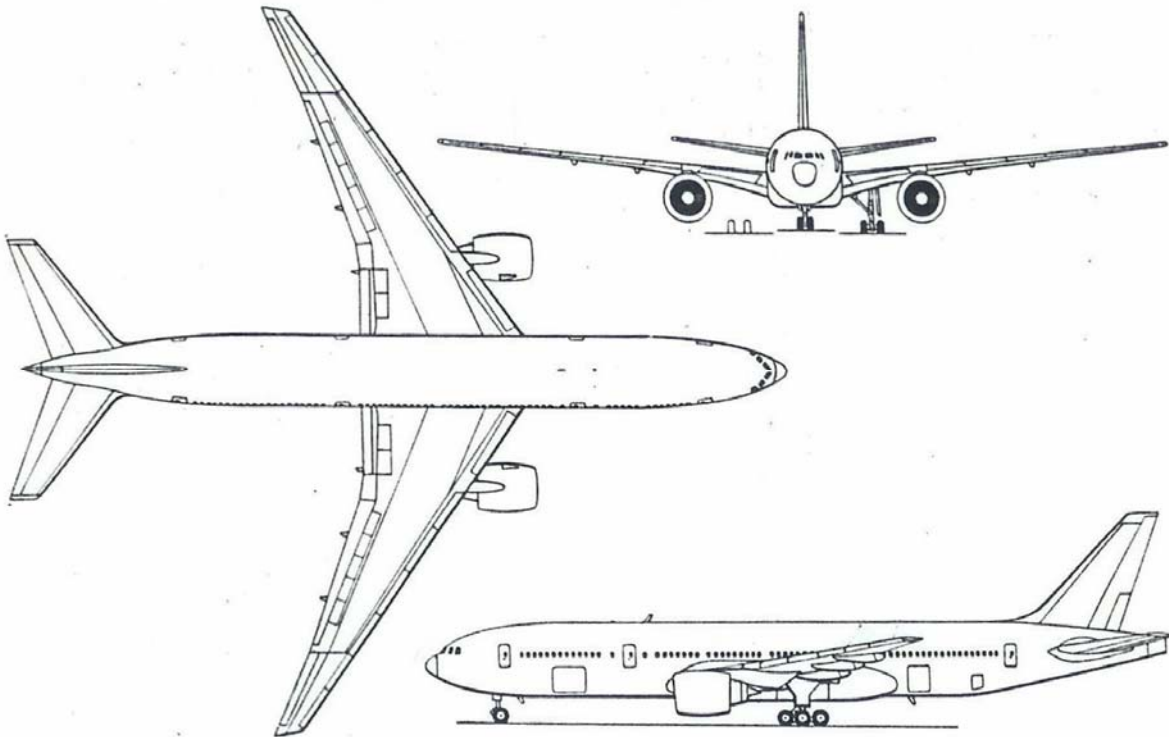


Figure 1. B-777-200ER Three-View Drawing

3. AIRLINE DATA COLLECTION AND EDITING SYSTEMS.

The airline data collection and editing systems consist of two major components: the data collection system installed onboard the aircraft and the ground data editing station. A schematic overview of the system is shown in figure 2. The data collection and editing systems are discussed in more detail below.

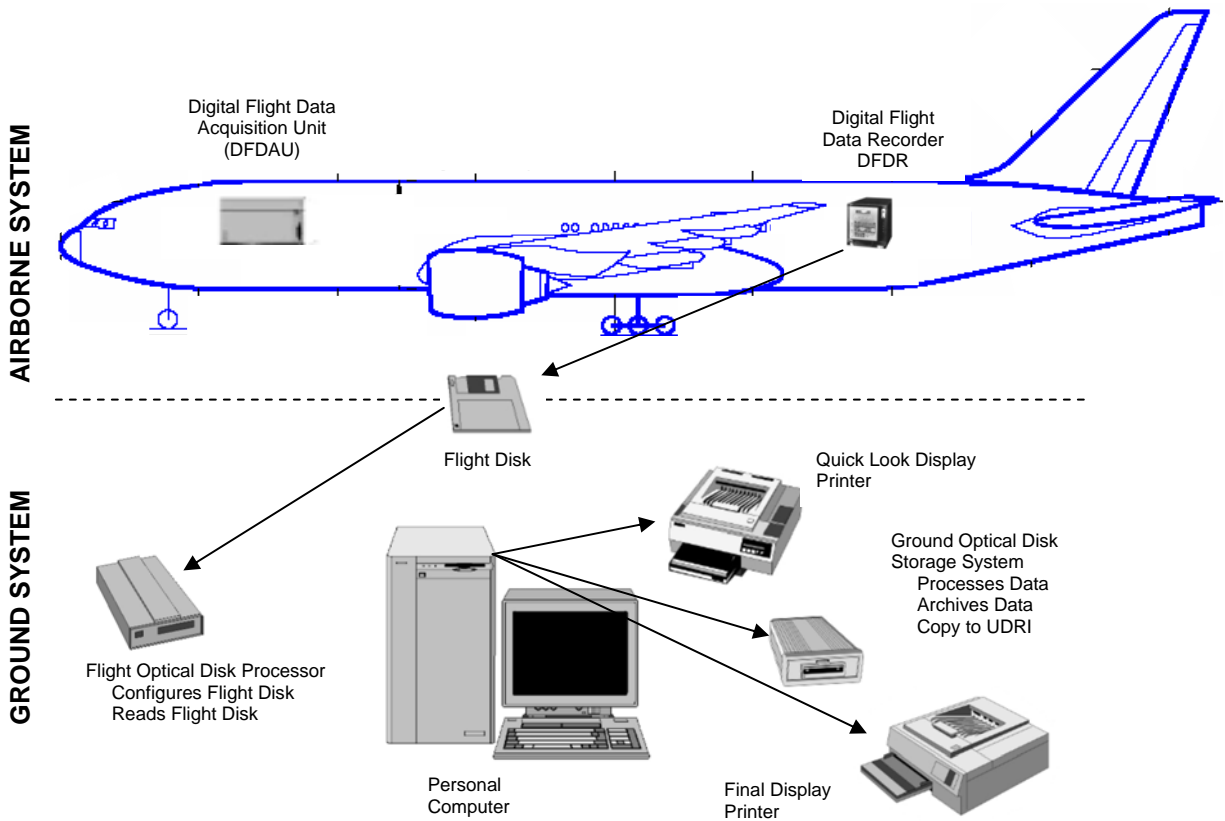


Figure 2. Airline Recording and Editing System

3.1 AIRLINE DATA COLLECTION SYSTEM.

The onboard data collection system for the B-777-200ER consists of a Digital Flight Data Acquisition Unit (DFDAU) and a 128-word per second Digital Flight Data Recorder (DFDR). The DFDAU collects sensor signals and transmits data signals to the DFDR. The DFDR uses a 25-hour solid-state electronic memory to store data. At the end of 25 hours, the DFDR will begin recording current data over the oldest data. No tape removal is required with this system. Previous Boeing airplanes obtained acceleration measurements from a multiaxis accelerometer package located near the nominal center of gravity (c.g.). However, for the B-777 acceleration sensors are located in the bay containing the Air Data Inertial Reference Unit (ADIRU) located near the crew station. The ADIRU system converts the measured accelerations at the crew station to accelerations at the c.g. The resulting c.g. accelerations are filtered with a second-order, 4-Hz Butterworth filter. They are further filtered with a notch filter to account for the first longitudinal body-bending mode and then transmitted to the flight data recorder. The equations used in the ADIRA are presented in appendix A.

3.2 AIRLINE DATA EDITING SYSTEM.

The airline ground data editing station consists of a computer, a disk drive, and flight data editing software. The software performs a number of functions during the process of transferring the raw flight data into a Disk Operating System (DOS) file format onto the hard disk. The most important of these functions includes a data integrity check and removal of flight sensitive information. Data considered sensitive are those that can be used to readily identify a specific flight. The desensitized data are forwarded to the University of Dayton Research Institute (UDRI) for flight loads processing and analysis.

4. UNIVERSITY OF DAYTON RESEARCH INSTITUTE DATA PROCESSING.

The recorded flight and ground loads parameter data are provided by the airline to UDRI on compact disk (CD) containing binary files for multiple flights for different airplanes. This section (1) lists the recorded parameters received from the airline, (2) identifies those parameters processed by UDRI, (3) describes the methods used to extract or compute parameters that are not recorded, and (4) describes how these data are then processed by UDRI through a series of computer software programs to extract the final data required to develop the statistical data formats.

4.1 RECORDED DATA PARAMETERS.

Table 2 lists the recorded data parameters provided by the airline to UDRI for each recorded flight.

Table 2. Recorded Parameters Provided to UDRI

Parameter	Sampling Rate	Parameter	Sampling Rate
Vertical acceleration	10 per second	Mach number	1 per second
Lateral acceleration	4 per second	Pressure altitude	1 per second
Longitudinal acceleration	4 per second	Gross weight	1 per second
Aileron position – 4 right and 4 left (2 inboard and 2 outboard)	2 per second each	Fuel quantity	1 per second
Elevator position – 4 right and 4 left (2 inboard and 2 outboard)	2 per second each	Bank angle	2 per second
Rudder position - upper and lower	1 per second	Pitch angle	4 per second
Horizontal stabilizer position	1 per second	Magnetic heading	1 per second
Flap position – 2 right and 2 left (1 inboard and 1 outboard)	1 per second each	True heading	1 per second
Spoiler/speed brake position - 4 and 12	1 per second each	Latitude	1 per second
Slats position – right and left	1 per second each	Longitude	1 per second
N1 Engine - right and left	1 per second each	Total air temperature	1 per second
N2 Engine - right and left	1 per second each	Radio altitude	1 per second
Thrust reverser status – right and left engine	1 per second each	Autopilot - left, center, right	1 per second each

TABLE 2. RECORDED PARAMETERS PROVIDED TO UDRI (Continued)

Parameter	Sampling Rate	Parameter	Sampling Rate
Exhaust gas temperature - 2 right and 2 left	1 per second each	Ground speed	1 per second
Squat switch - main, left	5 per second	Inertial vertical velocity	2 per second
Landing gear down and locked - main gear (right and left), nose gear	1 per second each	Glide slope - left, center, right	1 per second
Computer airspeed	1 per second	Wind speed (not available for all flights)	1 per second
True airspeed	1 per second	Wind direction (not available for all flights)	1 per second

However, not all parameters listed in table 2 are used for statistical analysis and data presentation. The recorded parameters that are used by UDRI to create time history files, compressed onto magneto-optical (MO) disks, and processed through the data reduction software for statistical analysis and data presentation are shaded.

The data system in the B-777 aircraft has the potential of having errors in the recorded c.g. accelerations. Title 14 Code of Federal Regulations 25.1459(a)(2) requires that the vertical acceleration sensor that provides acceleration data to the flight recorder be located within the appropriate c.g. limits, or at a distance forward or aft of these limits that does not exceed of 25 percent of the airplane's mean aerodynamic chord (MAC). However, for the B-777, a deviation from this requirement was approved by the responsible authority. The acceleration sensor package for the B-777 is located in the bay that contains the ADIRA, which forms part of the Airplane Information Management System. This bay is located in the cockpit area and not within the specified c.g. limits. This means that all the acceleration measurements for the B-777 must be corrected to account for their acceleration sensor position away from the c.g. area. The ADIRU system converts the measured accelerations at the crew station to accelerations at the c.g. using the relationships presented in appendix B. Subsequently, the resulting c.g. accelerations are filtered with a second-order, 4-Hz Butterworth filter. They are further filtered with a notch filter to account for the first longitudinal body-bending mode before transmittal to the flight data recorder. The conversion process used is assumed primarily applicable towards providing c.g. accelerations for in-flight conditions. Thus, it is likely that the accuracy of the recorded acceleration for other than flight conditions, such as touchdown and ground operation conditions, may be compromised.

4.2 COMPUTED PARAMETERS.

Certain information and parameters needed in subsequent data reduction are not recorded and need to be extracted or derived from available time history data. Derived gust velocity, U_{de} , and continuous gust intensity, U_{σ} , are important statistical load parameters, which are derived from measured vertical accelerations. This derivation of U_{de} and U_{σ} requires knowledge of atmospheric density, equivalent airspeed, and dynamic pressure. These values are calculated using equations that express the rate of change of density as a function of altitude based on the International Standard Atmosphere.

4.2.1 Atmospheric Density.

For altitudes below 36,089 feet, the density ρ is expressed as a function of altitude by

$$\rho = \rho_0 \left(1 - 6.876 \times 10^{-6} \times H_p\right)^{4.256} \quad (1)$$

where ρ_0 is air density at sea level (0.0023769 slugs/ft³) and H_p is pressure altitude (ft). Pressure altitude is a recorded parameter.

4.2.2 Equivalent Airspeed.

Equivalent airspeed (V_e) is a function of true air speed (V_T) and the square root of the ratio of air density at altitude (ρ) to air density at sea level (ρ_0) and is expressed as

$$V_e = V_T \sqrt{\frac{\rho}{\rho_0}} \quad (2)$$

True airspeed (V_T) is derived from Mach number (M) and speed of sound (a):

$$V_T = Ma \quad (3)$$

Mach number is dimensionless and is a recorded parameter. The speed of sound (a) is a function of pressure altitude (H_p) and the speed of sound at sea level and is expressed as

$$a = a_0 \sqrt{\left(1 - 6.876 \times 10^{-6} \times H_p\right)} \quad (4)$$

Substituting equations 1 and 4 into equation 2 gives

$$V_e = M \times a_0 \times \left(1 - 6.876 \times 10^{-6} \times H_p\right)^{0.5} \times \left(1 - 6.876 \times 10^{-6} \times H_p\right)^{2.128} \quad (5)$$

which simplifies to

$$V_e = M \times a_0 \times \left(1 - 6.876 \times 10^{-6} \times H_p\right)^{2.626} \quad (6)$$

where the speed of sound at sea level a_0 is 1116.4 fps or 661.5 knots.

4.2.3 Dynamic Pressure.

The dynamic pressure (q) is calculated from the air density and velocity as

$$q = \frac{1}{2} \rho V_T^2 \quad (7)$$

where

$$\begin{aligned}\rho &= \text{air density at altitude (slugs/ft}^3\text{)} \\ V_T &= \text{true airspeed (ft/sec)}\end{aligned}$$

4.2.4 Derived Gust Velocity.

The derived gust velocity, U_{de} , is computed from the peak values of gust incremental vertical acceleration as

$$U_{de} = \frac{\Delta n_z}{\bar{C}} \quad (8)$$

where Δn_z is gust peak incremental vertical acceleration and \bar{C} is the aircraft response factor considering the plunge-only degree of freedom and is calculated from

$$\bar{C} = \frac{\rho_0 V_e C_{L_\alpha} S}{2W} K_g \quad (9)$$

where

$$\begin{aligned}\rho_0 &= 0.002377 \text{ slugs/ft}^3, \text{ standard sea level air density} \\ V_e &= \text{equivalent airspeed (ft/sec)} \\ C_{L_\alpha} &= \text{aircraft lift-curve slope per radian} \\ S &= \text{wing reference area (ft}^2\text{)} \\ W &= \text{gross weight (lb)} \\ K_g &= \frac{0.88\mu}{5.3 + \mu} = \text{gust alleviation factor} \\ \mu &= \frac{2W}{\rho g \bar{C} C_{L_\alpha} S} \\ \rho &= \text{air density, slug/ft}^3, \text{ at pressure altitude (Hp), from equation 1} \\ g &= 32.17 \text{ ft/sec}^2 \\ \bar{C} &= \text{wing mean geometric chord (ft)}\end{aligned}$$

In this program, the lift-curve slope, C_{L_α} , is the lift-curve slope for the entire airplane.

4.2.5 Continuous Gust Intensity.

Power spectral density (PSD) functions provide a turbulence description in terms of the probability distribution of the root mean square (rms) gust velocities. The rms gust velocities or continuous gust intensities, U_σ , are computed from the peak gust value of vertical acceleration using the PSD technique as described in reference 1 as

$$U_\sigma = \frac{\Delta n_z}{A} \quad (10)$$

where Δn_z = gust peak incremental vertical acceleration

$$\bar{A} = \text{aircraft PSD gust response factor} = \frac{\rho_0 V_e C_{L\alpha} S}{2W} F(PSD) \text{ in } \frac{1}{\text{ft/sec}} \quad (11)$$

ρ_0 = 0.002377 slugs/ft³, standard sea level air density
 V_e = equivalent airspeed (ft/sec)
 $C_{L\alpha}$ = aircraft lift-curve slope per radian
 S = wing reference area (ft²)
 W = gross weight (lb)

$$F(PSD) = \frac{11.8}{\sqrt{\pi}} \left[\frac{\bar{c}}{2L} \right]^{\frac{1}{3}} \sqrt{\frac{\mu}{110 + \mu}}, \text{ dimensionless} \quad (12)$$

\bar{c} = wing mean geometric chord (ft)
 L = turbulence scale length, 2500 ft

$$\mu = \frac{2W}{\rho g \bar{c} C_{L\alpha} S}, \text{ dimensionless} \quad (13)$$

ρ = air density (slugs/ft³)
 g = 32.17 ft/sec²

To determine the number of occurrences (N) for U_σ , calculate

$$N = \frac{N_0(o)_{ref}}{N_0(o)} = \frac{\pi \bar{c}}{203} \left[\frac{\rho}{\rho_0} \mu \right]^{0.46}, \text{ dimensionless} \quad (14)$$

where \bar{c} , ρ , ρ_0 , and μ are defined above. Then each U_σ peak is counted as N counts at that U_σ value. This number of counts is used to determine the number of counts per nautical mile (nmi), or

$$\frac{\text{counts}}{\text{nmi}} = \left(\frac{N}{\text{distance flown in counting interval}} \right) \quad (15)$$

Finally, the number of such counts is summed from the largest plus or minus value toward the smallest to produce the cumulative counts per nautical mile.

4.2.6 Lift-Curve Slope.

For this study, the wing lift-curve slope was obtained from the one-dimensional approximation given in reference 2 as

$$C_{l_\alpha} = \frac{2\pi A_r}{2 + \left(4 + A_r^2 \beta^2 \left(1 + \frac{\tan^2 \Lambda}{\beta^2} \right) \right)^{1/2}} \quad (16)$$

$$A_r = \frac{b^2}{S} = \text{Wing aspect ratio}$$

$$b = \text{Wing span}$$

$$\beta = \sqrt{1 - M^2}$$

$$C_{l_\alpha} = \text{Lift-curve slope per radian or per degree}$$

$$\Lambda = \text{Quarter chord sweep angle}$$

$$M = \text{Mach number}$$

Equation 16 provides an estimate of the wing lift curve slope. Airplane gust response calculations are based on the use of the airplane lift curve slope. Reference 3 suggests a factor of 1.15 to represent the average airplane to wing lift curve slope. Therefore, the wing lift curve slope values were multiplied by 1.15. In this program, the lift-curve slope, C_{L_α} , is the untrimmed rigid lift-curve slope for the entire airplane.

4.2.7 Flight Distance.

The flight distance was obtained either by determining the stage length of the flight or by integrating the range with respect to changes in aircraft velocity as a function of time. The stage length is defined as the distance from departure airport to destination airport and is determined as the great circle distance in nautical miles between the point of liftoff (departure) and the point of touchdown (destination). Appendix B describes the calculation of great circle distance. The time histories of longitude and latitude are matched against the UDRI-generated phase of flight file to determine the geographical location of the aircraft at the point of liftoff and the point of touchdown. The integrated flight distance (D) is obtained by the numerical integration from the time at liftoff (t_0) to the time of touchdown (t_n), and V_T is the average true velocity during Δt .

$$D = \sum_{t_0}^{t_n} \Delta t \cdot V_T \quad (17)$$

4.2.8 Rate of Climb.

Although the rate of climb (RC) was a recorded value on the B-777-200ER, it was not always a recorded value on other aircraft. Therefore, UDRI continued its previous practice of calculating these values. The RC is obtained by numerical differentiation of the change in pressure altitude with time.

$$RC = \sum_{t_1}^{t_2} \frac{\Delta H_p}{\Delta t} \quad (18)$$

4.3 DATA REDUCTION OPERATIONS.

The data reduction phase retrieves the data from the CDs provided by the airline, transfers it to MO disk, processes it through a series of computer programs that convert the data to UDRI-compatible formats, and provides statistical information on aircraft usage, ground loads, flight loads, and systems operation. The data processing flow chart is illustrated in figure 3, and the flow of the processed data is discussed in subsequent paragraphs.

4.3.1 Initial Quality Screening.

All incoming data files are screened for acceptability. Individual flights are edited to remove erroneous or meaningless data such as discontinuous elapsed time data, evidence of nonfunctional channels or sensors, incomplete flight phases, and duplicate data sets. Files with missing, incomplete, or duplicate data are identified.

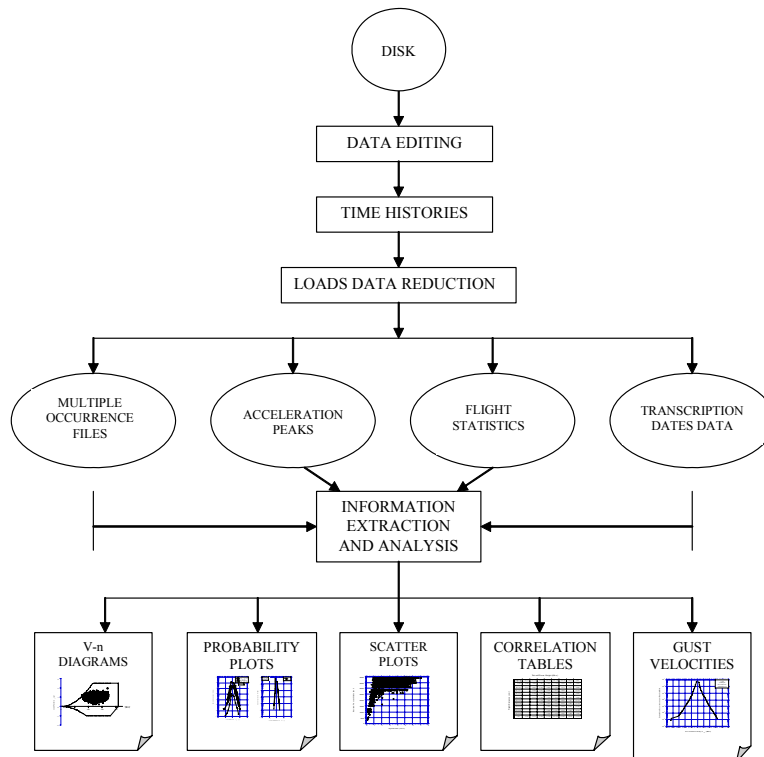


Figure 3. Data Processing Flow Chart

4.3.2 Time History Files.

Each CD provided by the airline contains multiple flights for each airplane. The files on CD are separated into individual parameter time history files for each flight. Then these time history files are compressed and stored on 230-megabyte MO disks for later recall by the flight loads processing software. Data editing and verification are performed on the data as the time histories are being prepared. Message alerts indicate that obviously erroneous data have been removed or that questionable data have been retained but need to be manually reviewed prior to their acceptance. Table 3 lists the limits against which the data are compared. Some of the parameters from table 2 are edited and retained even though they are not currently being used.

Table 3. Parameter Editing Values

Number	Parameter	Min	Max
1.	Gross weight	400,000 lb	875,000 lb
2.	Pressure altitude (Hp)	-2,000 ft	45,000 ft
3.	Calibrated airspeed	0 kts	450 kts
4.	Vertical acceleration	-2.0 g	+4.0 g
5.	Lateral acceleration	-1.0 g	+1.0 g
6.	Longitudinal acceleration	-1.0 g	+1.0 g
7.	Flap handle position	0°	40°
8.	Elevator position	-31°	+20°
9.	Aileron position	-26°	+26°
10.	Rudder position	-60°	+60°
11.	Trim position	-13.5°	+4°
12.	Speed brake position	0°	51°
13.	Throttles 1 and 2	-25°	45°
14.	Engine N ₁ and N ₂	0%	120%
15.	Thrust reverser status	0	1
16.	Squat switch (main gear)	0	1
17.	Pitch attitude	-10°	+30°
18.	Bank attitude	-40°	+40°
19.	Mach number	0	0.95
20.	Ground speed	0 kts	600 kts
21.	Fuel quantity	0	390,000 lb
22.	Latitude	-90°	+90°
23.	Longitude	-180°	+180°
24.	Magnetic heading	0°	360°
25.	Radio altitude	-20 ft	< 2,500 ft
26.	Anti-ice	0	1
27.	Autopilot	0	1
28.	Landing gear	0	1
29.	Glide slope	-10	10
30.	Inertial vertical velocity	-9,000 fpm	9,000 fpm
31.	Total air temperature	All	All
32.	Wind direction	0°	360°
33.	Wind speed	0 kts	500 kts

4.3.3 Relational Database.

Important characteristics about each set of flights received from the airline are recorded in a relational database. The airline identifier, aircraft tail number, and disk identifier of the disk received from the airline are in the data. Each flight is assigned a unique flight sequence number. The flight sequence number assigned to the first flight of the set, and the number of flights in the set are also entered. The disk identifier is also recorded, which contains the compressed time history files of all flights in the set.

4.3.4 Permanent Data Files.

In addition to the time history files, two other files are created and permanently stored with the time history files. The first file contains the chronologically sorted list of the phases of flight and their corresponding start times. This file provides the means to separate flight by flight phases in subsequent data analysis processing. The second file contains the accumulated time and distance for various combinations of phase of flight and altitude band. This file provides the capability to present data results in terms of normalized unit time and distance.

4.3.5 Loads Data Reduction.

The loads data reduction program uses the compressed time history files to derive statistical information on aircraft usage, ground loads, flight loads, and systems operations. These data are then reduced in accordance with specific data reduction criteria.

4.4 DATA REDUCTION CRITERIA.

To process the measured data into statistical loads formats, specific data reduction criteria were developed for (1) separating the phases of ground and flight operations, (2) identifying specific events associated with operation of the aircraft and its onboard systems, (3) assigning sign conventions, (4) determining maximum and minimum values and load cycles, and (5) distinguishing between gust and maneuver load factors. These criteria are discussed in the following sections.

4.4.1 Phases of Flight Profile.

The ground and flight phases were determined by UDRI from the recorded data. Each time history profile was divided into nine phases, consisting of four ground phases (taxi-out, takeoff roll, landing roll with and without thrust reverser deployed, and taxi-in) and five airborne phases (departure, climb, cruise, descent, and approach). Figure 4 shows the nine phases of a typical flight profile.

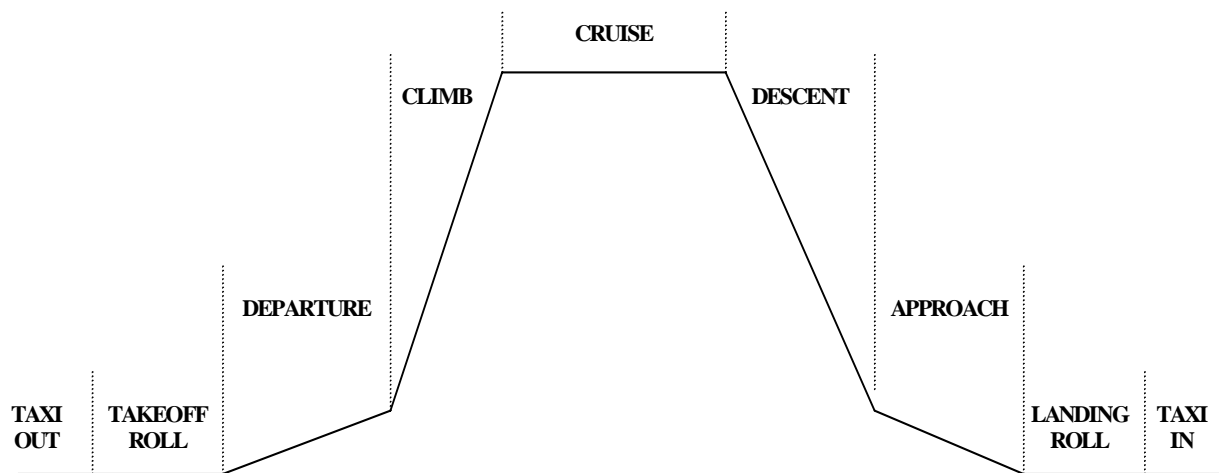


Figure 4. Description of Flight Profile Phases

The criteria used to define each of these phases are summarized in table 4 and discussed in more detail in the following sections.

Table 4. Flight Phase Criteria

Phase of Flight	Defining Condition at Start of Phase
Taxi-out	Engine start-up until beginning of takeoff roll
Takeoff roll	Time that begins first ground acceleration $> 2\text{kts/sec}$ for a 20 second duration
Departure	Liftoff, radio altitude 7 ft greater than average radio altitude during takeoff roll
Climb	Rate of climb $\geq 250\text{ ft/min}$ maintained for at least 1 minute with flaps retracted
Cruise	Rate of climb is between $\pm 250\text{ ft/min}$ and flaps retracted
Descent	Rate of descent $\geq 250\text{ ft/min}$ occurs for at least 1 minute and flaps retracted
Approach	Rate of descent $\leq 250\text{ ft/min}$ occurs for at least 1 minute with flaps extended
Landing roll	Immediately after touchdown event to start of turnoff
Taxi-in	End of runway turnoff until parked at the gate or recorder shutdown

4.4.1.1 Ground Phases.

UDRI separated the ground portion of each flight from the time it departed the gate area to its return to the gate into four phases: taxi-out, takeoff roll, landing roll, and taxi-in. Specific data reduction criteria were developed by UDRI and used to identify the beginning and end of each phase.

UDRI defined all aircraft movement from engine start-up until the aircraft begins its takeoff roll as being taxi-out.

UDRI identified the beginning of the takeoff roll by searching for ground speeds that accelerated at rates greater than 2 kts/sec for a minimum duration of 20 seconds. Then, when these values were found, the beginning of the takeoff roll was assigned as being the time slice where the first ground speed rate change greater than 2 kts/sec for that sequence occurred. The takeoff roll ends at liftoff, which is determined by the radio altitude.

The landing roll phase is defined as beginning immediately after the touchdown event and ending when the aircraft begins its turnoff from the active runway. The criteria for the touchdown and the runway turnoff are discussed further in sections 4.4.2.2 and 4.4.2.4 respectively.

Taxi-in is defined from the point where the aircraft completed its turnoff from the active runway after its landing roll to the position when the aircraft was either parked at the gate or the recorder had been shutdown.

4.4.1.2 Airborne Phases.

The airborne portion of each flight profile was separated into five phases: departure, climb, cruise, descent, and approach. These phases occur between the time that the aircraft lifts off until it touches down. The beginning of each flight phase is defined based on combinations of the squat switch position, flap settings, and the calculated RC or descent over a period of at least 1 minute as shown in table 4. Also, by definition, the departure phase cannot be less than 1 minute in length.

It should be noted that an airborne phase could occur several times per flight because it is determined by the RC and the position of the flaps. When this occurs, the flight loads data are combined and presented as a single flight phase. The UDRI software then creates a file that chronologically lists the phases of flight and their corresponding starting times.

4.4.2 Specific Events.

In addition to the ground and airborne phases, a unique set of criteria was also required to identify certain specific events such as liftoff, landing touchdown, thrust reverser deployment and stowage, and start and completion of turnoff from the active runway after landing. Figure 5 shows a sketch depicting these phases and events.

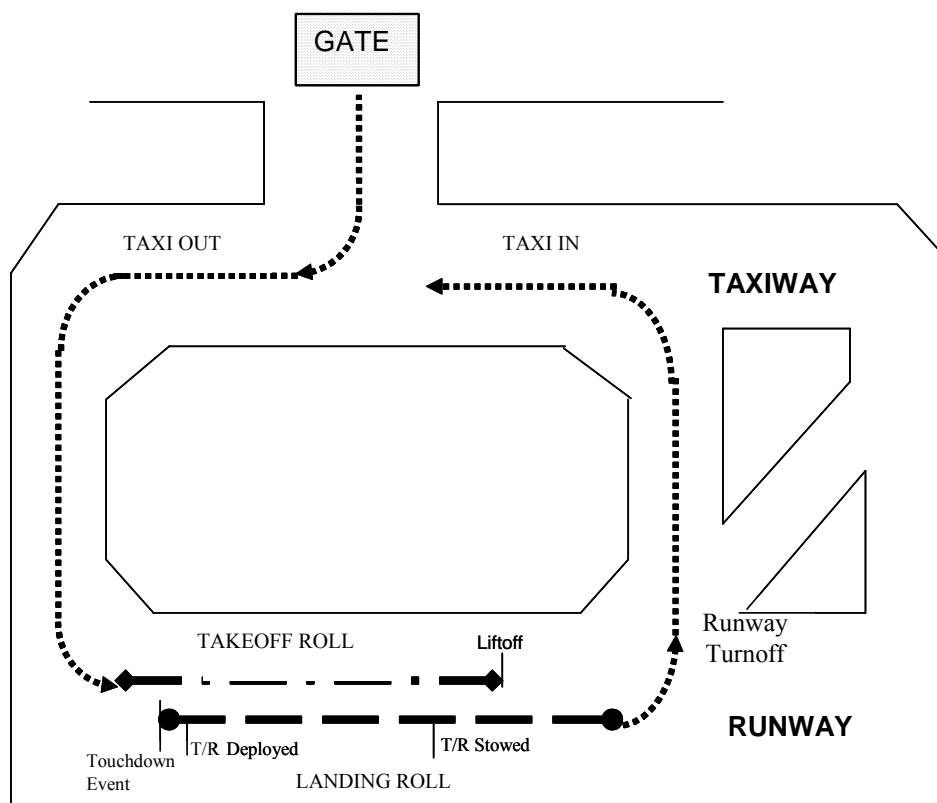


Figure 5. Sketch of Ground Phases and Specific Events

The criteria used to define each of the specific events are summarized in table 5 and discussed in more detail in reference 4 and the following sections.

Table 5. Summary of Specific Events Criteria

Phase/Event	Defining Conditions
Liftoff	Point of first reading in series of increasing radio altitude values greater than 7 feet higher than the average radio altitude value calculated during the takeoff roll
Landing touchdown	Three seconds prior to main gear squat switch to first point where average pitch angle during landing roll plus 0.5 degrees is crossed
Thrust reverser deployment and stowage	Thrust reverser switch on for deployment and off for stowage
Runway turnoff	From first sequential magnetic heading change in same direction from runway centerline and heading sequence changes >13.5 degrees to a straight line heading or turn in opposite direction

4.4.2.1 Liftoff.

Liftoff for the B-777-200ER was determined from an algorithm that identifies the liftoff point as the first reading in the series of increasing radio altitude values that was greater than 7 feet higher than the average radio altitude value that it calculated during the takeoff roll.

4.4.2.2 Landing Touchdown.

The primary objective when identifying the touchdown event was to ensure that accelerations, particularly n_y occurrences related to the landing event, were not mistakenly included in the landing roll phase. To accomplish this task, the touchdown event was defined to include closure of the nose gear squat switch. Since the nose gear squat switch was not an available parameter in the UDRI database for the B-777, an alternative method to identify the end of the touchdown event was used. Analysis of the touchdown event began three seconds prior to main gear squat switch closure and ended based on a method that used the pitch angle of the aircraft. The average pitch angle of each flight during a period of time 15 to 30 seconds after main gear squat switch was calculated as the initial reference line and identified when the aircraft had become level with the runway, i.e., constant pitch angle. The reference line was then shifted half a degree to make sure that the criteria would identify when the nose gear was down for every flight. The nose gear was assumed to be down and the touchdown event over when the aircraft's pitch angle first crossed the reference plus 0.5 degree mark. The end of the touchdown event also served as the start of the landing roll.

4.4.2.3 Thrust Reverser Deployment and Stowage.

An on/off switch identifies when deployment or stowage of the thrust reverser occurs. Thus, by identifying when this occurs as a special event, load factor acceleration data can be obtained at the instant of thrust reverser deployment and during the time of thrust reverser usage and stowage.

4.4.2.4 Runway Turnoff.

Changes in the aircraft's magnetic heading were used to identify the beginning and end of the aircraft's turnoff from the active runway after the landing roll. After the aircraft touched down, subsequent magnetic heading readings were averaged. This average heading was defined as the runway centerline. Subsequent magnetic heading changes were then tested to identify continuous movement in the same direction away from this centerline. When the aircraft's sequential magnetic heading change exceeded 13.5° from the direction of the landing centerline, the time slice associated with the first sequential heading change from the landing centerline in the direction of the turn was defined as the beginning of the turnoff from the runway.

An alternate method was used to identify flights involving shallow turns from the runway that did not exceed the 13.5° turn criteria. This method uses aircraft ground speed and magnetic heading to calculate the aircraft's position relative to the runway centerline by identifying when the aircraft's position perpendicular to the runway centerline exceeded 100 feet. The time slice associated with the first aircraft movement away from the landing centerline in the direction of the turn was defined as the beginning of the aircraft's turnoff from the runway.

The end point of the first turnoff from the active runway was also identified using magnetic heading readings. An algorithm was developed that uses the changes in magnetic heading, while the aircraft was in its turn, to identify when the aircraft had either returned to taxiing in a straight line or was turning in the opposite direction. The first point that provided this indication was then defined as the end point of the turnoff from the runway. This point is also the beginning of the taxi-in phase.

4.4.3 Sign Conventions.

Acceleration data are recorded in three directions: vertical (z), lateral (y), and longitudinal (x). As shown in figure 6, the positive z direction is up; the positive y direction is airplane starboard; and the positive x direction is forward.

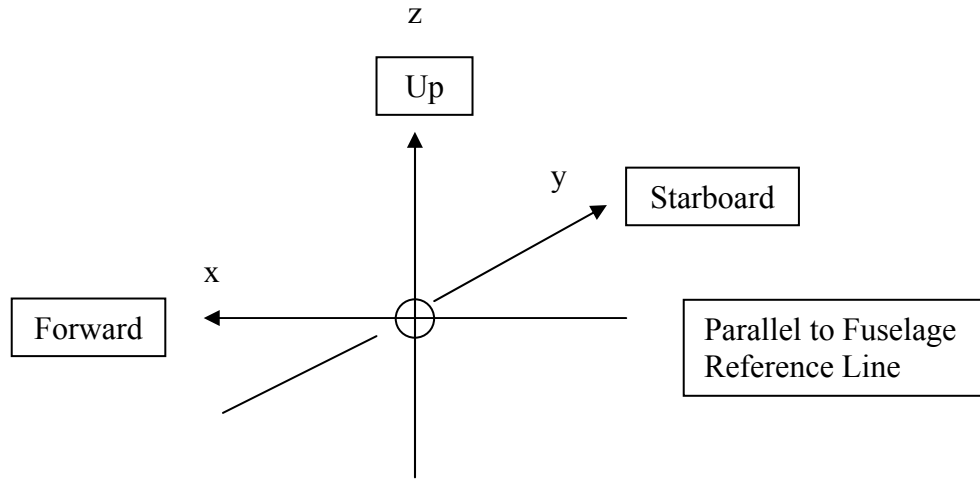


Figure 6. Sign Convention for Airplane Accelerations

4.4.4 Peak Selection Technique.

The peak-between-means method presented in reference 1 is used to identify positive and negative peaks in the acceleration data. This method is consistent with past practices and pertains to all accelerations (n_x , n_y , Δn_z , $\Delta n_{z_{gust}}$, and $\Delta n_{z_{man}}$). A brief description of the peak-between-means technique follows.

One peak is identified between each two successive crossings of the mean acceleration, which is the zero load factor condition for lateral, longitudinal, and incremental vertical accelerations. Peaks greater than the mean are considered positive, and those less than the mean negative. A threshold zone is defined around the mean, when acceleration peaks are ignored because they have been shown to be irrelevant. The threshold zone is ± 0.05 g for the vertical accelerations Δn_z , $\Delta n_{z_{gust}}$, and $\Delta n_{z_{man}}$, ± 0.005 g for lateral acceleration n_y , and ± 0.0025 g for longitudinal acceleration n_x .

Figure 7 demonstrates the acceleration peak selection technique. The sample acceleration trace contains 8 zero crossings that are circled, set off by vertical dashed lines, and labeled C_i , $i = 0$ to 7. For each of seven intervals between successive mean crossings, C_{i-1} to C_i , $i = 1$ to 7, one peak, which is located at P_i , is identified. Peaks lying outside the threshold zone (P_1 , P_2 , P_5 , P_6 , and P_7) are accepted and retained, whereas peaks lying inside the threshold zone (P_3 and P_4) are ignored.

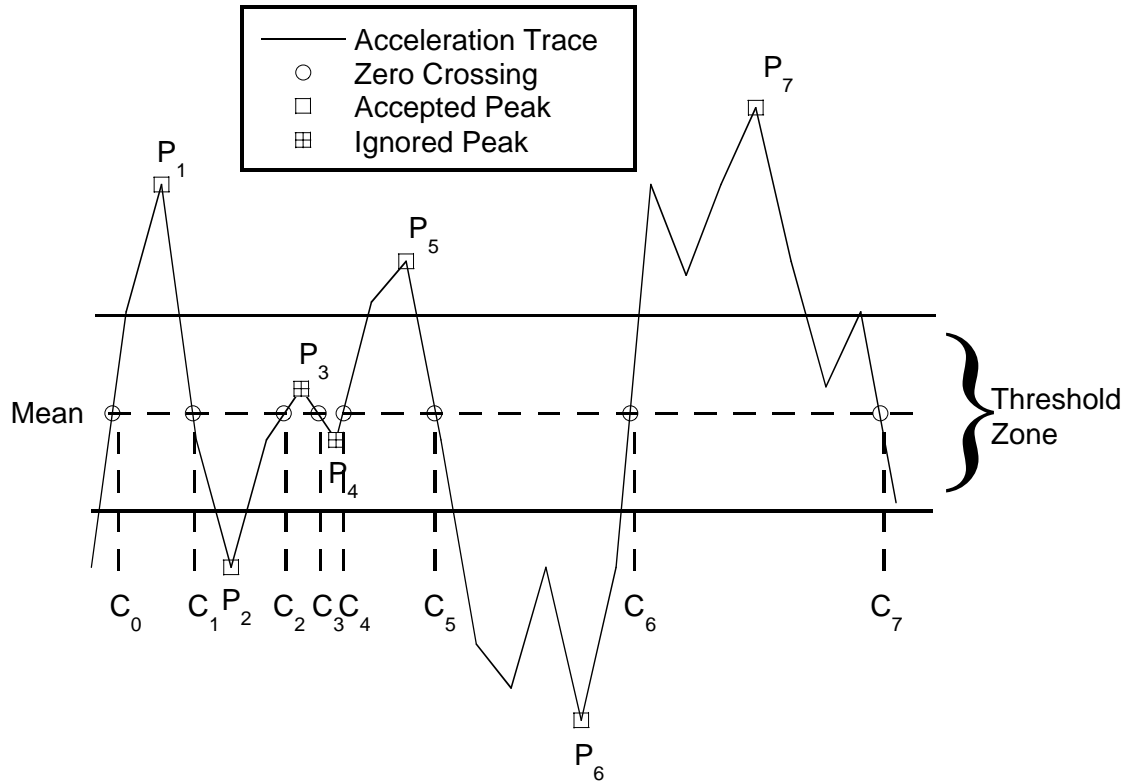


Figure 7. The Peak-Between-Means Classification Criteria

4.4.5 Separation of Maneuver and Gust Load Factors.

The incremental vertical acceleration Δn_z at the c.g. is obtained by subtracting the 1-g condition from the measured total load factor n_z . The incremental acceleration measured at the c.g. of the aircraft in flight may be the result of either maneuvers or gusts. To derive gust and maneuver statistics, the maneuver-induced acceleration ($\Delta n_{z_{man}}$) and the gust response acceleration ($\Delta n_{z_{gust}}$) must be separated from the total acceleration history. Reference 5 reported the results of a UDRI study to evaluate methods of separating maneuver and gust load factors from measured acceleration time histories. As a result of this study, UDRI uses a cycle duration rule to differentiate maneuver-induced acceleration peaks from those peaks caused by gust loading. Review of the B-777-200ER response characteristics has shown that a cycle duration of 2.0 seconds is appropriate for the aircraft and thus was used.

4.4.6 Flap Detents.

When flaps are extended, the effective deflection is considered to be that of the applicable detent, as indicated in table 6.

Table 6. Flap Detents (B-777-200ER)

Flap/Slat Detent	Minimum Flap Setting	Maximum Flap Setting
1	$> 0^{\circ}$	$\leq 1^{\circ}$
5	$> 1^{\circ}$	$\leq 4.6^{\circ}$
10	$> 4.6^{\circ}$	$\leq 9.6^{\circ}$
20	$> 9.6^{\circ}$	$\leq 19.6^{\circ}$
25	$> 19.6^{\circ}$	$\leq 24.6^{\circ}$
30	$> 24.6^{\circ}$	$\leq 32.6^{\circ}$

5. DATA PRESENTATION.

The statistical data presented in this section provide the FAA, aircraft manufacturers, and the operating airline with the information that is needed to assess how the B-777-200ER aircraft is actually being used in operational service versus its original design or intended usage. The statistical data presented herein can be used by the FAA as a basis to evaluate existing structural certification criteria, to improve requirements for the design, evaluation, and substantiation of existing aircraft, and to establish design criteria for future generations of new aircraft. The aircraft manufacturer can use these data to assess the aircraft's structural integrity by comparing the actual in-service usage of the B-777-200ER aircraft versus its originally intended design usage. It can also use these data to derive typical flight profiles and to update structural strength, durability, and damage tolerance analyses to establish or revise maintenance and inspection requirements for critical airframe and structural components. The airline and aircraft operator can use these data to evaluate the aircraft's current usage with respect to established operational procedures and placard limitations. They can also use these data to identify where changes in current operational procedures could provide additional safety margins, increase the service life of structural components, and improve on the economics of its operations.

Table 7 lists all the statistical formats for which the data were processed. The various data formats have been grouped together within the table in an attempt to categorize the B-777-200ER data being presented on the basis of whether it pertains to aircraft usage, ground or flight loads data, or systems operational data. The aircraft usage data section describes the aircraft's operational usage in terms of distributions of flight lengths, flight duration, flight phase, flight altitudes, flight speeds, takeoff and landing gross weights, etc. The loads and system data section describes the flight and ground environment and the induced system cyclic loadings experienced by the aircraft while the aircraft performs its intended usage.

Table 7. Statistical Data Formats

Data Description	Figure
AIRCRAFT USAGE DATA	
WEIGHT AND FLIGHT DISTANCE DATA	
Cumulative Probability of Takeoff Gross Weight	C-1
Cumulative Probability of Landing Gross Weight	C-2
Cumulative Probability of Great Circle Flight Length	C-3
Correlation of Great Circle Flight Length and Integrated Flight Distance	C-4
Correlation of Takeoff Gross Weight and Great Circle Flight Length	C-5
Correlation of Takeoff Gross Weight and Great Circle Flight Length, Percent of Flights	C-6
Correlation of Takeoff and Landing Gross Weight, Percent of Flights	C-7
Percent of Integrated Flight Distance in Altitude Bands	C-8
ALTITUDE AND SPEED DATA	
Correlation of Maximum Altitude and Flight Duration	C-9
Cumulative Probability of Maximum Ground Speed During Taxi	C-10
Maximum Mach Number and Coincident Altitude, All Flight Phases	C-11
Maximum Computed Airspeed and Coincident Altitude, All Flight Phases	C-12
Cumulative Probability of Ground Speed at Liftoff	C-13
Cumulative Probability of Ground Speed at Touchdown	C-14
ATTITUDE DATA	
Cumulative Probability of Pitch Angle at Liftoff	C-15
Cumulative Probability of Pitch Angle at Touchdown	C-16
Cumulative Probability of Maximum Pitch Angle During Departure	C-17
Cumulative Probability of Maximum Pitch Angle During Approach	C-18
GROUND LOADS DATA	
LATERAL LOAD FACTOR, n_y	
Cumulative Frequency of Maximum Lateral Load Factor at Touchdown	C-19
Maximum Lateral Load Factor and Coincident Incremental Vertical Load Factor at Touchdown	C-20
Cumulative Frequency of Maximum Lateral Load Factor During Runway Turnoff	C-21
Cumulative Frequency of Maximum Lateral Load Factor During Ground Turns	C-22
Probability Distributions of Turning Angle During Runway Turnoff	C-23
Maximum Lateral Load Factor and Coincident Ground Speed During Runway Turnoff, 0-60 Degree Turns	C-24
Maximum Lateral Load Factor and Coincident Ground Speed During Runway Turnoff, 60-120 Degree Turns	C-25
Maximum Lateral Load Factor and Coincident Ground Speed During Runway Turnoff, 120-240 Degree Turns	C-26
Maximum Lateral Load Factor at Touchdown vs Maximum Yaw Angle Before Touchdown	C-27
Maximum Lateral Load Factor at Touchdown vs Mean Yaw Angle Before Touchdown	C-28
Maximum Lateral Load Factor at Touchdown vs Maximum Bank Angle Before Touchdown	C-29
LONGITUDINAL LOAD FACTOR, n_x	
Cumulative Frequency of Longitudinal Load Factor During Taxi Operations	C-30
Cumulative Frequency of Longitudinal Load Factor at Touchdown and During Landing Roll	C-31
VERTICAL LOAD FACTOR, n_z	
Cumulative Frequency of Incremental Vertical Load Factor During Taxi Operations	C-32
Cumulative Frequency of Incremental Vertical Load Factor During Takeoff Roll	C-33
Cumulative Frequency of Incremental Vertical Load Factor at Spoiler Deployment and at Touchdown	C-34
Cumulative Frequency of Incremental Vertical Load Factor During Landing Roll	C-35
Maximum Incremental Vertical Load Factor at Touchdown vs Maximum Yaw Angle Before Touchdown	C-36
Maximum Incremental Vertical Load Factor at Touchdown vs Mean Yaw Angle Before Touchdown	C-37
Maximum Incremental Vertical Load Factor at Touchdown vs Maximum Bank Angle Before Touchdown	C-38

TABLE 7. STATISTICAL DATA FORMATS (Continued)

Data Description	Figure
FLIGHT LOADS DATA	
Maximum Incremental Vertical Load Factor at Touchdown vs Coincident Airspeed	C-39
Aircraft Runway Acceleration Response	C-40
GUST VERTICAL LOAD FACTOR DATA	
Cumulative Occurrences of Incremental Vertical Gust Load Factor per 1000 Hours by Flight Phase	C-41
Cumulative Occurrences of Incremental Vertical Gust Load Factor per 1000 Hours, Combined Flight Phases	C-42
Cumulative Occurrences of Incremental Vertical Gust Load Factor per Nautical Mile by Flight Phase	C-43
Cumulative Occurrences of Incremental Vertical Gust Load Factor per Nautical Mile, Combined Flight Phases	C-44
Gust Load Factor and Coincident Speed for Flaps Retracted	C-45
Gust Load Factor and Coincident Speed for Flaps Extended	C-46
DERIVED GUST VELOCITY DATA	
Cumulative Occurrences of Derived Gust Velocity per Nautical Mile, < 500 Feet	C-47
Cumulative Occurrences of Derived Gust Velocity per Nautical Mile, 500-1500 Feet	C-48
Cumulative Occurrences of Derived Gust Velocity per Nautical Mile, 1500-4500 Feet	C-49
Cumulative Occurrences of Derived Gust Velocity per Nautical Mile, 4500-9500 Feet	C-50
Cumulative Occurrences of Derived Gust Velocity per Nautical Mile, 9500-19,500 Feet	C-51
Cumulative Occurrences of Derived Gust Velocity per Nautical Mile, 19,500-29,500 Feet	C-52
Cumulative Occurrences of Derived Gust Velocity per Nautical Mile, 29,500-39,500 Feet	C-53
Cumulative Occurrences of Derived Gust Velocity per Nautical Mile, 39,500-44,500 Feet	C-54
Cumulative Occurrences of Derived Gust Velocity per Nautical Mile, Flaps Extended	C-55
Cumulative Occurrences of Derived Gust Velocity per Nautical Mile, Flaps Retracted	C-56
CONTINUOUS GUST INTENSITY DATA	
Cumulative Occurrences of Continuous Gust Intensity per Nautical Mile, Flaps Extended	C-57
Cumulative Occurrences of Continuous Gust Intensity per Nautical Mile, Flaps Retracted	C-58
MANEUVER VERTICAL LOAD FACTOR DATA	
Cumulative Occurrences of Incremental Vertical Maneuver Load Factor per 1000 Hours During Departure by Altitude	C-59
Cumulative Occurrences of Incremental Vertical Maneuver Load Factor per 1000 Hours During Climb by Altitude	C-60
Cumulative Occurrences of Incremental Vertical Maneuver Load Factor per 1000 Hours During Cruise by Altitude	C-61
Cumulative Occurrences of Incremental Vertical Maneuver Load Factor per 1000 Hours During Descent by Altitude	C-62
Cumulative Occurrences of Incremental Vertical Maneuver Load Factor per 1000 Hours During Approach by Altitude	C-63
Cumulative Occurrences of Incremental Vertical Maneuver Load Factor per Nautical Mile During Departure by Altitude	C-64
Cumulative Occurrences of Incremental Vertical Maneuver Load Factor per Nautical Mile During Climb by Altitude	C-65
Cumulative Occurrences of Incremental Vertical Maneuver Load Factor per Nautical Mile During Cruise by Altitude	C-66
Cumulative Occurrences of Incremental Vertical Maneuver Load Factor per Nautical Mile During Descent by Altitude	C-67
Cumulative Occurrences of Incremental Vertical Maneuver Load Factor per Nautical Mile During Approach by Altitude	C-68
Cumulative Occurrences of Incremental Vertical Maneuver Load Factor per 1000 Hours by Flight Phase	C-69
Cumulative Occurrences of Incremental Vertical Maneuver Load Factor per 1000 Hours, Combined Flight Phases	C-70
Cumulative Occurrences of Incremental Vertical Maneuver Load Factor per Nautical Mile by Flight Phase	C-71
Cumulative Occurrences of Incremental Vertical Maneuver Load Factor per Nautical Mile, Combined Flight Phases	C-72
Maneuver Load Factor and Coincident Speed for Flaps Retracted	C-73
Maneuver Load Factor and Coincident Speed for Flaps Extended	C-74

TABLE 7. STATISTICAL DATA FORMATS (Continued)

Data Description	Figure
FLIGHT LOADS DATA	
COMBINED MANEUVER AND GUST VERTICAL LOAD FACTOR DATA	
Cumulative Occurrences of Incremental Vertical Load Factor per 1000 Hours by Flight Phase	C-75
Cumulative Occurrences of Incremental Vertical Load Factor per 1000 Hours, Combined Flight Phases	C-76
Cumulative Occurrences of Incremental Vertical Load Factor per Nautical Mile by Flight Phase	C-77
Cumulative Occurrences of Incremental Vertical Load Factor per Nautical Mile, Combined Flight Phases	C-78
Cumulative Occurrences of Lateral Load Factor per 1000 Hours by Flight Phase	C-79
Maximum Lateral Load Factor vs Coincident Gross Weight During Departure	C-80
Maximum Lateral Load Factor vs Coincident Gross Weight During Climb	C-81
Maximum Lateral Load Factor vs Coincident Gross Weight During Cruise	C-82
Maximum Lateral Load Factor vs Coincident Gross Weight During Descent	C-83
Maximum Lateral Load Factor vs Coincident Gross Weight During Approach	C-84
GROUND-AIR-GROUND CYCLE DATA	
Ground-Air-Ground Cycle Occurrences of Maximum and Minimum Incremental Vertical Load Factor	C-85
3-D Plot of Ground-Air-Ground Cycles	C-86
SYSTEMS OPERATIONAL DATA	
FLAP USAGE DATA	
Cumulative Probability of Maximum Airspeed in Flap Detent During Departure	C-87
Relative Probability of Maximum Airspeed in Flap Detent During Departure	C-88
Cumulative Probability of Maximum Airspeed in Flap Detent During Approach	C-89
Relative Probability of Maximum Airspeed in Flap Detent During Approach	C-90
Percent of Time in Flap Detent During Departure	C-91
Percent of Time in Flap Detent During Approach	C-92
THRUST REVERSER DATA	
Cumulative Probability of Time With Thrust Reversers Deployed	C-93
Cumulative Probability of Speed at Thrust Reverser Deployment and Stowage	C-94
PROPULSION DATA	
Cumulative Probability of Percent of N_1 During Takeoff, at Thrust Reverser Deployment, and During Thrust Reverser Deployment	C-95

Figures C-1 through C-95 are presented in appendix C. The figures present information on aircraft usage, repeated ground and flight loadings, and flap and thrust reverser operations. To present the large amount of processed data in the most visible and comprehensive manner and to facilitate easy comparison between variables, most information is presented in graphical form with a minimum of tabular summaries. The graphical presentations include line plots of both cumulative and relative probability, frequency distribution histograms, pie charts, and scatter plots. The scatter plots are included to show the relationship between coincident parameters that are considered to be of interest and to show visible evidence of relationships, outliers, or suspicious data. The scatter plots presented in this report show that many of the plotted parameters are not related but occur in an independent random manner.

It should also be noted that the data presented in these figures are not always based on an identical number of flights or flight hours. During data reduction, it was discovered that some data frames and parameters exhibited random errors and were thus judged to be unacceptable for use. When this occurred, those questionable data that could influence the presentation of the other data measurements were eliminated from the statistical database for any application, either

directly or indirectly. As a result, not all figures are necessarily based on data from identical number of flights, hours, or nautical miles.

5.1 AIRCRAFT USAGE DATA.

Figures C-1 through C-18 provide statistical data on the aircraft's operational usage. Information on takeoff and landing gross weights, operational flight speeds and altitudes, aircraft attitude, and flight lengths based on normal everyday flight operations are presented. These data are useful in defining typical flight profiles in terms of gross weight, speed, altitude, and the numbers of flights associated with each type profile.

5.1.1 Weight and Flight Distance Data.

This section presents statistical data on operational takeoff and landing gross weights, flight distances, and plots showing the correlation between weight and flight distance. The flight distances in these figures are based on the great circle distance (sometimes referred to as stage length) between departure and arrival points except for figure C-4, which compares two methods of determining flight distance.

The cumulative probability distributions of gross weight during takeoff and landing are presented in figures C-1 and C-2. The occurrences of takeoff gross weight show a wide variation as one would expect due to differing fuel weights required for the different flight lengths shown in figures C-3 and C-4. It is noteworthy that some landing gross weights observed are close to the maximum design landing gross weight of 445,000 lb listed in table 1. These are possibly associated with short flights at high takeoff weights where the airplane is fueled through, that is, the aircraft is not refueled between flights or a turn back. Figure C-6 shows the occurrence of such flights.

Figure C-3 shows the cumulative probability distribution of the great circle flight length for all Boeing-777-200ER flights. The distribution shows that 80% of all flights exceed 2500 nmi in length.

Figure C-4 presents a scatter plot comparison of the differences in the great circle flight length and the integrated flight distance. The great circle flight length reflects the calculated straight-line flight distance between two points in still air. The integrated flight distances represent the airborne distance flown relative to the ambient air and accounts for the impact of winds, deviations from straight-line flight, and loiter on the total distance flown by the aircraft. These distances will always be different because of deviations that occur during the flight resulting from directional flight changes directed by the air traffic control center, increased distance flown due to holding patterns, wind direction, and to a much lesser extent, the climb and descent distances that are slightly larger than the level flight distance. Figure C-4 indicates that for flights of the B-777-200ER exceeding 1000 nmi, the integrated flight distance may be considerably longer than the great circle flight length. Thus, the aircraft is subjected to the loading environment for a much longer period of time than if only the great circle flight length was considered.

Figures C-5 and C-6 compare aircraft gross weight at takeoff with distance flown to determine whether there is any correlation between the two parameters. Figure C-5 compares the takeoff gross weight versus the great circle flight distance flown for each individual flight as a scatter plot. Figure C-6 contains a tabular listing of the percent of flights that took off within the interval of gross weight shown and those that landed within the specified flight distance. While both figures indicate there is a wide variation in takeoff gross weights and flight lengths, the data does show a correlation between gross weight and great circle flight length, although considerable scatter is evident. The data also indicate that the aircraft is mostly used for flight distances exceeding 2500 nmi.

Figure C-7 provides a tabular listing of the percent of flights that takeoff and land within the gross weight ranges indicated. The data indicate that very few flights takeoff at gross weights above 600,000 pounds and about 98 percent of the flights land at weights between 350,000 and 450,000 pounds.

Figure C-8 shows the distribution, expressed in percent, of the integrated flight distance by pressure altitude bands. Each column represents 100% of the flights that fall within the specified distance range. The table shows that the aircraft operate consistently above 29,000 feet for flights longer than 1000 nmi.

5.1.2 Altitude and Speed Data.

This section presents information about the altitudes and speeds at which the aircraft operate.

Figure C-9 shows the maximum altitude attained during each flight plotted versus the duration of the flight. The data indicate that as the flight length increases, the maximum altitude attained by the aircraft increases. Flight altitudes are assigned by air traffic control and are generally below 35,000-36,000 feet. For long duration flights and flights in areas of less congested traffic, a stepped cruise altitude may be allowed for improved performance. The scatter plot supports the fact that as flight length increases, especially above 5 hours duration, higher cruise altitudes are allowed. Airline performance is judged strongly by block time rather than operating performance. Hence, for short flights, climbs to higher altitudes for better performance is not important, and lower maximum cruise altitudes may be requested and granted. The scatter plots show a reduction in maximum altitude for short flights less than 1.5 hours.

The cumulative probabilities of ground speed for taxi-in and taxi-out operations are presented in figure C-10. The taxi-in speed is somewhat higher than the taxi-out speed, which agrees with what has been observed with other aircraft models. This probably occurs because ground movement of inbound traffic to the terminal after landing is generally accomplished faster due to less traffic than when moving from the terminal to the takeoff position. It should be noted for this report that the taxi-in phase of operation begins after the first turnoff from the active runway compared to previous UDRI reports that included the runway turnoff speeds as part of the taxi-in phase of operation. The higher taxi-in speeds, as observed in these earlier reports, probably occurred as the aircraft was exiting the runway during the turnoff.

Figures C-11 and C-12 show measured speeds plotted versus Mach number and airspeed limits, M_{MO} or V_{MO} , as defined in the aircraft flight manual. Each plotted point represents the airspeed

or Mach number that yielded the greatest difference between the observed airspeed and Mach number, and the speed or Mach number limit at its coincident altitude, regardless of flight phase. For example, in one flight, the maximum speed with respect to the limit might have been attained in the climb phase, while in another flight, the maximum speed might have occurred in a different phase. Also, it should be noted that the Mach number and airspeed points as plotted do not necessarily occur simultaneously. Both plots indicate there are many flights that operate at speeds or Mach number values approaching or, in a few cases, slightly exceeding the airspeed limits.

Figures C-13 and C-14 show the cumulative probabilities of ground airspeed at liftoff and touchdown respectively. They show that most of the takeoffs occur at speeds between 130 and 170 knots. Most touchdown speeds occur between 110 and 135 knots. Comparison of the two flight phases also shows that the liftoff speeds for the Boeing-777-200ER are approximately 25 to 35 knots higher than the touchdown speeds.

5.1.3 Attitude Data.

This section presents statistical pitch angle data for selected phases of flight.

Figure C-15 provides the cumulative probability of maximum pitch angle at liftoff. The criteria used to identify the maximum pitch angle at liftoff selects the value of the maximum pitch angle occurring within an interval of 5 seconds after the squat switch indicated liftoff.

Figure C-16 shows the cumulative probability distribution of pitch angle at touchdown, where touchdown is identified as squat switch activation. Because the landing gear strut needs to compress a finite distance to activate the squat switch, the squat switch is not always a reliable indicator of the exact instant of touchdown. However, time history data shows that the pitch angle is quite constant during the end of flare until squat switch activation, and the squat switch signal was considered to be adequate for purposes of determining the pitch angle at touchdown. The figure shows that the pitch angle during touchdown varied from 2 to 6 degrees with most touchdowns occurring at pitch angles between 2.5 and 4.5 degrees.

Figures C-17 and C-18 present the cumulative probability of maximum pitch angle during the departure and approach phases of flight. The data show that the pitch angle of the aircraft during departure varies from approximately 13 to 20 degrees, while during its approach, the pitch angle varies from 3 to 9 degrees. In reference 4, Chai and Mason attributed this difference to the fact that “with the flaps in the fully deflected position, the critical angle of attack of the wing during landing [and approach] is smaller than during takeoff [and departure].” Consequently, the pitch angle during landing is smaller than that during takeoff.

5.2 GROUND LOADS DATA.

Figures C-19 through C-40 provide statistical loads data based on the B-777-200ER’s ground operations. The ground loads data include frequency and probability information on vertical, lateral, and longitudinal accelerations during takeoff, landing, taxi, and turning operations. These loads primarily affect the landing gear and landing gear backup structure and, to a lesser

extent, the wing, fuselage, and empennage. (Statistical ground loads data for other aircraft models can be found in references 4, 6, 7, 8, 9, and 10.)

5.2.1 Lateral Load Factor Data.

This section presents lateral load factor statistical data during ground turning operations and at touchdown.

Figure C-19 presents the cumulative occurrences of maximum lateral load factor that occur per 1000 flights at touchdown. Because of the delay in the squat switch indication of touchdown and to ensure that the maximum n_y load factor peak associated with touchdown was identified, UDRI scanned an interval of 3 seconds prior to main gear squat switch closure until nose gear down to identify the maximum n_y load factor peak during touchdown. The data show that n_y peaks during the landing touchdown fall between approximately -0.3 and +0.3 g's. Comparison with the lateral load factor occurrences experienced on other aircraft, such as reported in references 6-10, show the acceleration levels recorded for the B-777-200ER are considerably higher. Comparison with the B-747-400, which exhibited the highest load factors of all referenced aircraft, the B-777-200ER shows load factors equal to 0.1 g higher than the B-747-400. It is suspected that the load factors for this aircraft recorded during touchdown are in error because, as discussed in section 4.1.1, the transfer functions and filtering techniques used are oriented towards flight conditions only and do not account for the dynamics of landing conditions.

Figure C-20 presents the peak lateral load factor and coincident incremental vertical load factor measured at touchdown (the same 3-second interval as defined above was used to identify touchdown). The same errors in the lateral load factors as discussed for figure C-19 apply to this figure.

Figure C-21 presents the cumulative frequency of the maximum lateral load factor that occurred per 1000 flights during the first turnoff from the active runway after landing. The frequencies and magnitudes of the lateral load factors experienced by the B-747-200ER compare very well with those experienced on the B-747-400. Perhaps this is not surprising considering that no major structural deflection modes are involved during ground operations and the lateral load factor is primarily a function of the ground speed and the radius of turn. The turning angles and ground speeds for these two aircraft are very similar.

Figure C-22 shows the cumulative occurrences of the maximum lateral load factor that occur during each ground turn (excludes the runway turnoff). The information is presented per 1000 flights for both pre- and postflight taxi and contains data for both left and right turns. The magnitudes of lateral load factor during taxi-in are slightly higher than during taxi-out. Data for the B-737-400, MD-82/83, B-767-200, A320, and CRJ100 aircraft, as reported in references 6, 7, 8, 9, and 10, also showed higher load factors during taxi-in. It is surmised that the lateral load factors are probably a little higher during taxi-in due to possible higher speeds associated with taxi-in. Also, figure C-22 shows no significant difference between the number of left and right turns or their magnitudes. Maximum lateral load factors experienced during ground turning for the B-777-200ER are again consistent with the load factors experienced on the B-747-400.

Figure C-23 shows the probability of the turn angle (total angular measurement) experienced during 10,047 turnoffs from the active runway. The plot indicates that turns are grouped mostly in the 25-, 90-, and 180-degree range. The scatter plots, figures C-24 through C-26, show the peak lateral load factor experienced during each turnoff versus its corresponding ground speed. The range of turn angles in each of these figures was selected to span the three turn angles, which occurred most often. The data show there is considerable variation in ground speeds during the runway turnoff. There also appears to be a correlation between speed during the turn and magnitude of the lateral load factor.

Figures C-27 through C-29 contain scatter plots showing the maximum lateral load factor at touchdown versus the yaw angle and bank angle before touchdown. Since yaw angle was not a recorded parameter, it had to be derived for each landing. This was accomplished by assuming that the calculated average magnetic heading of the aircraft on the runway after landing represented the direction of the runway. Then, the calculated difference in the aircraft heading prior to touchdown, with the magnetic heading of the aircraft on the runway after landing, resulted in the estimated yaw angle. The maximum yaw angle reflects the highest value that was calculated during an interval from -10 to -3 seconds prior to the squat switch indication of touchdown. The interval was terminated at -3 seconds prior to touchdown to ensure that the data from touchdown were not included. The mean yaw angle was determined by averaging the maximum yaw angles that occurred during the -10 to -3-second interval just prior to touchdown. At most, a minimal correlation exists between yaw angle and lateral acceleration at touchdown. The maximum bank angle reflects the maximum value recorded during the 50-second interval prior to touchdown. Again it is important to remember that the lateral load factors recorded during touchdown are of questionable accuracy.

5.2.2 Longitudinal Load Factor Data.

Longitudinal load factor statistics are presented for the pre- and postflight taxi, at touchdown, and during the landing roll phases of ground operations.

Figure C-30 presents the cumulative occurrences of longitudinal load factor during pre- and postflight taxi operations per 1000 flights. The cumulative occurrences of longitudinal load factor during taxi occur primarily due to braking and throttle changes. The magnitude of longitudinal load factors observed during taxi vary between -0.3 and +0.3 g's. The longitudinal load factors recorded appear reasonable when compared to the experience of other aircraft.

Figure C-31 shows the cumulative frequency of the maximum and minimum longitudinal load factor measured at touchdown and during the landing rollout with and without thrust reverser deployment. It appears that additional braking, which results from deployment of the thrust reversers, increases the negative longitudinal load factor spectra by approximately 0.1 g over the values seen when the thrust reversers are not in use. The maximum longitudinal load factor observed was -0.44 g, which occurred during operation of the thrust reversers. The occurrence of positive longitudinal load factors, even though very small, probably occurs due to the variations in retardation forces caused by the thrust reversers, hydraulic brakes, and rolling friction. For pre- and postflight taxi, the longitudinal load factors recorded appear reasonable when compared to the experience of other aircraft even for the touchdown condition.

5.2.3 Vertical Load Factor Data.

This section presents vertical load factor statistics during ground operations involving touchdown, taxi, and takeoff and landing roll (with and without thrust reverser), and at spoiler deployment. Also included are the aircraft's acceleration response due to operations within this operator's system.

Figure C-32 presents cumulative occurrences of incremental vertical load factor per 1000 flights for the taxi-in and taxi-out phases of ground operations. The data show that the magnitude of the incremental vertical load factor during taxi-in is higher than that for taxi-out. This slight difference was also observed on the B-737-400, MD-82/83, B-767, A320, and CRJ100 aircraft [5, 6, 7, 8, and 9]. The magnitudes of the incremental vertical load factors experienced on the B-777-200ER are also consistent with those experienced on the referenced aircraft. However, these magnitudes of the vertical accelerations are approximately twice as high as those seen for the B-747-400.

Figure C-33 presents the cumulative occurrences of positive and negative incremental vertical load factors per 1000 flights that occurred during the takeoff roll. While the magnitudes of load factor appear to be consistent with what one would expect during the takeoff roll, these values are primarily a function of the condition or roughness of the runway. With the incremental vertical load factors experienced during taxi operations, the load factors experienced during the takeoff roll agree well with those experienced on other aircraft. Again, these magnitudes of the vertical accelerations are approximately 0.1 g higher than those seen for the B-747-400.

Figure C-34 presents the cumulative occurrences of the minimum and maximum incremental vertical load factor per 1000 flights associated with touchdown and deployment of the ground spoilers. This figure shows that approximately the same minimum load factor, -0.4 g's are attributable to each event. However, at touchdown the maximum load factor was about 1.0 g's, while at spoiler deployment the maximum was around 0.6 g's. The data shows that during touchdown, high incremental vertical load factors were recorded much more frequently than recorded on any other aircraft for which UDRI has processed data. As discussed in section 4.1.1, the transfer functions and filtering techniques are oriented towards flight conditions only and do not account for the dynamics of landing conditions and how these conditions would affect the accuracy of the conversion of vertical accelerations in the same manner as the lateral accelerations.

Figure C-35 presents the cumulative occurrences of incremental vertical load factor per 1000 flights during the landing roll for operations with and without thrust reversers. These curves may also include the effects of ground spoiler usage on vertical load factor because the spoilers are normally used during the landing rollout concurrently with the thrust reversers. The frequencies of incremental vertical load factor agree quite well with the experience of other aircraft, including the B-747-400.

Figures C-36 through C-39 contain scatter plots that show the maximum incremental vertical load factor at touchdown versus the yaw angle and bank angle. The values of the yaw angle and bank angle used here are the same as those derived and used previously in figures C-27 through

C-29. Again, caution should be used in the interpretation of these plots because of the expected errors in the recorded incremental vertical load factors during touchdown.

Figure C-37 is a scatter plot that shows the maximum incremental vertical load factor versus the coincident-computed airspeed at touchdown. The negative values shown indicate that the vertical load factor response during some of the landing touchdowns were higher than the positive load factor due to landing. Again, caution should be used in the interpretation of these plots because of the expected errors in the recorded incremental vertical load factors during touchdown.

Figure C-40 compares the rms acceleration response to various runways used by the airline involved with this program. An rms value was calculated using the takeoff and landing roll vertical acceleration data from each airport. However, because of the close proximity of parallel runways at some airports and the questionable accuracy involved with presenting these data by runway, the rms data presented reflect the average of all runways used at each airport. The acceleration response provides a filtered representation of the runway roughness as determined by the landing gear characteristics. The data show that in terms of B-777-200ER acceleration response, the roughest runway location (DLC) is over twice as rough as the smoothest runway location (TER).

5.3 FLIGHT LOADS DATA.

The statistical flight loads data in this section, figures C-41 through C-86, describe the aircraft's operating gust, maneuver, and combined maneuver and gust load environment.

The gust loads data are presented in the form of incremental vertical load factors, derived gust velocity, U_{de} , and continuous gust intensity, U_{σ} . The derived gust velocity and continuous gust intensity are computed values, as described in section 4.2. Gust and maneuver incremental vertical acceleration data are plotted as either cumulative occurrences per 1,000 hours or as cumulative occurrences per nautical mile and also may be plotted by phase of flight, altitude, flap position, etc.

This section also presents the combined total vertical and lateral load factor occurrences, due to the maneuver and gust environment, presented per 1000 hours or per nautical mile by phase of flight and for vertical load factor for all flight phases combined. Cumulative occurrences of maximum lateral load factor versus gross weight are presented by phase of flight. Also, the excursion between the largest negative and highest positive load factor that occurs once per flight are paired together and presented as the ground-air-ground or (GAG) cycle data. In contrast to the significant differences seen in load factors recorded during touchdown, the load factor data recorded during flight, as discussed in the following sections, appear to be consistent with those recorded on other aircraft. This provides a further indication that the cockpit measured acceleration conversion in the ADIRU is applicable to flight conditions only.

5.3.1 Gust Vertical Load Factor Data.

Cumulative occurrences of incremental vertical gust load factor are plotted as either cumulative occurrence per 1000 hours or per nautical mile by phase of flight.

Figure C-41 shows the cumulative occurrences of incremental vertical gust load factor per 1000 hours by phase of flight, and figure C-42 shows the cumulative occurrences of incremental vertical gust load factor for all the airborne phases combined per 1000 hours. The maximum incremental vertical gust load factor encountered by the B-777-200ER was about 1.0 g and occurred, as shown in figure C-39, during the descent phase of flight.

Figure C-43 presents the cumulative occurrences of incremental vertical gust load factor per nautical mile by phase of flight. Figure C-44 shows the cumulative occurrences of incremental vertical gust load factor for all the airborne phases combined per nautical mile.

Figures C-45 and C-46 show the coincident gust acceleration and airspeed measurements for the flaps retracted and extended configurations, respectively. For the flap extended case, all flap detent positions for which data were available (1, 5, 15, 20, 25, and 30) were combined.

5.3.2 Derived Gust Velocity Data.

The magnitudes for the derived gust velocities were calculated from the measured accelerations in accordance with the procedures presented in section 4.2.4. In figures C-47 through C-54, the derived gust velocity, U_{de} , is plotted as cumulative occurrences per nautical mile for altitudes from sea level to 44,500 feet. In each figure, the derived gust velocities are compared to the gust velocity distributions presented in reference 11. The gust velocity distributions from reference 11 have been used in the past in establishing structural design criteria for repeated gust loads. These comparisons must be interpreted with caution. The derived gust velocities are based on lift-curve slope values calculated from an empirical formula, as shown in section 4.2.4. This lift-curve slope equation provides estimates of the rigid wing lift-curve slope as a function of Mach number. The rigid estimates are quite acceptable up to Mach numbers of 0.7. However, at Mach numbers above approximately 0.75 Mach the accuracy deteriorates rapidly. In addition, flexibility effects on the lift-curve slope, which are not accounted for in the equation, can be significant at higher dynamic pressures. Consequently, the derived gust velocities may contain significant errors, particularly at the lower altitudes where flexibility effects would be more prominent.

Figures C-55 and C-56 present derived gust velocity, U_{de} , per nautical mile for the flaps extended and retracted conditions, respectively.

5.3.3 Continuous Gust Intensity Data.

The magnitudes of the continuous gust intensities, U_{σ} , were derived from the measured accelerations in accordance with the procedures presented in section 4.2.5. The cumulative occurrences of continuous gust intensity per nautical mile for the flaps extended and the flaps retracted conditions are presented in figures C-57 and C-58, respectively.

5.3.4 Maneuver Vertical Load Factor Data.

The maneuver loads data are presented in the form of incremental vertical load factors, either per 1000 hours or per nautical mile by phase of flight and altitude, or as combined phases.

Figures C-59 through C-63 provide the cumulative occurrences of incremental maneuver load factor per 1000 hours by altitude for each of the airborne flight phases, i.e., departure, climb, cruise, descent, and approach.

Figures C-64 through C-68 display the cumulative occurrences of incremental maneuver load factor by altitude per nautical mile (instead of per 1000 hours) in the airborne phases of flight.

Figure C-69 shows the total cumulative occurrences of incremental maneuver load factor per 1000 hours for each phase of flight, regardless of altitude. Figure C-70 contains the total cumulative occurrences of incremental maneuver load factor per 1000 hours for all flight phases combined.

Figure C-71 shows the total cumulative occurrences of incremental maneuver load factor per nautical mile for each phase of flight regardless of altitude. Figure C-72 contains the total cumulative occurrences of incremental maneuver load factor per nautical mile for all flight phases combined.

The maximum incremental vertical maneuver load factor encountered by the B-777-200ER was 0.8 g and occurred during the descent and cruise phases of flight. However, the occurrences during the descent phase were approximately six times more frequent. The most negative load factor encountered was -1.4 g's and also occurred during the descent phase.

Figures C-73 and C-74 show the coincident maneuver acceleration and speed measurements for the flaps retracted and extended, respectively. As with the gust loads, all flap detent positions for which data were available (1, 5, 10, 20, 25, and 30) were combined.

5.3.5 Combined Maneuver and Gust Vertical Load Factor Data.

Figure C-75 shows the cumulative occurrences of the combined maneuver and gust incremental vertical load factor per 1000 hours by phases of flight. Figure C-76 shows the incremental vertical load factor occurrences for all flight phases combined.

Figures C-77 and C-78 contain the same vertical load factor data as figures C-75 and C-76, but are plotted as occurrences per nautical mile by phases of flight and for all flight phases combined. The highest positive 1.0-g incremental load factor encountered during the descent phase of flight results from a gust encounter while the most negative load factor of -1.5 g's is associated with a maneuver.

5.3.6 Combined Maneuver and Gust Lateral Load Factor Data.

Figure C-79 presents the cumulative occurrences of lateral load factor per 1000 hours by phase of flight. Maximum lateral load factor values between approximately -0.36 and +0.22 g were observed during flight operations of the B-777-200ER. In general, the departure phase resulted in the highest level of lateral load factor occurrences, with the approach phase a close second.

Figures C-80 through C-84 contain scatter plots that show the maximum lateral load factor versus the coincident gross weight of the aircraft during airborne phases of flight. It is interesting to observe the reduction in the maximum gross weight at which points are plotted

when viewing the scatter plots from departure to approach. This is, of course, consistent with fuel consumption during the flights.

5.3.7 Ground-Air-Ground Cycle Data.

Figures C-85 and C-86 display occurrences of the maximum and minimum incremental vertical load factor that occurs once per flight. The load excursion between the largest negative and highest positive load factor is often referred to by aircraft design engineers as the ground-air-ground or GAG cycle. Figure C-85 presents the number of GAG cycle occurrences in tabular form, and figure C-86 shows the number of GAG cycle occurrences plotted as a three-dimensional bar chart. The GAG cycle usually contributes the most damaging fatigue cycle experienced by the aircraft wing and carry through structural assemblies. The GAG cycle that contained the widest range between incremental negative and positive values occurred was between -1.45 and +0.80 g's.

5.4 SYSTEMS OPERATIONAL DATA.

This section contains operational usage data for the flaps, thrust reversers, and the propulsion system. Although control surface position information was available for the aileron, rudder, and elevator systems, it was not processed because the sampling rates were deemed to be too slow to provide reliable statistical usage information for these components.

5.4.1 Flap Usage Data.

Flap usage data showing airspeed and percent of time spent by flap detent and phase of flight are presented in this section. These data can be used to characterize the sources of repeated loads on the flaps and backup structure and other flap components. The B-777-200ER flap operational speed limits for each detent setting were listed in table 6.

Figures C-87 and C-88 present the probability of the maximum airspeed encountered in various flap detents during the departure phase of flight. Figures C-89 and C-90 present similar probability data for the approach phase of flight. Figure C-90 shows that the most probable speed at which the flaps are first deployed during the approach phase of flight for detent 5 occurs at about 200 knots, for detent 15 about 180 knots, for detent 20 about 160 knots, detents 25 and 30 about 155 knots.

Figures C-91 and C-92 present the percent of time spent in each flap detent setting during the departure and approach phases of flight, respectively. Flap detents 01 and 05 are the most frequently used setting during the departure phase (23.56% and 68.8 % of the time, respectively), while flap detents 05 (33.94%) and 30 (30.49%) are the most often used settings during the approach phase.

5.4.2 Thrust Reverser Data.

The times and speeds associated with thrust reverser operations were derived from the measured data. Figure C-93 presents the cumulative probability of time during which the thrust reversers are deployed. The data show that for 90% of the flights, the thrust reversers are deployed for

approximately less than 50 seconds. Figure C-94 presents the cumulative probability of the speed at the time the thrust reversers were deployed and stowed. Most (90% or more) thrust reverser deployment cycles begin at speeds between 115 and 150 knots. Approximately 92% of the time, the thrust reversers are stowed at speeds below 50 knots. Thrust reverser data was available for 1262 flights of the 10,046 flights processed for this report. During these flights, the reversers were used during 1182 flights, or approximately 94% of the flights for which data was available.

5.4.3 Propulsion Data.

Figure C-95 presents the cumulative probability of the maximum engine fan speed N_1 during takeoff, at the instant of thrust reverser deployment during the landing roll, and during the time that the thrust reverser is deployed. Most takeoffs occur at fan speed values ranging greater than 80%. The fan speed at thrust reverser deployment ranges between 40% and approximately 50% and then increases up to a maximum value of over 75% during the time the thrust reverser is deployed.

6. CONCLUSIONS.

This report provides valuable information about how the Boeing 777-200ER aircraft are being used during normal flight and ground operations by the airline.

The participating airline fully supported this program and provided the University of Dayton Research Institute (UDRI) with 10,047 flights, representing 67,000 flight hours and 30.5 million nmi of useable B-777-200ER data from typical revenue flights. Except for some gaps and repeated frames, the recorded data were acceptable and compatible with UDRI's data processing software. The 10,047 flights were judged as sufficient to provide a representative statistical baseline of the aircraft's ground, airborne, and systems operational usage.

The 95 statistical data formats presented in this report provide the Federal Aviation Administration (FAA), airline, and aircraft manufacturer with beneficial information about the B-777-200ER's actual operational service usage.

The B-777-200ER exceeds a flight length of 3000 nautical miles (nmi) on approximately 50% of the flights. Comparison with data from the B-767-200ER, an extended range aircraft, shows a 3000 nmi flight length on approximately 90% of the flights.

Lateral load factors during ground turning are lower than observed on previous smaller aircraft such as the B-767-200ER, A320, B-737-400, and the MD-82. The lateral load factors are comparable to those encountered on the B-747-400. A comparison of the lateral load factors frequency distributions seen on the B-777-200ER with those previously seen on the above-mentioned aircraft makes it clear that there is an inverse relationship between the lateral load factor during ground turning and airplane size.

Longitudinal load factors during taxi operations are slightly lower for the B-777-200ER than were measured on either the B-767-200ER or the A320. The longitudinal load factors during touchdown and landing roll are also lower when compared to the other aircraft.

Vertical load factors during taxi operations, takeoff roll, and landing roll are slightly lower for the B-777-200ER than for the B-767-200ER or the A320. In contrast, the vertical load factors at touchdown appear to be slightly higher.

Vertical gust load factors and maneuver load factors extracted from the vertical load factor measurements for the B-777-200ER are not significantly different from the B-767-200ER and the A320.

The derived gust velocities for the B-777-200ER were calculated using lift-curve slope values based on an empirical formula for a rigid wing. In contrast, the derived gust velocities published in prior loads data reports were calculated using flexible airplane lift-curve slope data from the aircraft manufacturer. Therefore, comparisons of the B-777-200ER derived gust velocities with those published in previously referenced reports are subject to misinterpretation.

The installation of acceleration sensors in the cockpit rather than near the center of gravity is a deviation, albeit approved by the appropriate airworthiness authorities, from the Federal Aviation Regulation specifications. The transfer functions and filtering techniques used in the transfer of the sensed accelerations at the cockpit to those expected at the center of gravity are oriented towards flight conditions. As a result, the aircraft dynamics experienced during landing conditions are not properly accounted for and the recorded accelerations for these conditions will include unknown errors. These errors were clearly manifested in the vertical and lateral load factors recorded for the touchdown condition when comparing the B-777-200ER load factors with those of other aircraft. This is of particular concern if vertical load factors recorded during touchdown were to be used by the airlines for routine hard landings identification or by the National Transportation Safety Board in landing accident investigations. In such cases, the use of the recorded values would be very questionable. It is recommended that a task be considered that will install a center of gravity accelerometer in one airplane and record both the converted and direct measured accelerations to determine the extent of the differences that may exist. Perhaps some airline might be willing to consider such a task on one airplane for a few hundred hours to at the very least resolve any hard landing concerns.

7. REFERENCES.

1. de Jonge, J.B., "Reduction of Incremental Load Factor Acceleration Data to Gust Statistics," DOT/FAA/CT-94/57, August 1994.
2. Anonymous, USAF Stability and Control DATCOM," Flight Control Division, Air Force Flight Dynamics Laboratory, Wright-Patterson Air Force Base, Ohio, October 1960, revised April 1976.
3. Hoblit, Frederic M., et al., "Development of a Power Spectral Gust Design Procedure for Civil Aircraft," Technical Report FAC-ADS-53, 1966.
4. Tipps, Daniel O., Rustenburg, John W., and Skinn, Donald A., "Study of Side Load Factor Statistics from Commercial Aircraft Ground Operations," University of Dayton Research Institute report UDR-TR-2001-00005, January 2001.

5. Rustenburg, John W., Skinn, Donald A., and Tipps, Daniel O., "An Evaluation of Methods to Separate Maneuver and Gust Load Factors from Measured Acceleration Time Histories," FAA report DOT/FAA/AR-99/14, April 1999.
6. Rustenburg, John, Skinn, Donald, and Tipps, Daniel O., "Flight Loads Data for a Boeing 737-400 in Commercial Operation," FAA report DOT/FAA/AR-98/28, August 1998.
7. Skinn, Donald, Tipps, Daniel O., and Rustenburg, John, "Flight Loads Data for a MD-82/83 in Commercial Operation," FAA report DOT/FAA/AR-98/65, February 1999.
8. Tipps, Daniel O., Rustenburg, John W., and Skinn, Donald A., "Statistical Loads Data for B-767-200 Aircraft in Commercial Operation," FAA report DOT/FAA/AR-00/10, March 2000.
9. Rustenburg, John W., Skinn, Donald A., and Tipps, Daniel O., "Statistical Loads Data for the Airbus A-320 Aircraft in Commercial Operations," FAA report DOT/FAA/AR-02/35, April 2002.
10. Rustenburg, John W., Skinn, Donald A., and Tipps, Daniel O., "Statistical Loads Data for Bombardier CRJ100 Aircraft in Commercial Operations," FAA report DOT/FAA/AR-03/44, June 2003.
11. Press, Harry and Steiner, Roy, "An Approach to the Problem of Estimating Severe and Repeated Gust Loads for Missile Operations," National Advisory Committee for Aeronautics Technical Note 4332, Langley Aeronautical Laboratory, Langley Field, VA, September 1958.

APPENDIX A—BOEING 777 CENTER OF GRAVITY TRANSFER EQUATIONS

The Boeing 777 Air Data Inertial Reference Unit calculates center of gravity (c.g.) accelerations using the following equations

$$\begin{aligned}\alpha_{cgx} &= \alpha_{bx} + \omega_{by}^2 l_{xa} + \omega_{bz}^2 l_{xa} \\ \alpha_{cgy} &= \alpha_{by} - \omega'_{bz} l_{xa} - \omega_{bx} \omega_{by} l_{xa} \\ \alpha_{cgz} &= \alpha_{bz} + \omega'_{by} l_{xa} - \omega_{bx} \omega_{bz} l_{xa}\end{aligned}$$

where

- α_{cgx} : c.g. acceleration in the x axis
- α_{cgy} : c.g. acceleration in the y axis
- α_{cgz} : c.g. acceleration in the z axis
- α_{bx} : body acceleration in the x axis
- α_{by} : body acceleration in the y axis
- α_{bz} : body acceleration in the z axis
- ω_{bx} : body angular rate in the x axis
- ω_{by} : body angular rate in the y axis
- ω_{bz} : body angular rate in the z axis
- ω'_{by} : angular acceleration in the y axis
- ω'_{bz} : angular acceleration in the z axis
- l_{xa} : the distance from the ADIRU to the Airplane c.g.

α_{cgx} , α_{cgy} , and α_{cgz} are filtered with a second-order, 4-Hz Butterworth filter. They are further filtered with a notch filter to account for the first longitudinal body bending mode (18 rad/sec).

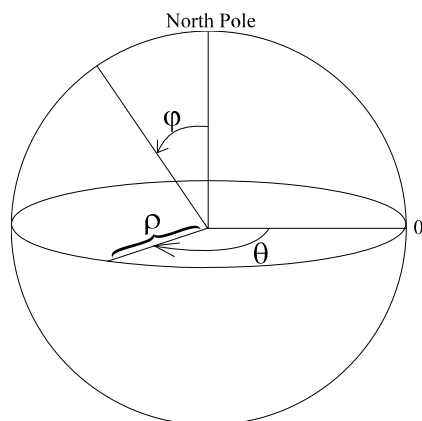
Final c.g. parameters are calculated as

$$\begin{aligned}\alpha_{cglong} &= \alpha_{cgfx} \\ \alpha_{cglat} &= \alpha_{cgfy} \\ \alpha_{cgnorm} &= -\alpha_{cgfz} - g\end{aligned}$$

where

- α_{cglong} : longitudinal cg acceleration
- α_{cglat} : lateral cg acceleration
- α_{cgnorm} : the normal cg acceleration
- α_{cgfx} : filtered cg acceleration in the x axis
- α_{cgfy} : filtered cg acceleration in the y axis
- α_{cgfz} : filtered cg acceleration in the z axis
- g : gravity

APPENDIX B—GREAT CIRCLE DISTANCE CALCULATION



Given:

Latitude and Longitude
of Departure and
Destination Airports

ρ = distance from center
 ϕ = angle from North Pole
 θ = angle E/W of prime meridian

Procedure: (see sketch)

The standard mathematical system for spherical coordinates is shown where three variables specify location: ρ , ϕ , and θ .

Let

a = Great Circle Distance in angular measure

Latitude is measured away from the Equator (0°) to the North Pole ($+90^\circ$) and the South Pole (-90°); whereas in the standard spherical coordinate system, the North Pole, Equator, and South Pole lie at 0° , 90° , and 180° , respectively. Therefore

$$\phi = 90^\circ - \text{latitude}$$

transforms latitude readings into equivalent angles (ϕ) in the standard spherical coordinate system.

Then

$$\begin{aligned} b &= 90^\circ - \text{Latitude}_{\text{Dep}} \\ c &= 90^\circ - \text{Latitude}_{\text{Des}} \end{aligned}$$

where b and c are values of ϕ for the departure and destination locations, respectively.

Longitude is measured away from the prime meridian (0°). Longitudes to the east are positive and to the west negative. However, the standard spherical coordinate system measures its angles in the opposite direction. Therefore

$$\theta = - \text{longitude}$$

transforms longitude readings into equivalent angles (θ) in the standard spherical coordinate system.

Then

$$\begin{aligned} A &= (-\text{Longitude}_{\text{Des}}) - (-\text{Longitude}_{\text{Dep}}) \\ &= \text{Longitude}_{\text{Dep}} - \text{Longitude}_{\text{Des}} \end{aligned}$$

where A is the value of θ between the departure and destination locations.

The following equation, based on the spherical coordinate system, allows the computation of the Great Circle Distance, a . (Law of cosines for oblique spherical triangles)

$$\cos a = \cos b \cos c + \sin b \sin c \cos A$$

Substituting for b , c , and A from the above equalities

$$\begin{aligned} \cos a &= \cos (90^\circ - \text{Lat}_{\text{Dep}}) \cos (90^\circ - \text{Lat}_{\text{Des}}) \\ &+ \sin (90^\circ - \text{Lat}_{\text{Dep}}) \sin (90^\circ - \text{Lat}_{\text{Des}}) \cos (\text{Lon}_{\text{Dep}} - \text{Lon}_{\text{Des}}) \end{aligned}$$

Since

$$\begin{aligned} \cos (90^\circ - \text{Lat}_{\text{Dep}}) &= \sin \text{Lat}_{\text{Dep}} \\ \cos (90^\circ - \text{Lat}_{\text{Des}}) &= \sin \text{Lat}_{\text{Des}} \\ \sin (90^\circ - \text{Lat}_{\text{Dep}}) &= \cos \text{Lat}_{\text{Dep}} \\ \sin (90^\circ - \text{Lat}_{\text{Des}}) &= \cos \text{Lat}_{\text{Des}} \end{aligned}$$

by replacement one obtains

$$\cos a = \sin (\text{Lat}_{\text{Dep}}) \sin (\text{Lat}_{\text{Des}}) + \cos (\text{Lat}_{\text{Dep}}) \cos (\text{Lat}_{\text{Des}}) \cos (\text{Lon}_{\text{Des}} - \text{Lon}_{\text{Dep}})$$

Thus, a , the angular measure of the great circle arc connecting the departure and destination locations, is obtained as

$$a = \cos^{-1} [\sin (\text{Lat}_{\text{Dep}}) \sin (\text{Lat}_{\text{Des}}) + \cos (\text{Lat}_{\text{Dep}}) \cos (\text{Lat}_{\text{Des}}) \cos (\text{Lon}_{\text{Des}} - \text{Lon}_{\text{Dep}})]$$

So, for a expressed in radians

$$GCD = a \text{ radians} \left(\frac{180 \text{ deg.}}{\pi \text{ radians}} \right) \left(\frac{60 \text{ min.}}{1 \text{ deg.}} \right) \left(\frac{1 \text{ nmi}}{1 \text{ min.}} \right) = \left(\frac{10800a}{\pi} \right) \text{ nmi}$$

and for a expressed in degrees,

$$GCD = a \text{ degrees} \left(\frac{60 \text{ min.}}{1 \text{ deg.}} \right) \left(\frac{1 \text{ nmi}}{1 \text{ min.}} \right) = 60a \text{ nmi}$$

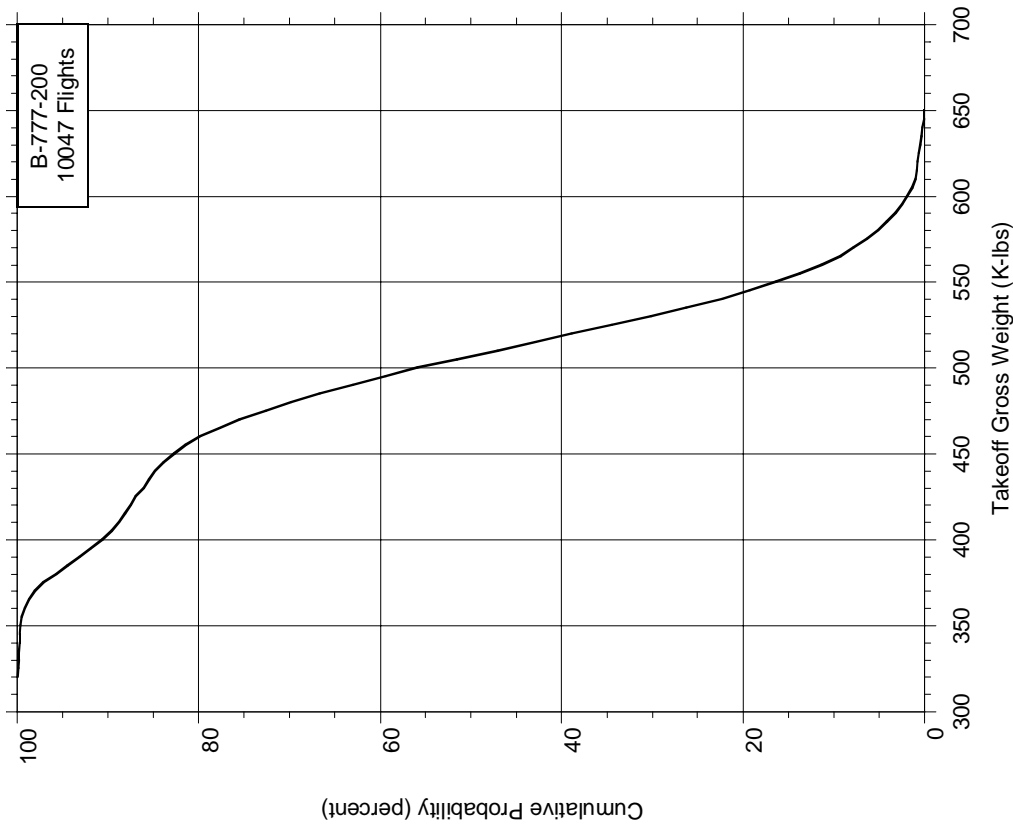


Figure C-1. Cumulative Probability of Takeoff Gross Weight

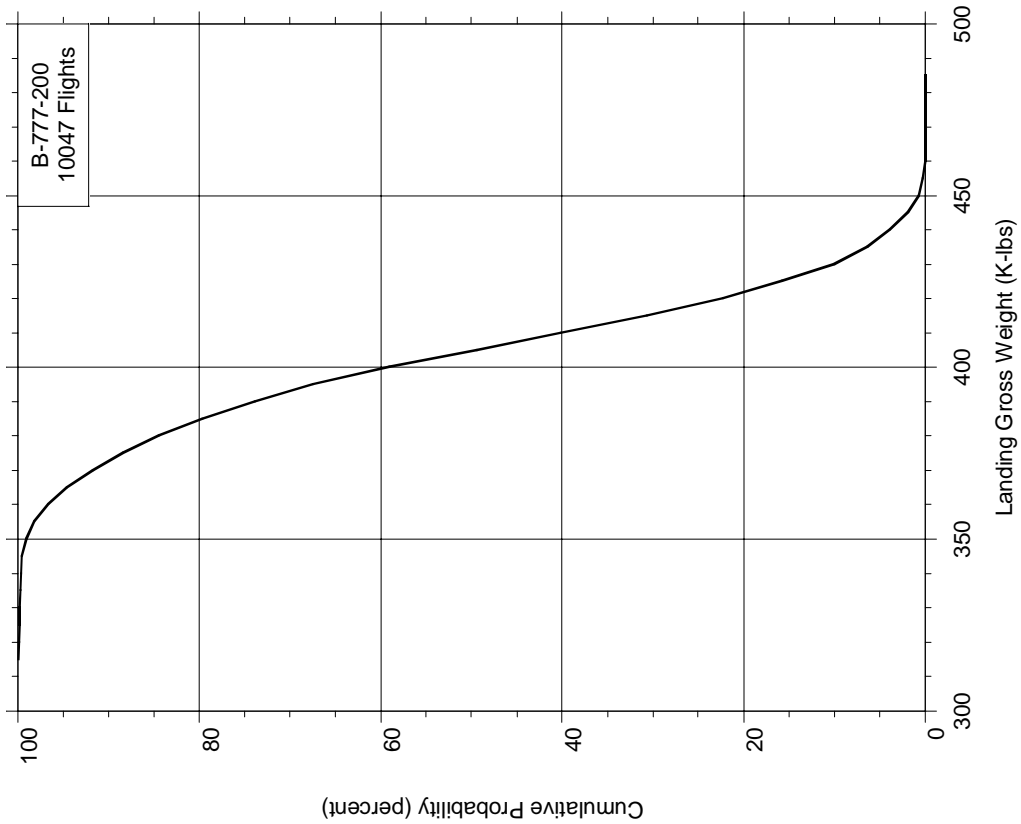


Figure C-2. Cumulative Probability of Landing Gross Weight

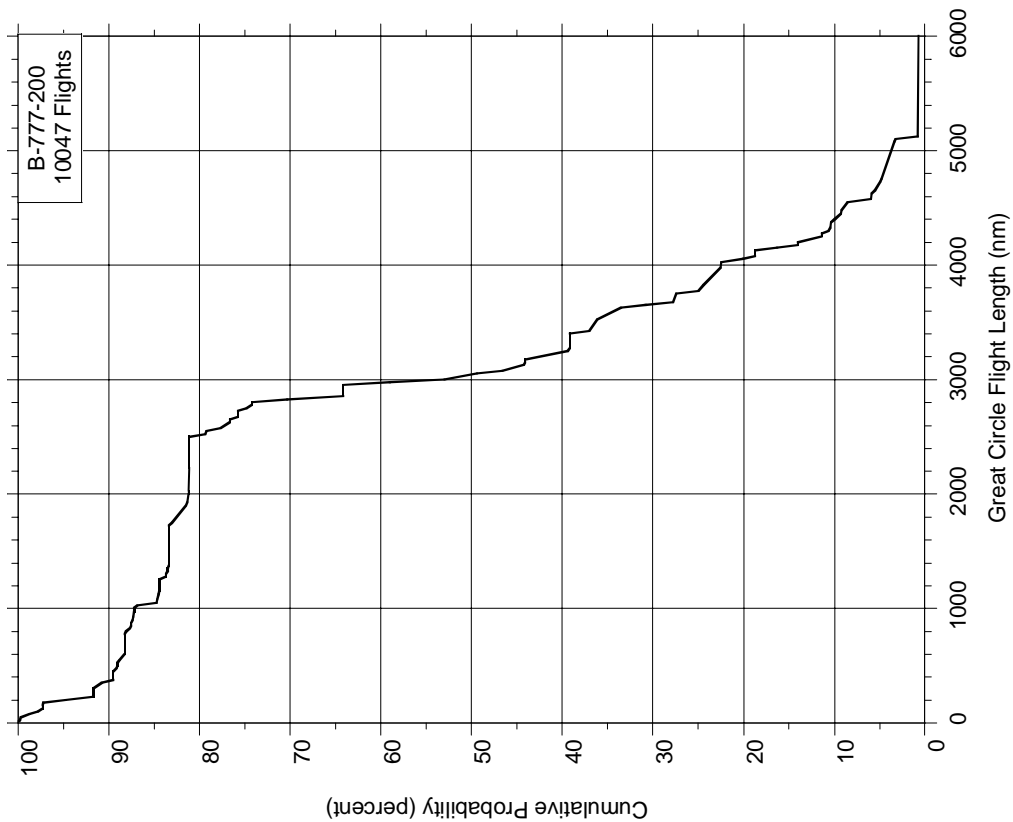


Figure C-3. Cumulative Probability of Great Circle Flight Length

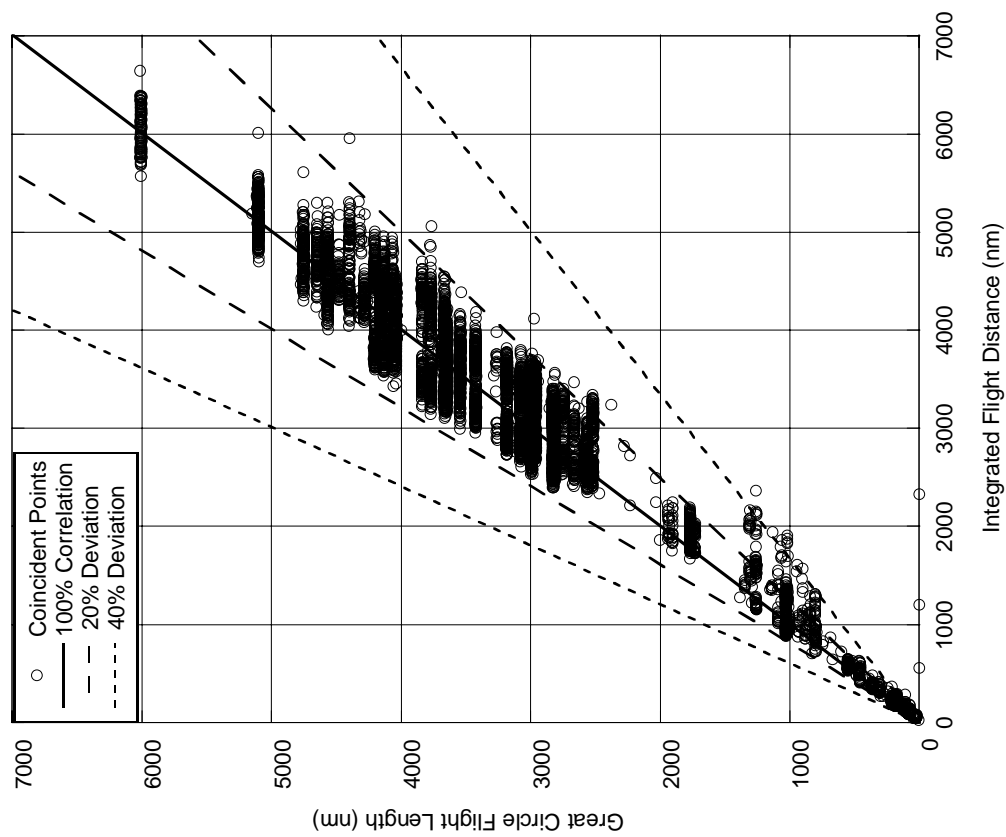


Figure C-4. Correlation of Great Circle Flight Length and Integrated Flight Distance

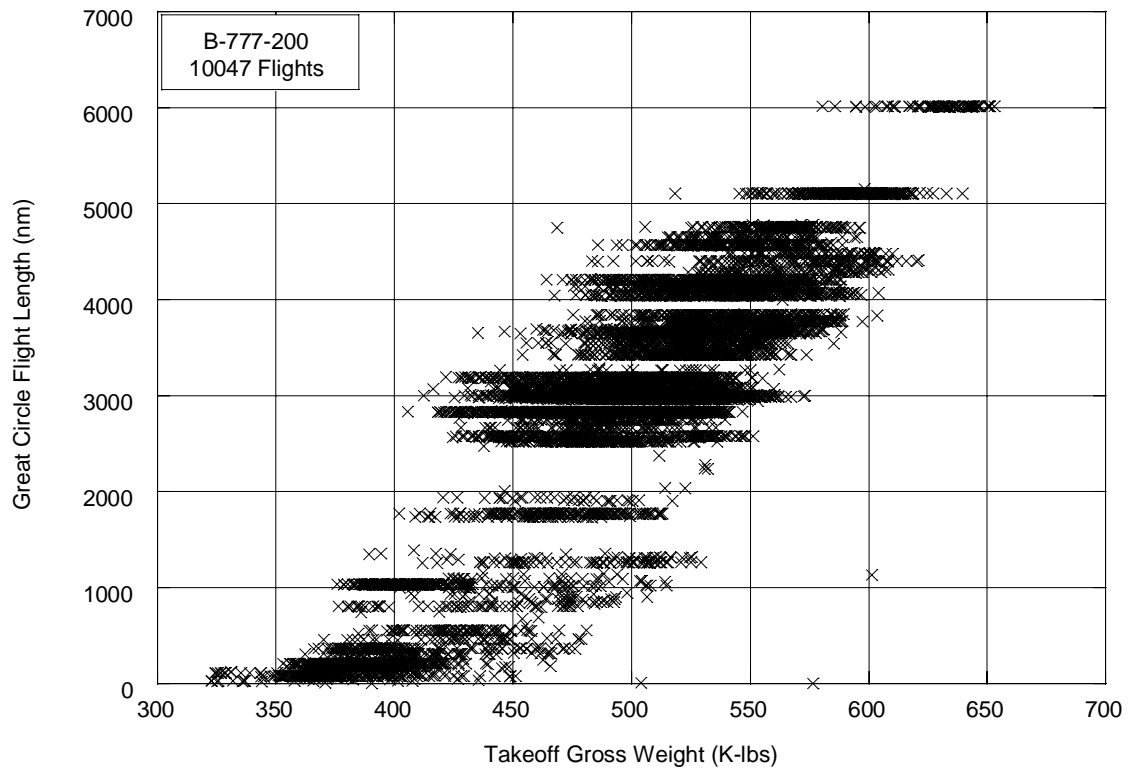


Figure C-5. Correlation of Takeoff Gross Weight and Great Circle Flight Length

Takeoff Gross Weight (K-lbs)										
Great Circle Flight Length (nm)	"10047Flts"	300-350	350-400	400-450	450-500	500-550	550-600	600-650	650-700	Total
	0- 500	0.27	7.98	2.36	0.29	0.01	0.01			10.92
	500-1000		0.25	1.05	0.56	0.01				1.87
	1000-1500		0.85	1.67	0.77	0.43		0.01		3.72
	1500-2000			0.50	1.44	0.20				2.14
	2000-2500			0.02		0.06				0.08
	2500-3000			1.65	14.67	11.42	0.31			28.05
	3000-3500			0.65	6.83	8.83	0.40			16.70
	3500-4000			0.02	1.27	9.09	3.46	0.01		13.85
	4000-4500				0.93	7.26	5.50	0.31		13.99
	4500-5000				0.04	2.20	2.98			5.22
	5000-5500					0.04	1.74	0.84		2.62
	5500-6000									
	6000-6500						0.05	0.74	0.05	0.84
Total	0.27	9.08	7.92	26.79	39.53	14.45	1.90	0.05	100.00	

Figure C-6. Correlation of Takeoff Gross Weight and Great Circle Flight Length, Percent of Flights

Takeoff Gross Weight (K-lbs)										
Landing Gross Weight (K-lbs)	10047 Flts	300-350	350-400	400-450	450-500	500-550	550-600	600-650	650-700	Total
	300-350	0.27	0.39	0.14	0.03					0.83
	350-400		8.69	5.69	17.88	7.37	0.48			40.11
	400-450			2.09	8.74	31.79	13.81	1.84	0.05	58.33
	450-500				0.15	0.37	0.16	0.06		0.74
	Total	0.27	9.08	7.92	26.79	39.53	14.45	1.90	0.05	100.00

Figure C-7. Correlation of Takeoff and Landing Gross Weight, Percent of Flights

		Integrated Flight Distance (nm)						
Altitude Band (feet)	10047 Flts	0-1000	1000-2000	2000-3000	3000-4000	4000-5000	5000-6000	6000-7000
	39500-44500	6.83	15.60	18.72	9.10	3.16	2.08	0.58
	29500-39500	31.37	67.76	72.45	82.81	90.92	92.86	94.97
	19500-29500	26.87	7.94	3.34	3.31	2.50	2.27	1.93
	9500-19500	18.07	4.32	2.84	2.58	1.90	1.55	1.24
	4500-9500	8.73	2.34	1.63	1.30	0.94	0.81	0.74
	1500-4500	6.27	1.56	0.76	0.69	0.44	0.35	0.42
	500-1500	1.26	0.32	0.17	0.14	0.09	0.06	0.08
	0-500	0.60	0.16	0.08	0.06	0.04	0.03	0.04
	Total	100.00	100.00	100.00	100.00	100.00	100.00	100.00

Figure C-8. Percent of Integrated Flight Distance in Altitude Bands

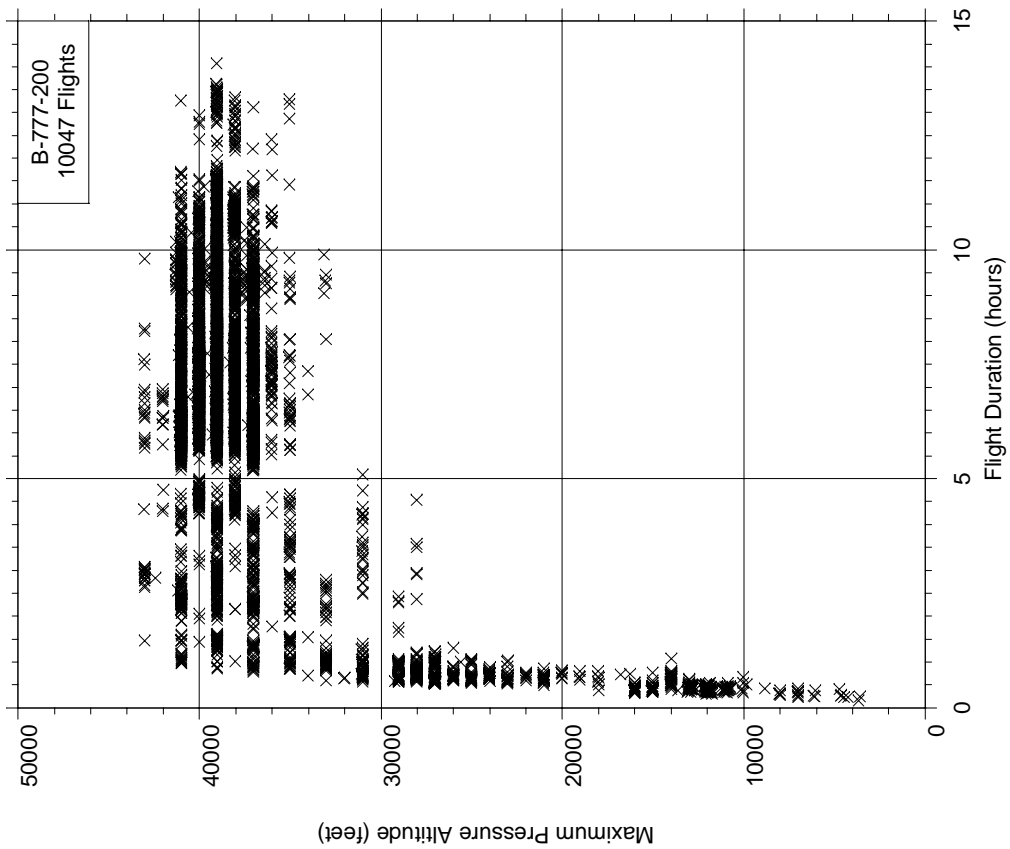


Figure C-9. Correlation of Maximum Altitude and Flight Duration

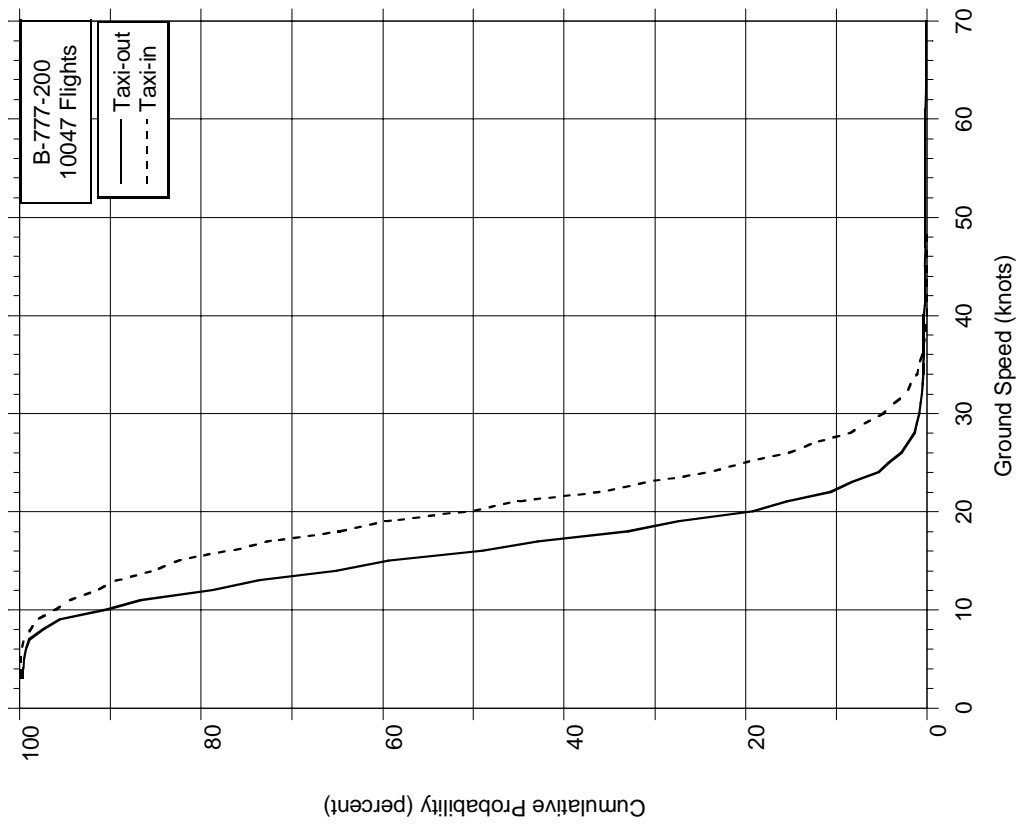


Figure C-10. Cumulative Probability of Maximum Ground Speed During Taxi

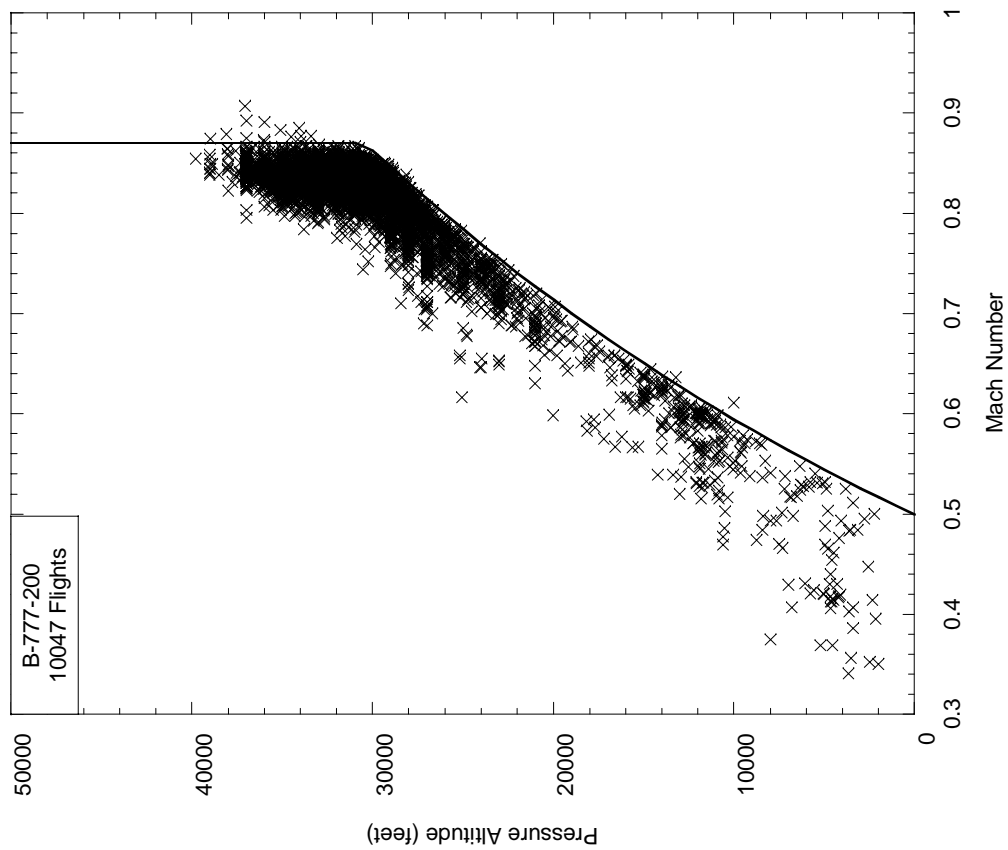


Figure C-11. Maximum Mach Number and Coincident Altitude,
all Flight Phases

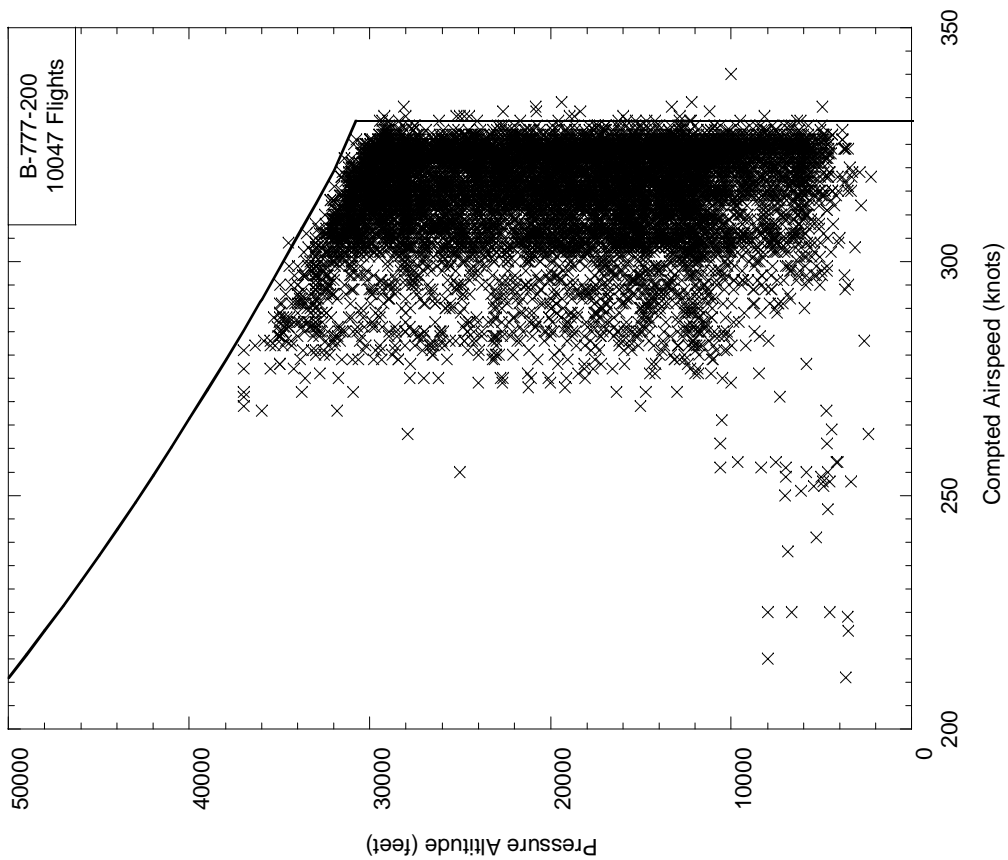


Figure C-12. Maximum Computed Airspeed and Coincident
Altitude, all Flight Phases

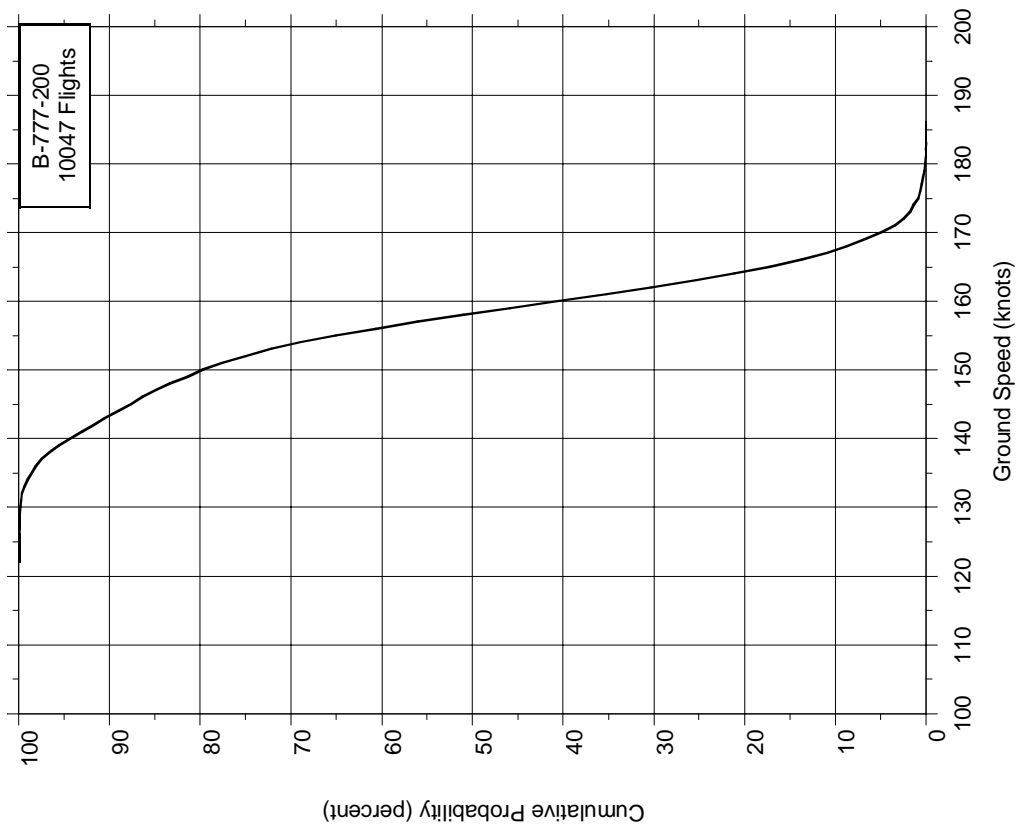


Figure C-13. Cumulative Probability of Ground Speed at Liftoff

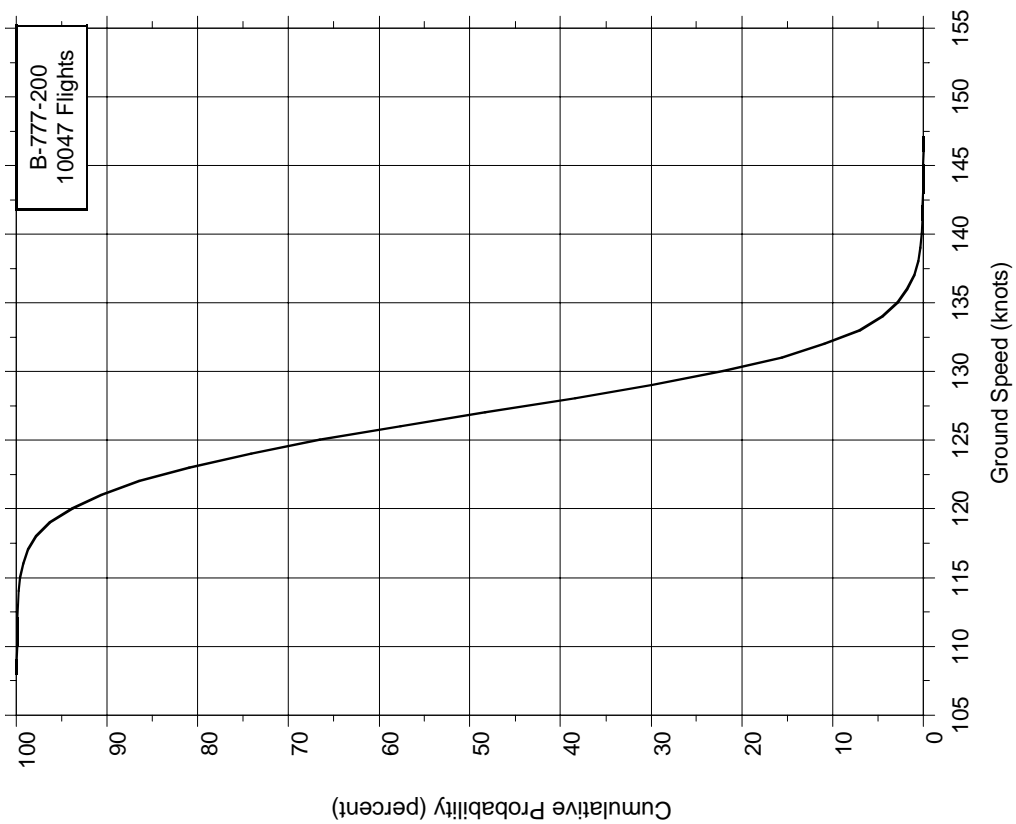


Figure C-14. Cumulative Probability of Ground Speed at Touchdown

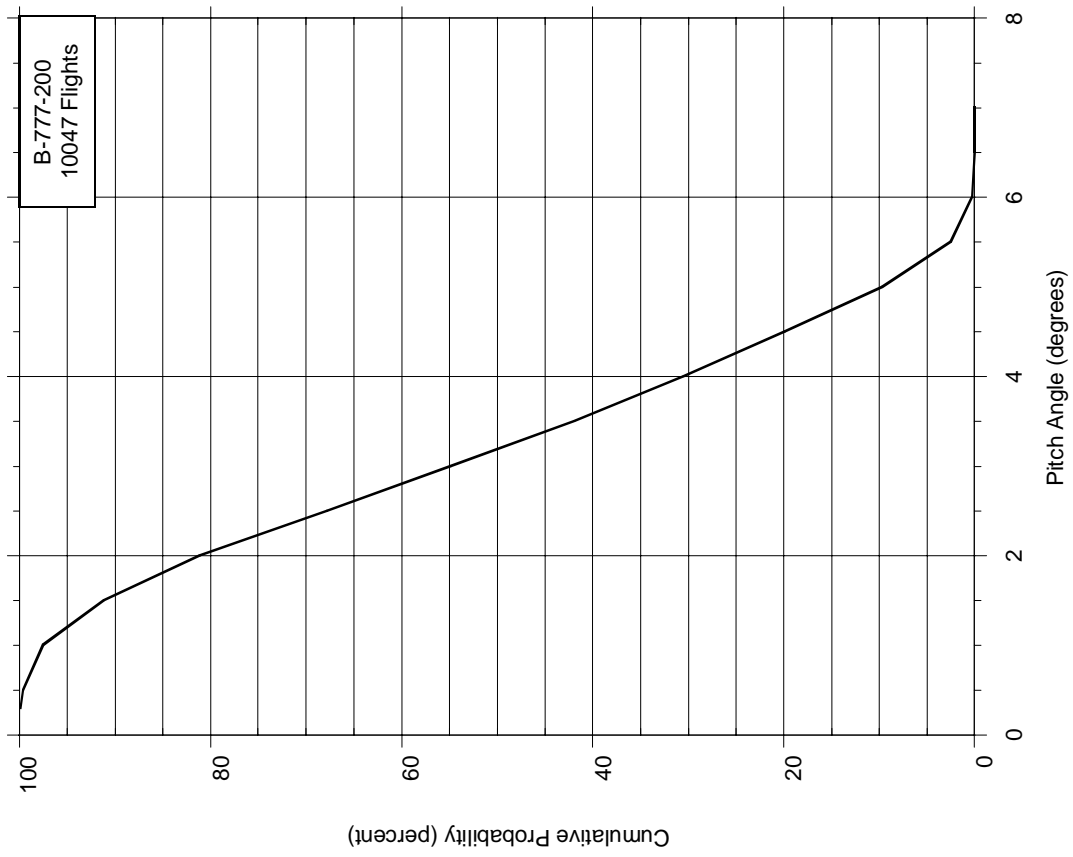


Figure C-15. Cumulative Probability of Pitch Angle at Liftoff

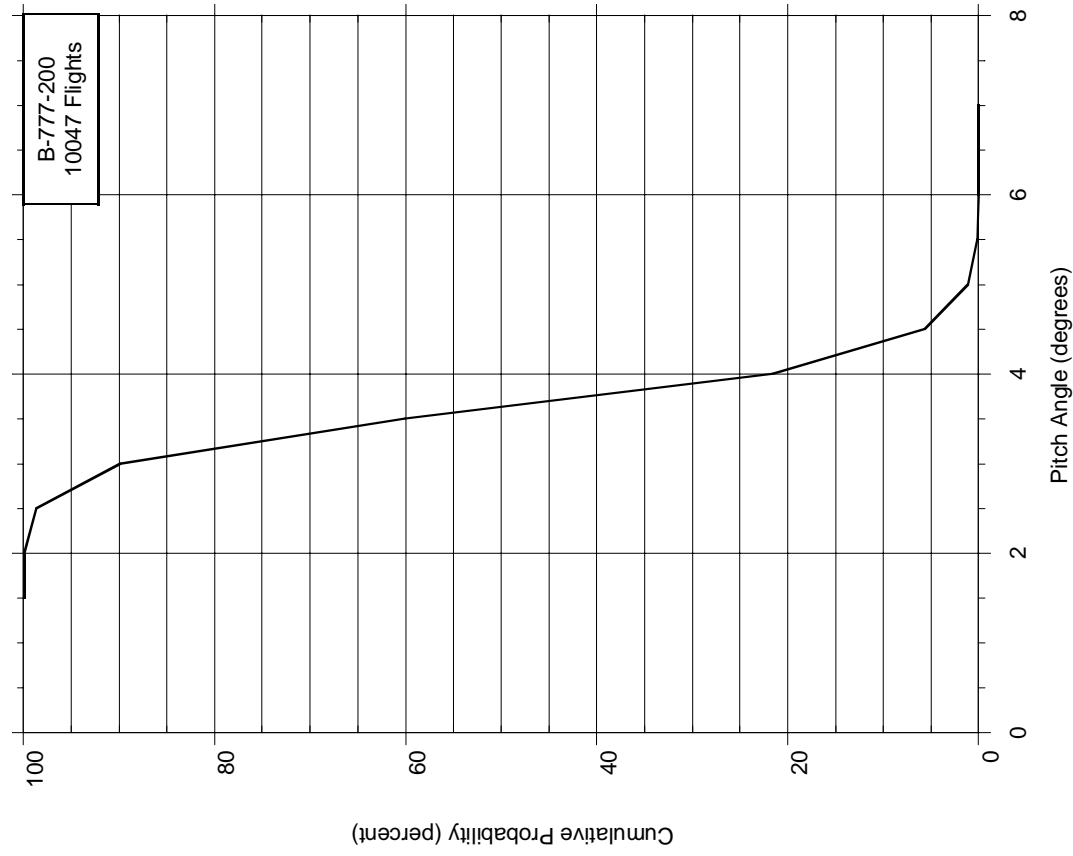


Figure C-16. Cumulative Probability of Pitch Angle at Touchdown

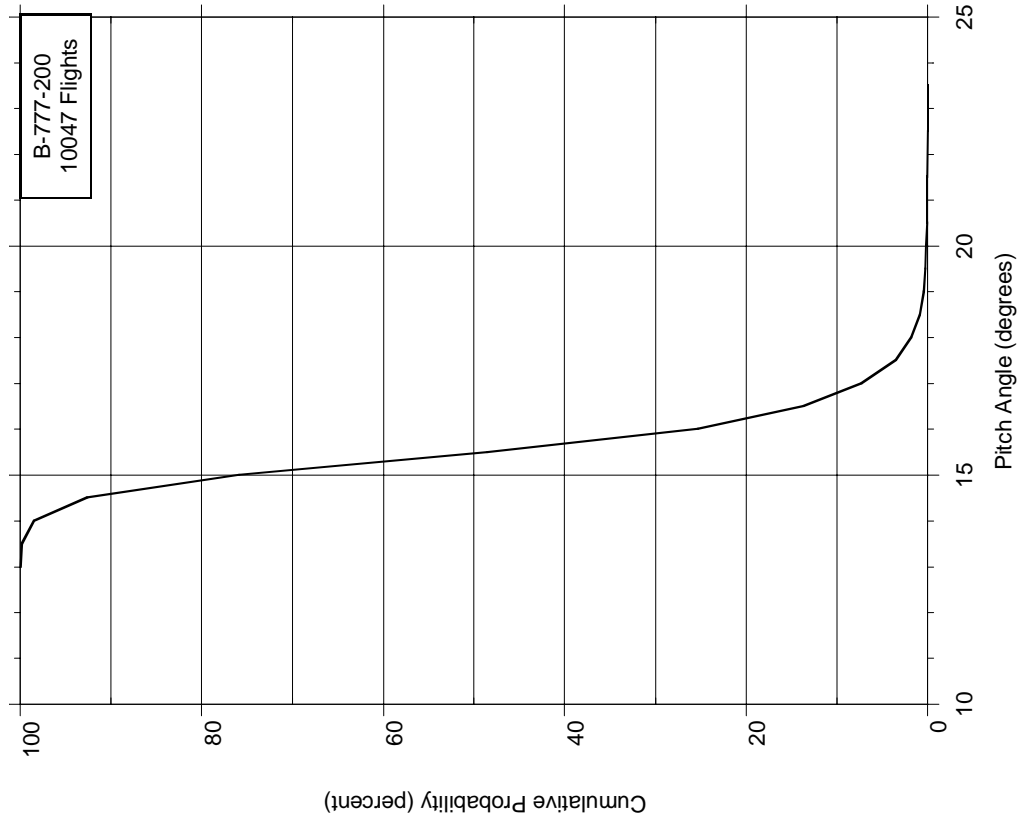


Figure C-17. Cumulative Probability of Maximum Pitch Angle During Departure

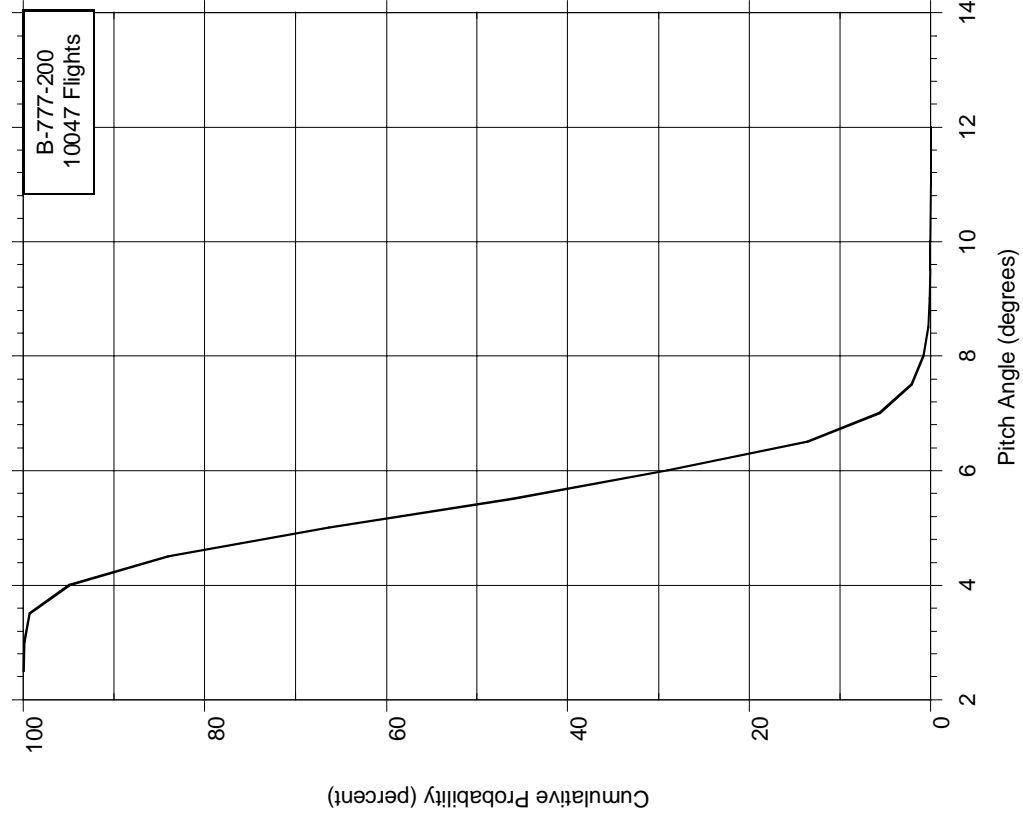


Figure C-18. Cumulative Probability of Maximum Pitch Angle During Approach

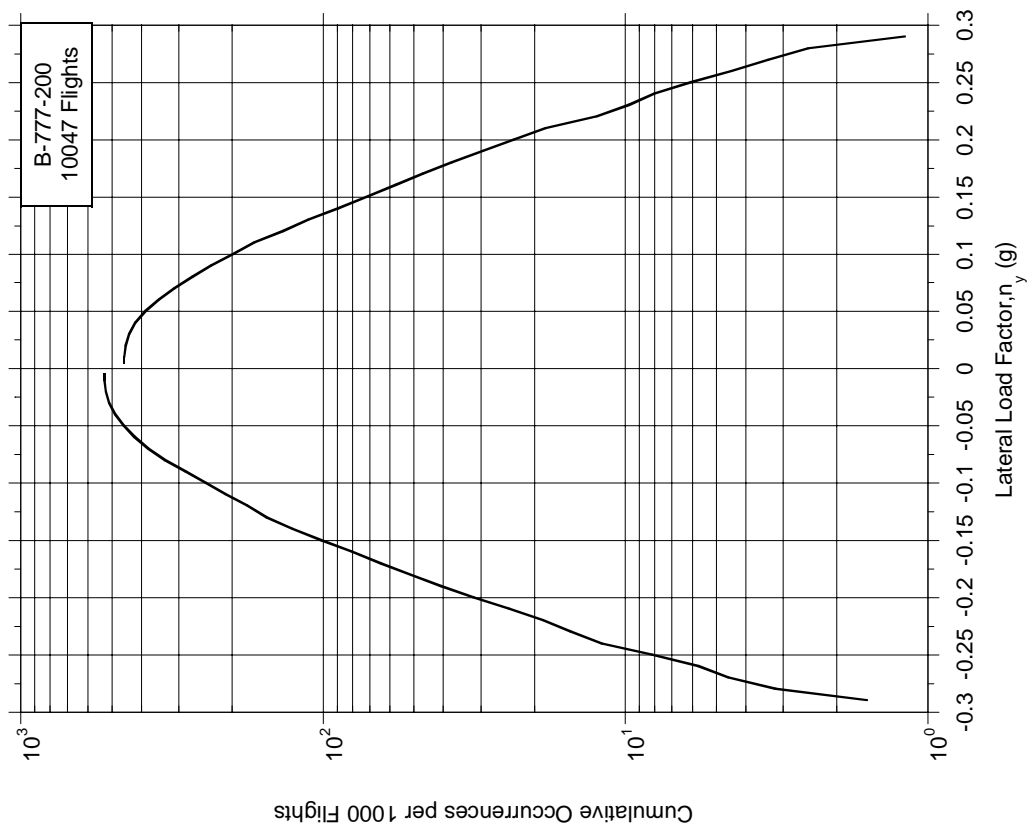


Figure C-19. Cumulative Frequency of Maximum Lateral Load Factor at Touchdown

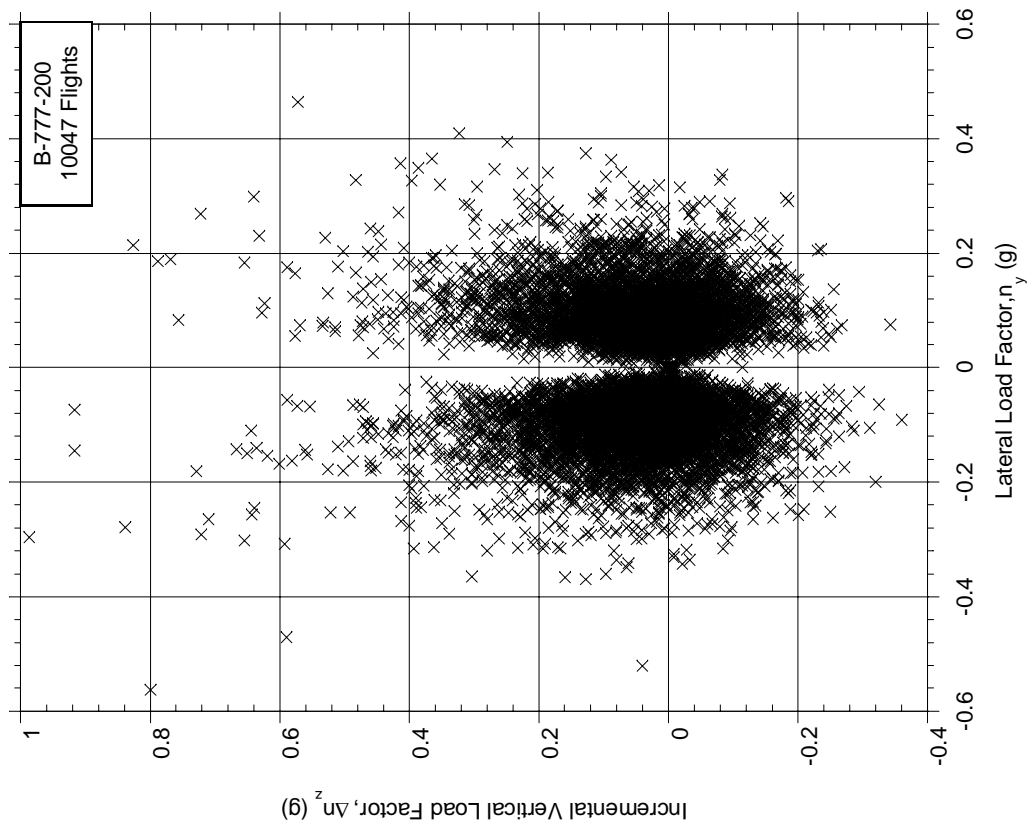


Figure C-20. Maximum Lateral Load Factor and Coincident Incremental Vertical Load Factor at Touchdown

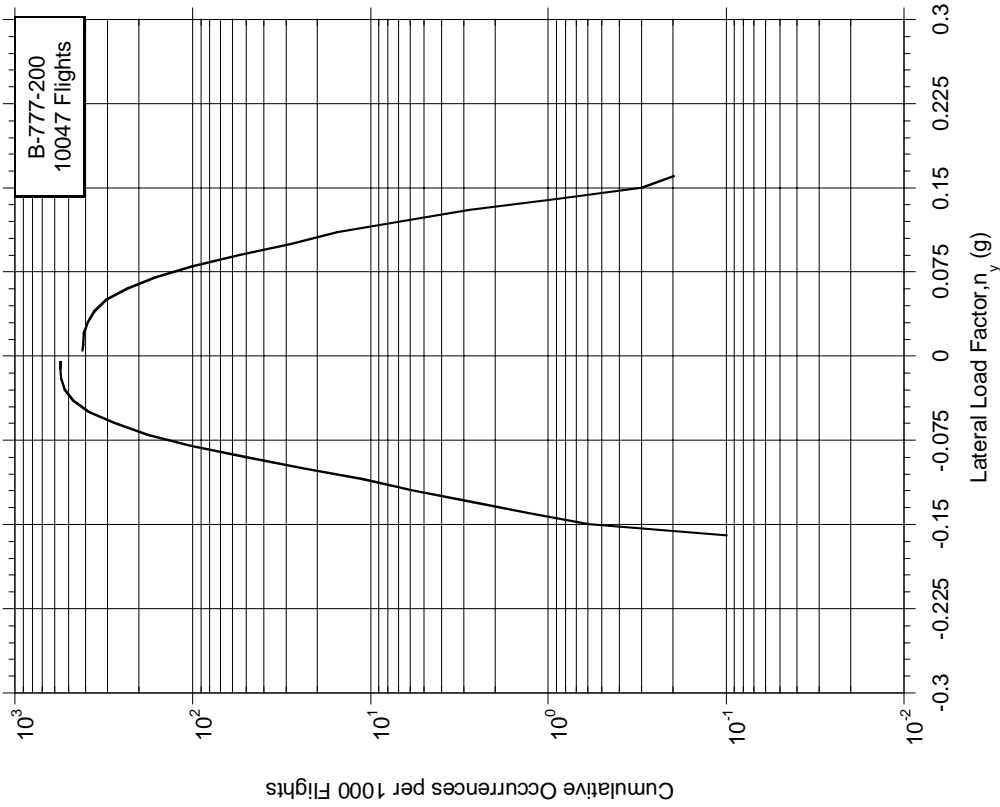


Figure C-21. Cumulative Frequency of Maximum Lateral Load Factor During Runway Turnoff

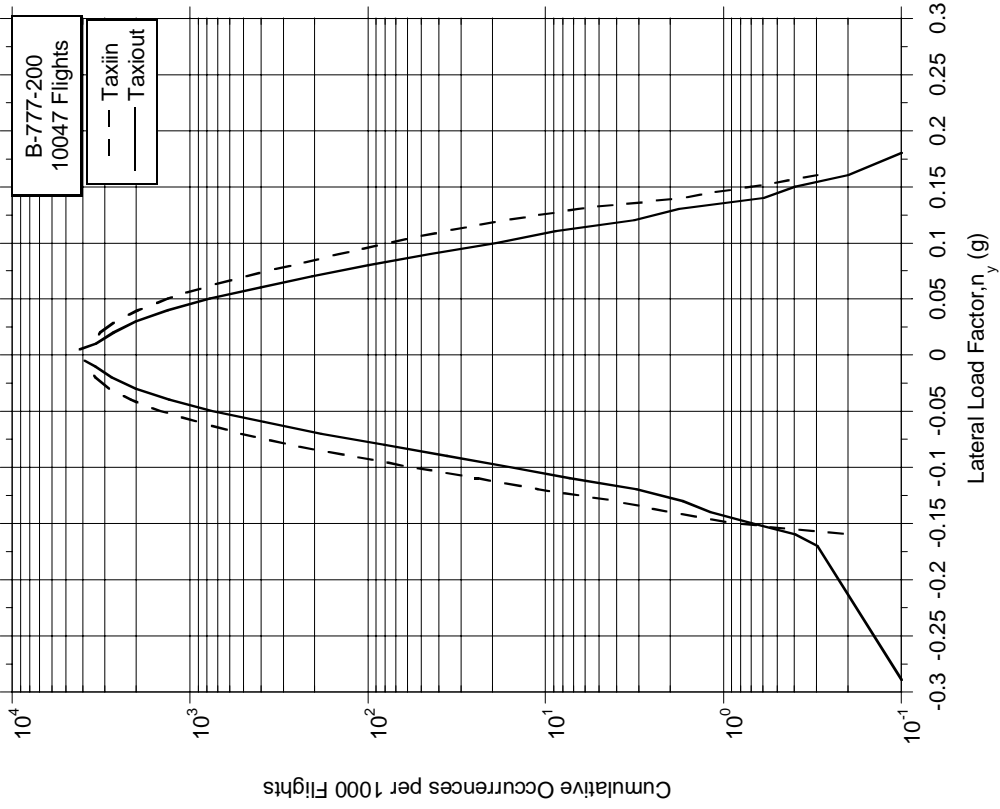


Figure C-22. Cumulative Frequency of Maximum Lateral Load Factor During Ground Turns

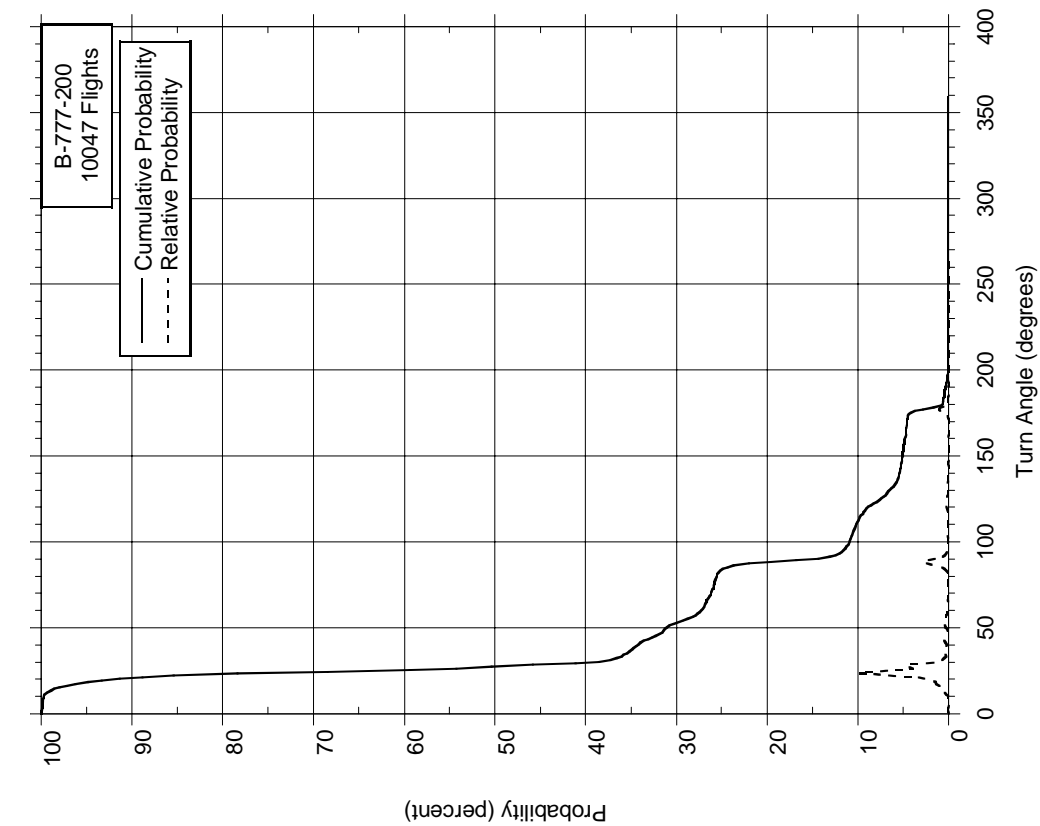


Figure C-23. Probability Distributions of Turning Angle During Runway Turnoff

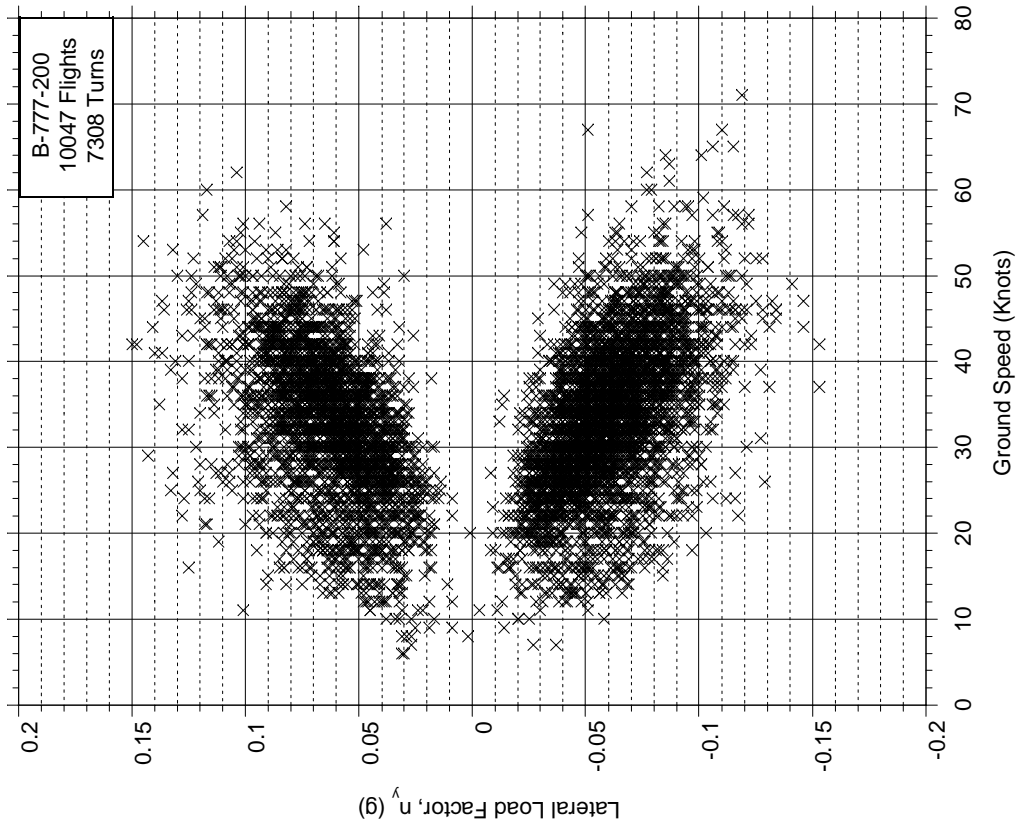


Figure C-24. Maximum Lateral Load Factor and Coincident Ground Speed During Runway Turnoff, 0-60 Degree Turns

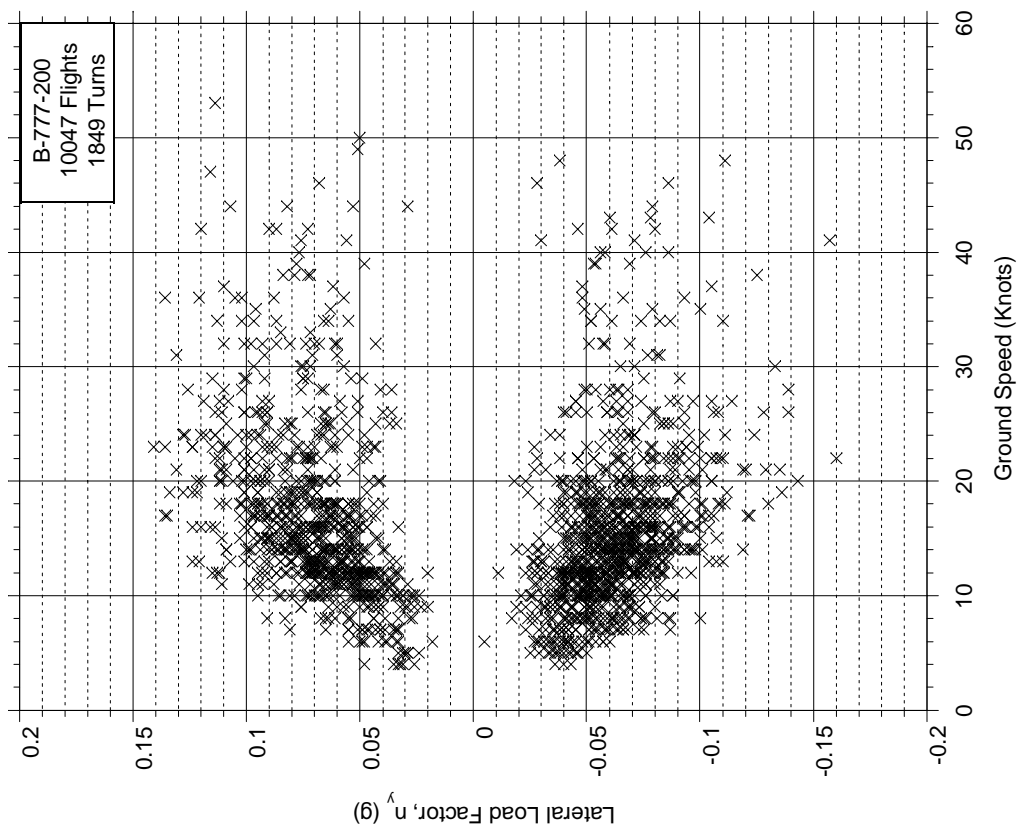


Figure C-25. Maximum Lateral Load Factor and Coincident Ground Speed During Runway Turnoff, 60-120 Degree Turns

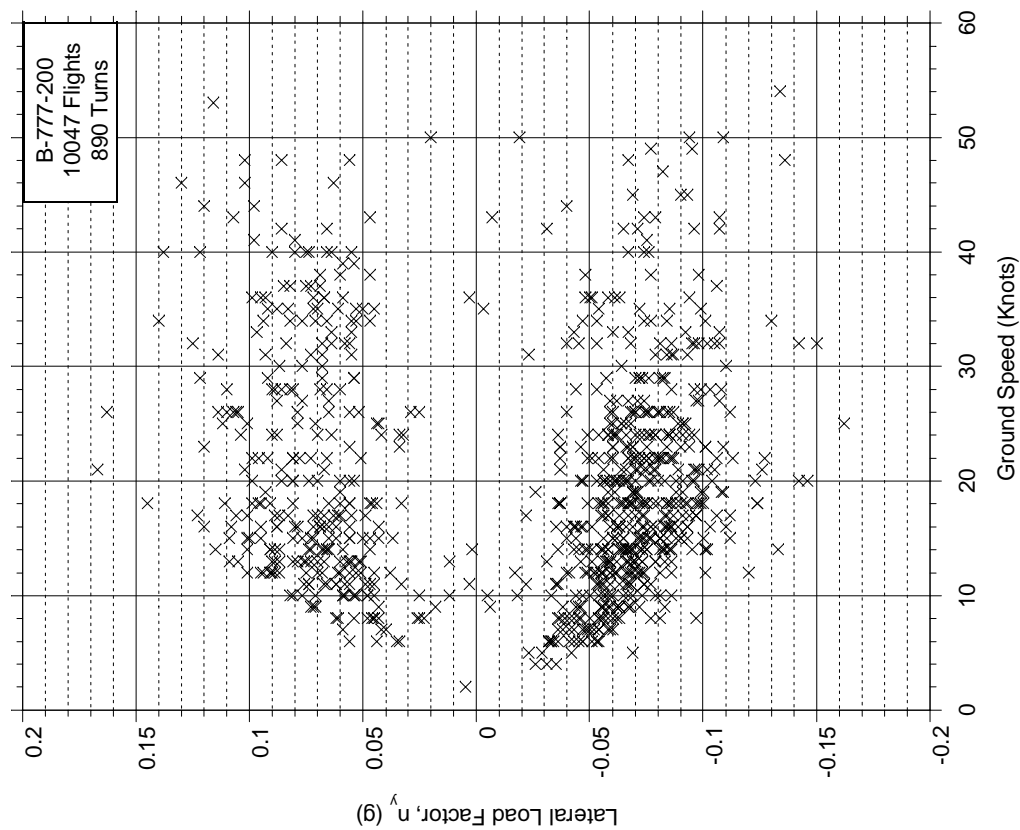


Figure C-26. Maximum Lateral Load Factor and Coincident Ground Speed During Runway Turnoff, 120-240 Degree Turns

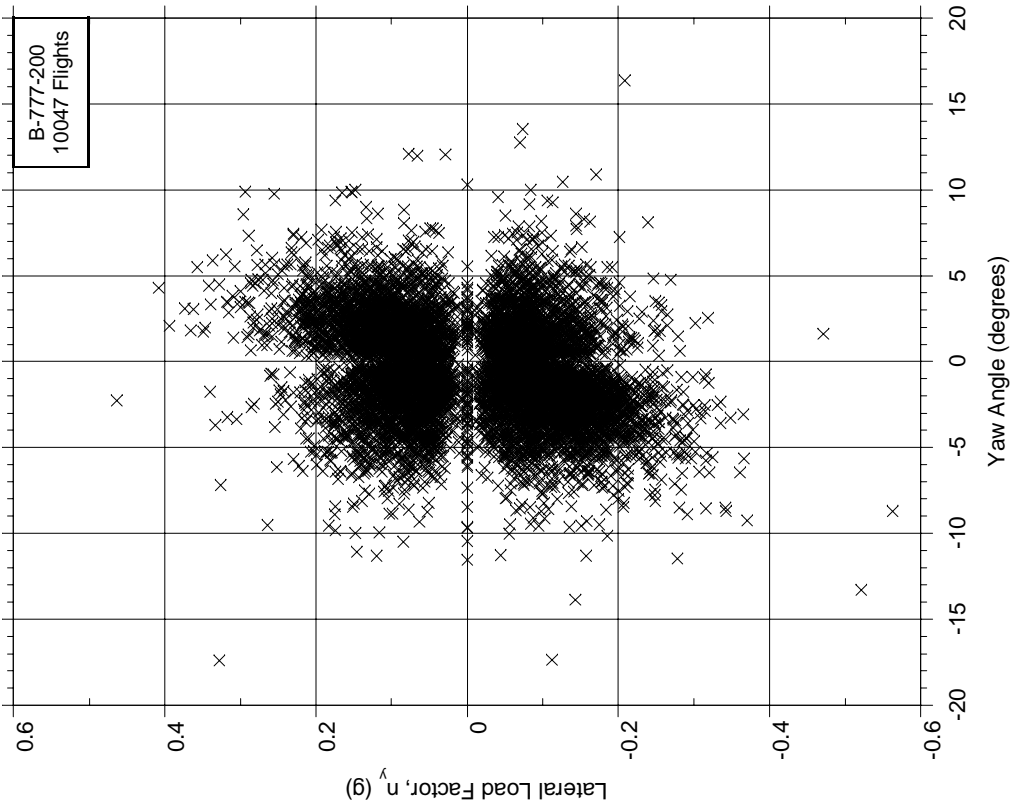


Figure C-27. Maximum Lateral Load Factor at Touchdown vs
Maximum Yaw Angle Before Touchdown

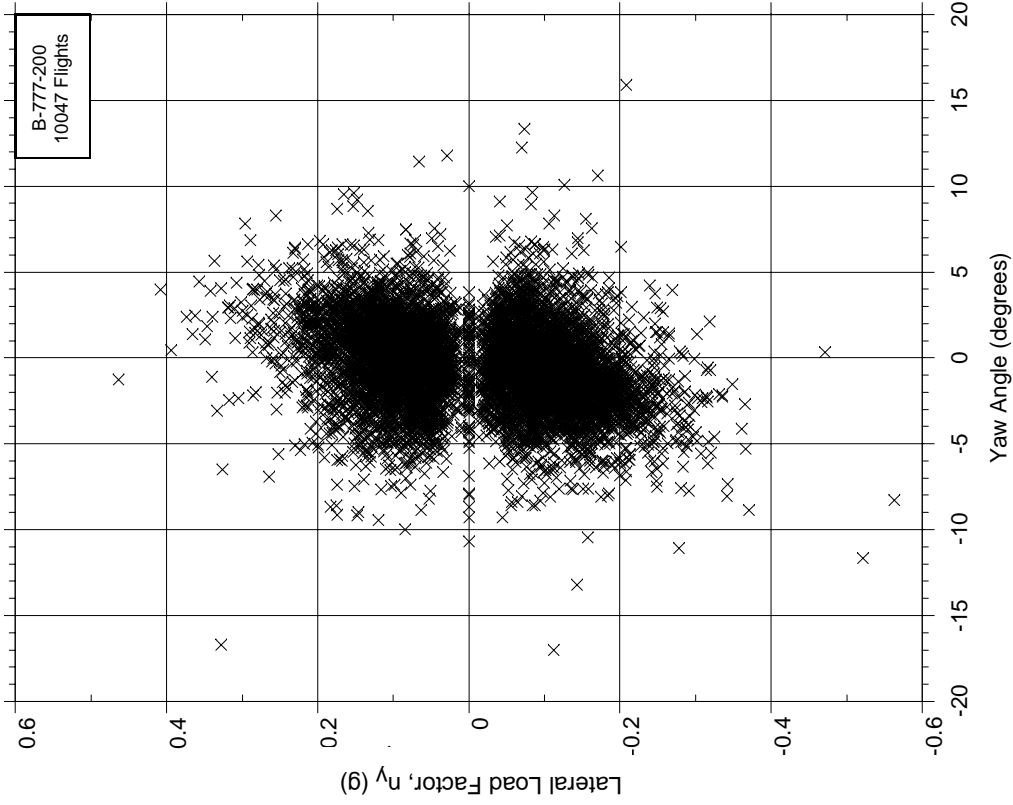


Figure C-28. Maximum Lateral Load Factor at Touchdown vs
Mean Yaw Angle Before Touchdown

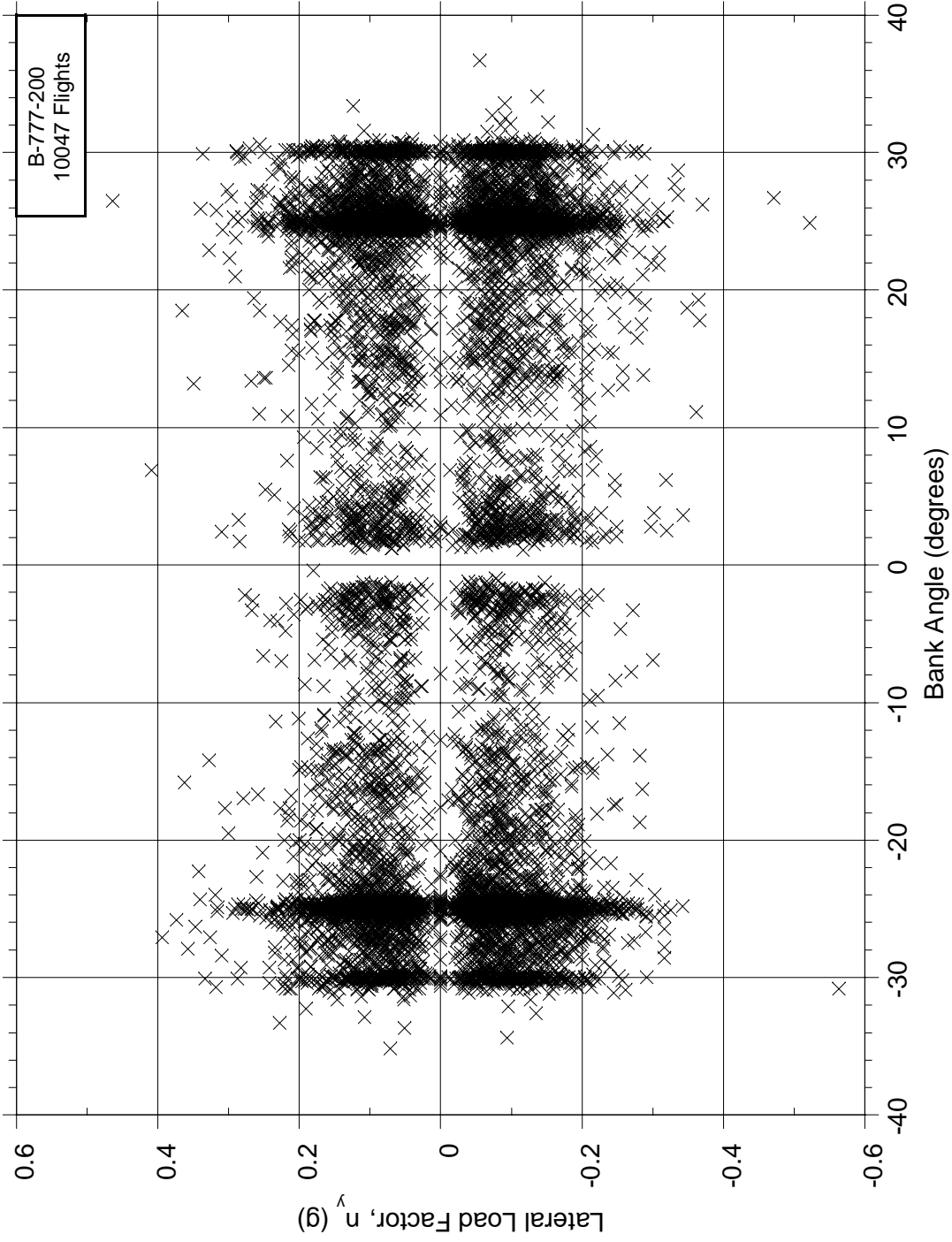


Figure C-29. Maximum Lateral Load Factor at Touchdown vs Maximum Bank Angle Before Touchdown

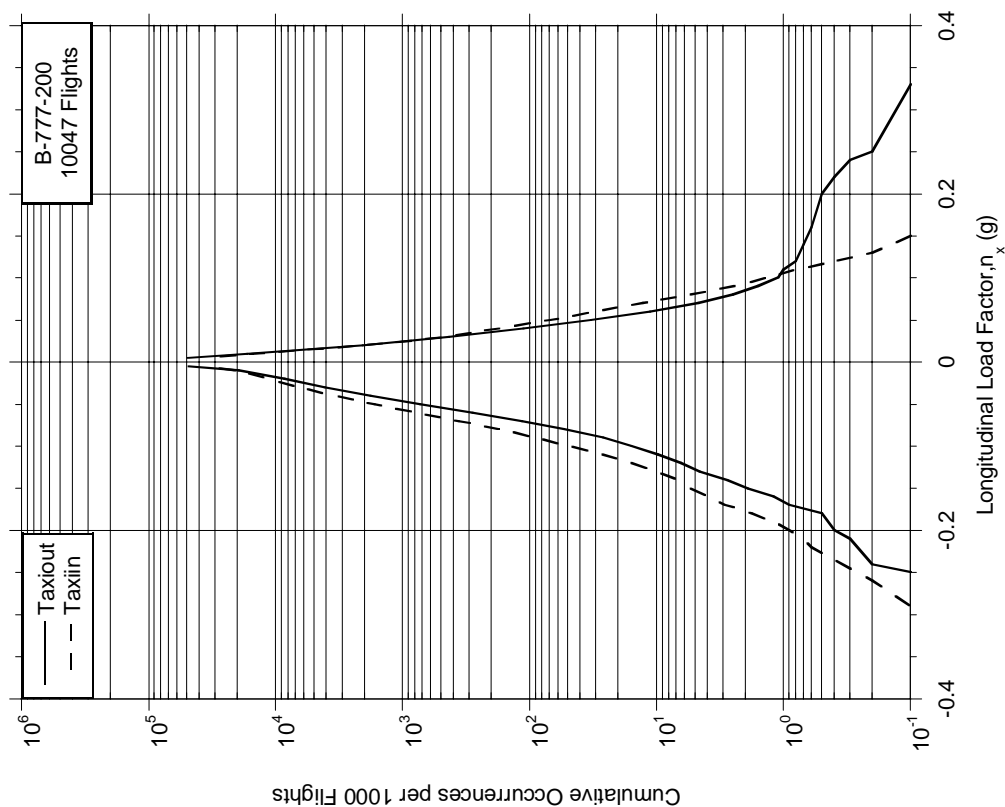


Figure C-30. Cumulative Frequency of Longitudinal Load Factor During Taxi Operations

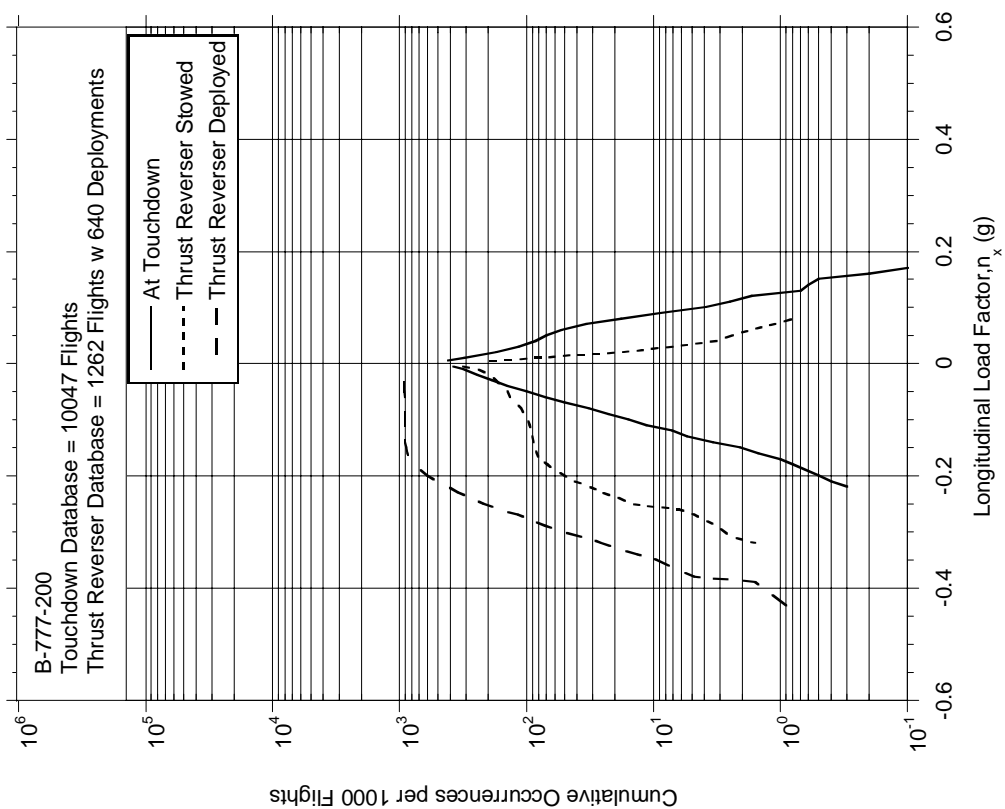


Figure C-31. Cumulative Frequency of Longitudinal Load Factor at Touchdown and During Landing Roll

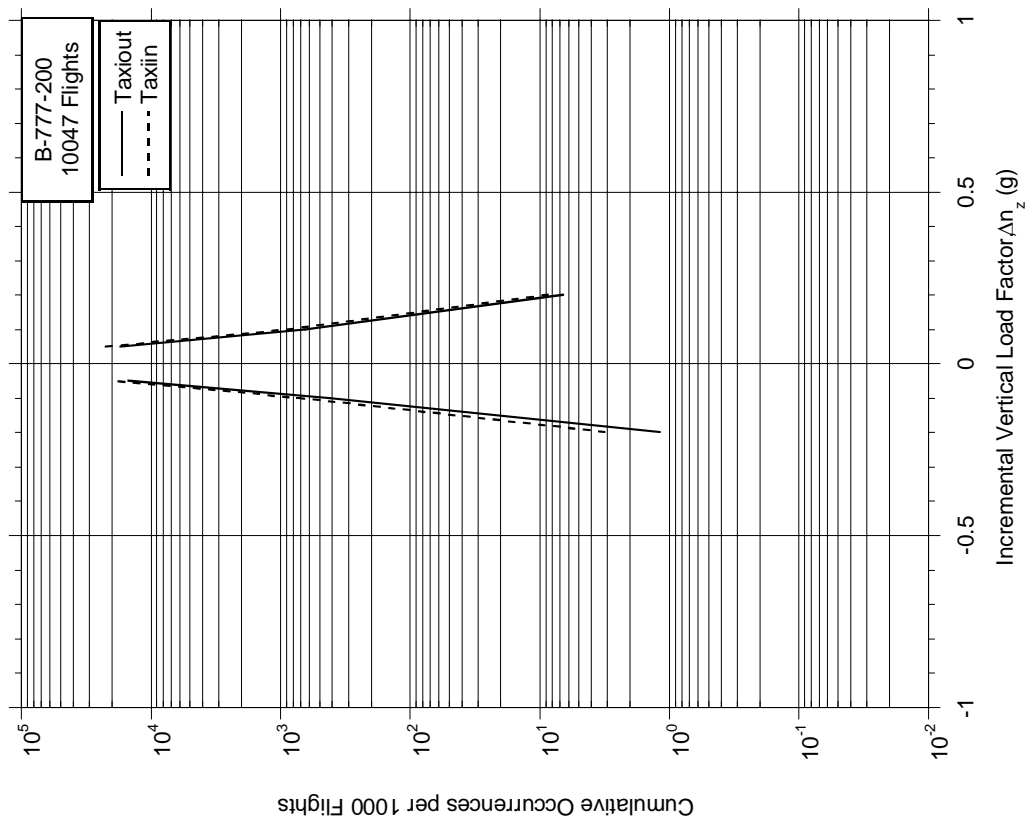


Figure C-32. Cumulative Frequency of Incremental Vertical Load Factor During Taxi Operations

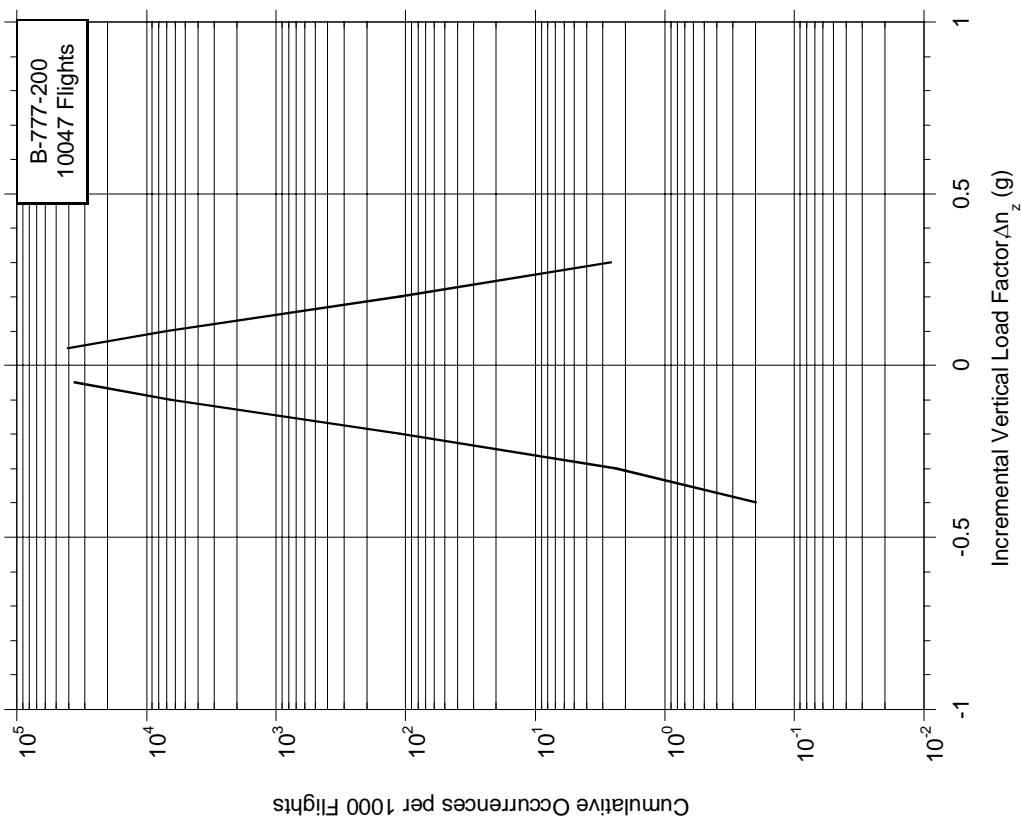


Figure C-33. Cumulative Frequency of Incremental Vertical Load Factor During Takeoff Roll

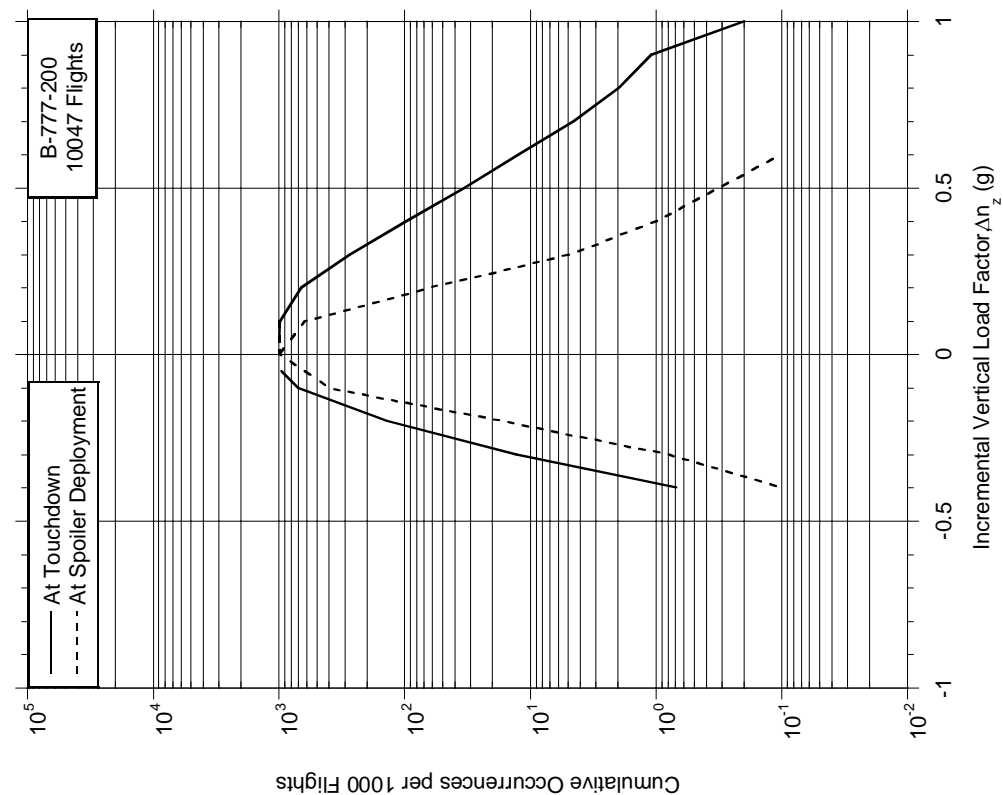


Figure C-34. Cumulative Frequency of Incremental Vertical Load Factor at Spoiler Deployment and at Touchdown

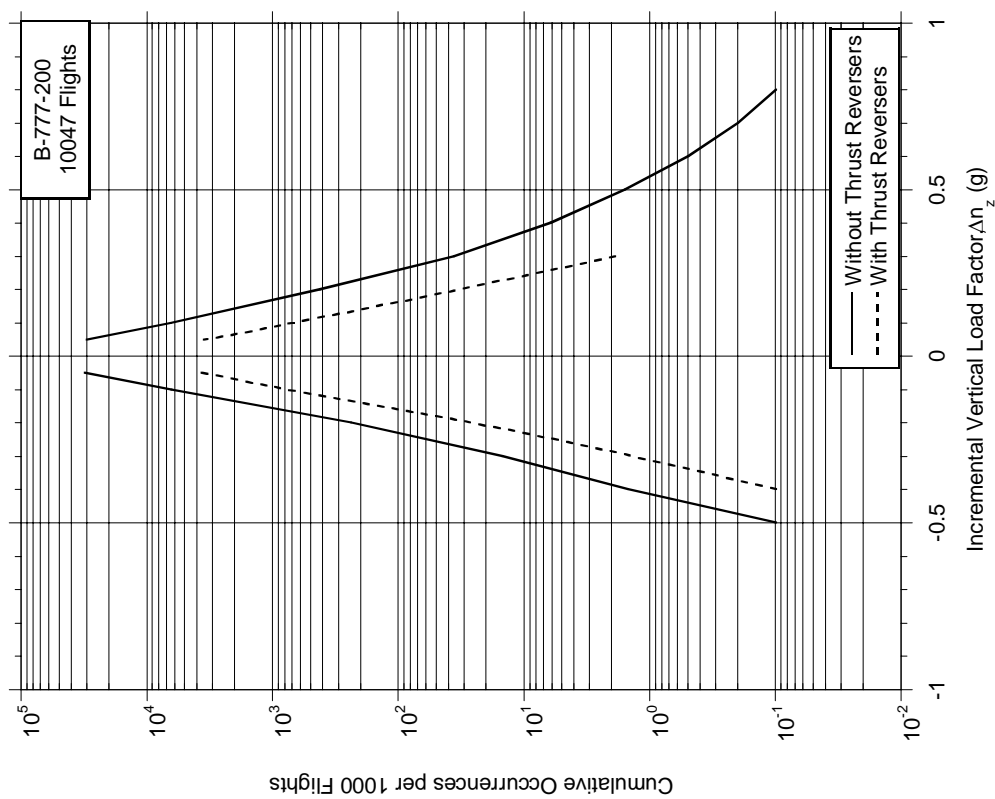


Figure C-35. Cumulative Frequency of Incremental Vertical Load Factor During Landing Roll

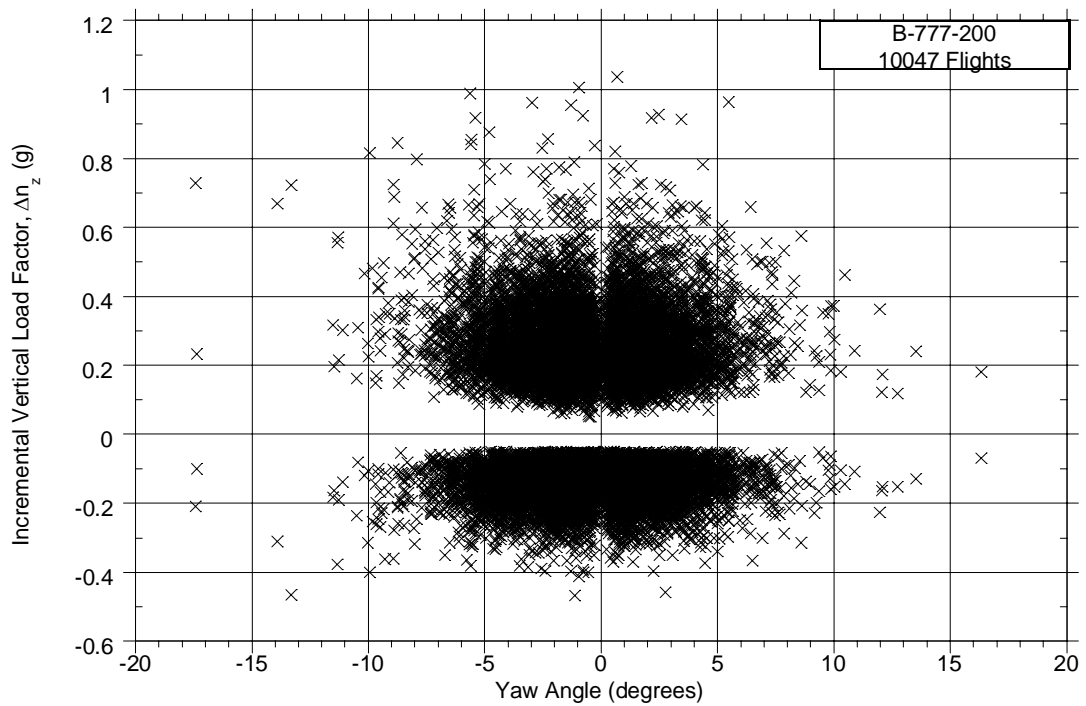


Figure C-36. Maximum Incremental Vertical Load Factor At Touchdown Vs. Maximum Yaw Angle Before Touchdown

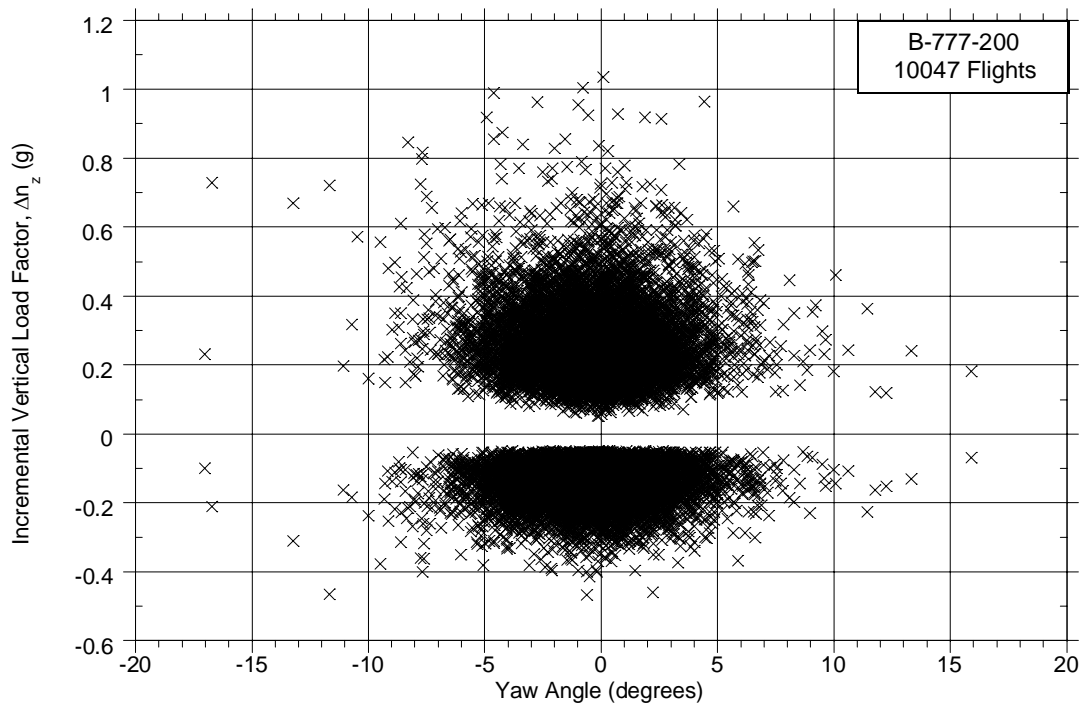


Figure C-37. Maximum Incremental Vertical Load Factor at Touchdown vs Mean Yaw Angle Before Touchdown

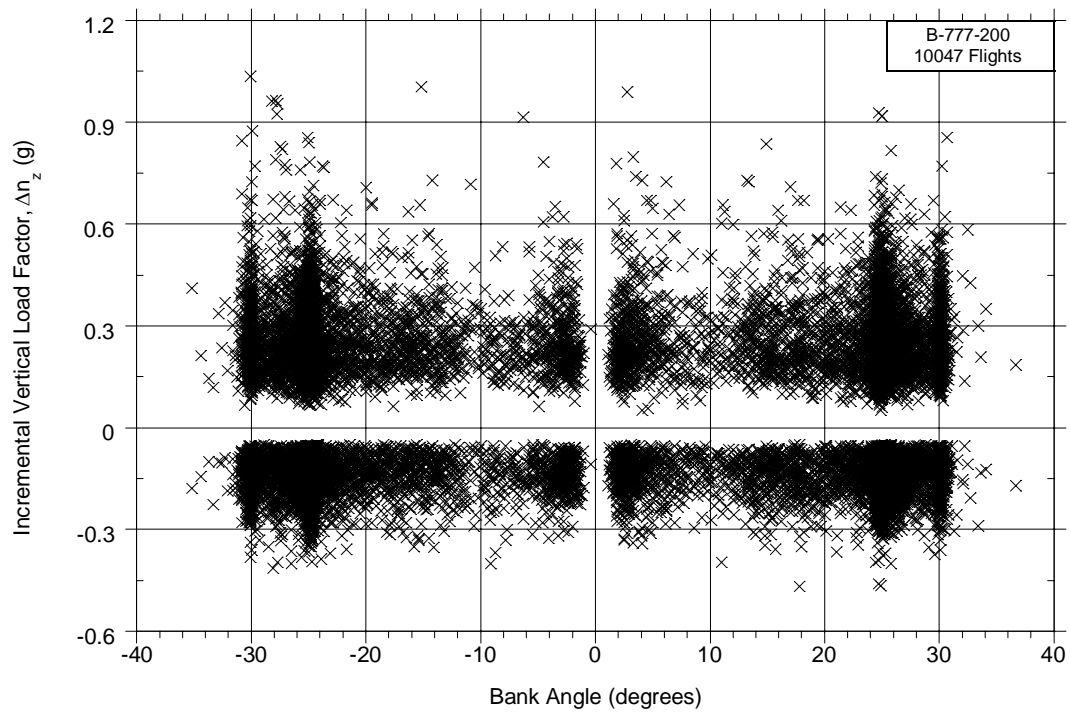


Figure C-38. Maximum Incremental Vertical Load Factor at Touchdown vs Maximum Bank Angle Before Touchdown

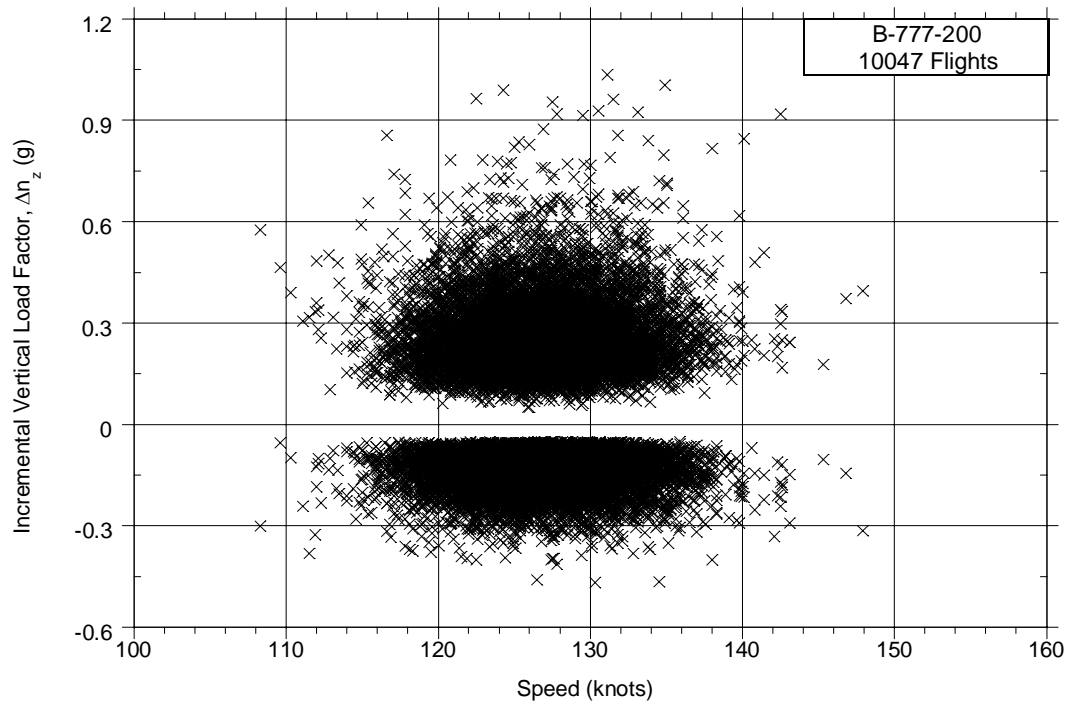


Figure C-39. Maximum Incremental Vertical Load Factor at Touchdown vs Coincident Air Speed

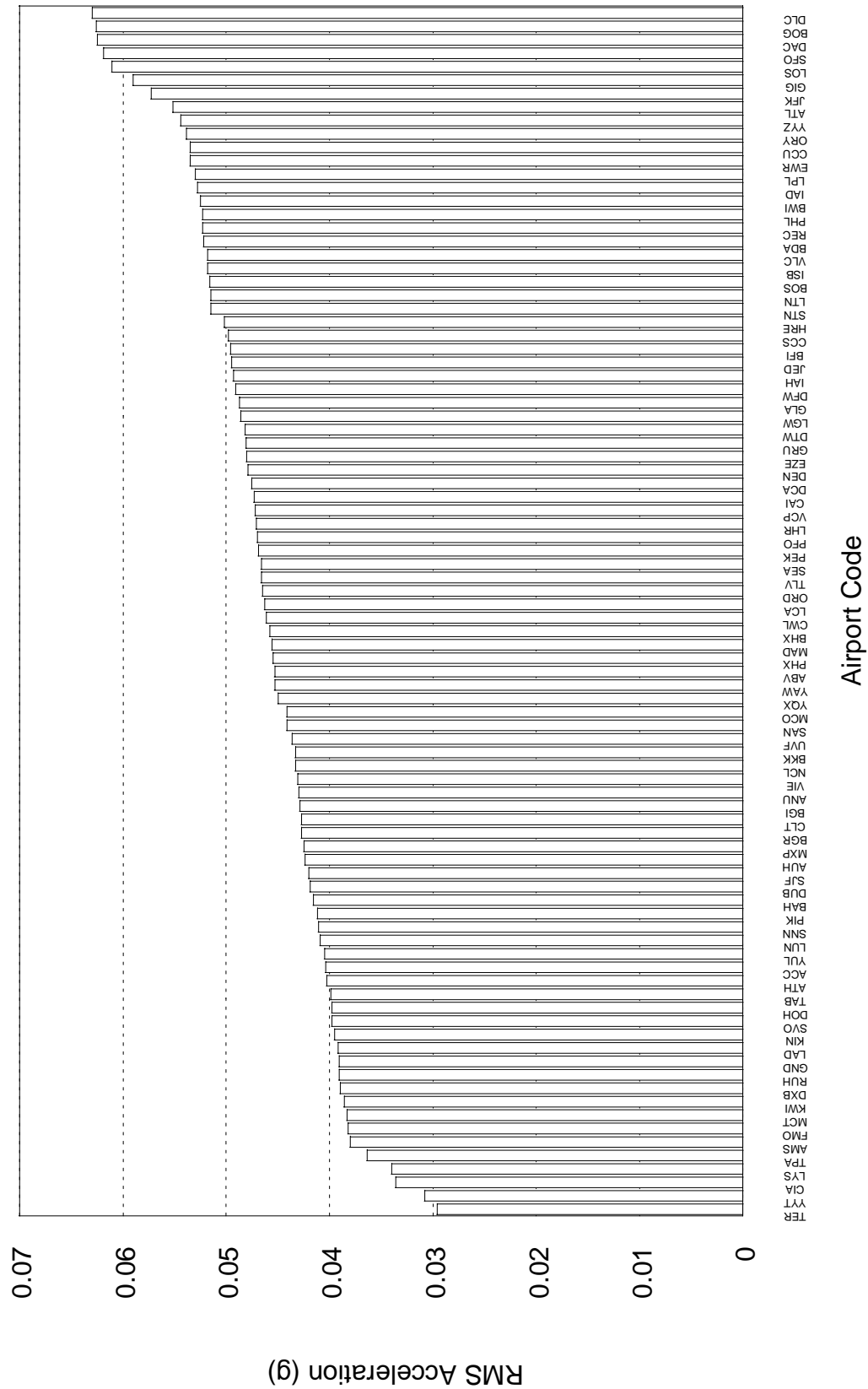


Figure C-40. Aircraft Runway Acceleration Response

Table C-1. List of Airport Codes

Airport Code	Airport	Airport Code	Airport
AUH	Abu Dhabi	LCA	Larnaca
ABV	Abuja	LPL	Liverpool
ACC	Accra	LGW	London (Gatwick)
AMS	Amsterdam	LHR	London (Heathrow)
ANU	Antigua	LAD	Luanda
ATH	Athens	LUN	Lusaka
ATL	Atlanta	LYS	Lyon
BAH	Bahrain	MAD	Madrid
BWI	Baltimore	MLP	Milan (Malpensa)
BKK	Bangkok	YUL	Montreal Dorval
BGR	Bangor	SVO	Moscow
PEK	Beijing	FMO	Munster
BDA	Bermuda	MCT	Muscat
BHX	Birmingham	JFK	New York (Kennedy)
BFI	Boeing Field Intl	EWR	Newark
BOG	Bogota	NCL	Newcastle
BOS	Boston	MCO	Orlando
BGI	Bridgetown	PFO	Paphos
EZE	Buenos Aires	ORY	Paris (Orly)
CAI	Cairo	PHL	Philadelphia
CCU	Calcutta	PHX	Phoenix
VCP	Campinas	GD	Pt. Saline
CCS	Caracas	REC	Recife (Guararapes)
CWL	Cardiff	GIG	Rio De Janeiro
CLT	Charlotte	RUH	Riyad
ORD	Chicago	CIA	Rome
DLC	Dalian (Zhoushuizi)	SAN	San Diego
DFW	Dallas/Fort Worth	SFO	San Francisco
DEN	Denver	GRU	Sao Paulo
DTW	Detroit	SEA	Seattle
DAC	Dhaka	SNN	Shannon
DOH	Doha	SJF	St. John
DXB	Dubai	CA	St Johns
DUB	Dublin	UVF	St. Lucia
YQX	Gander	TPA	Tampa
GLA	Glasgow	TLV	Tel Aviv
YAW	Halifax	TER	Terceira (Lajes)
HRE	Harare	YYZ	Toronto International
IAH	Houston	TAB	Trinidad
ISB	Islamabad	VLC	Valencia
JED	Jeddah	VIE	Vienna
KIN	Kingston	IAD	Washington Dulles
KWI	Kuwait	DCA	Washington National
LOS	Lagos		

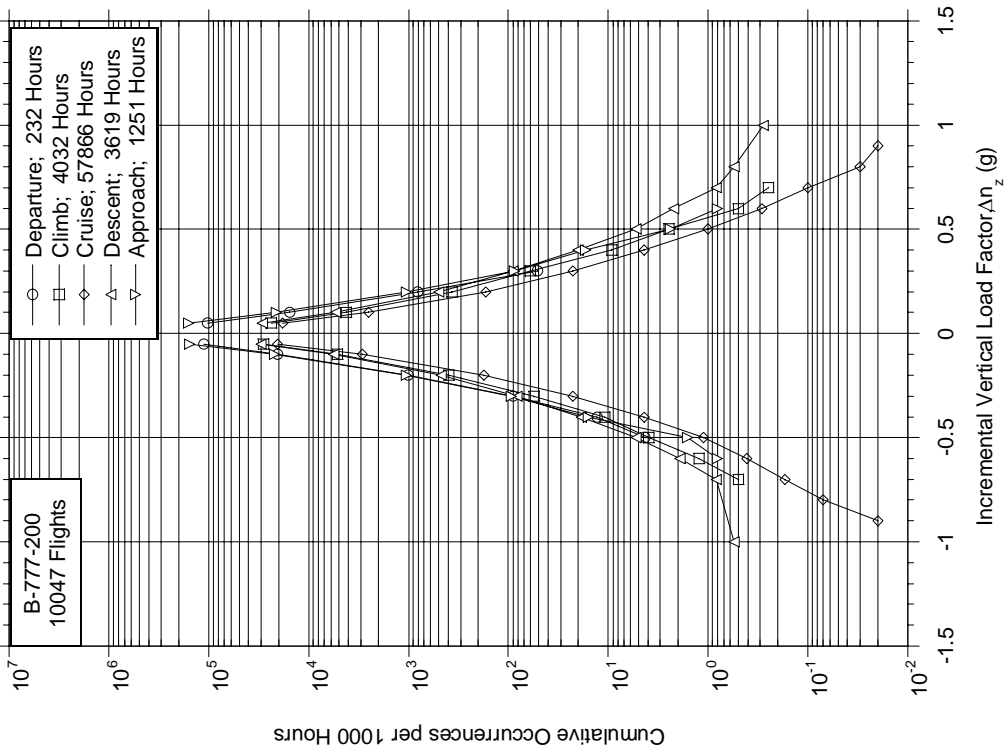


Figure C-41. Cumulative Occurrences of Incremental Vertical Gust Load Factor per 1000 Hours by Flight Phase

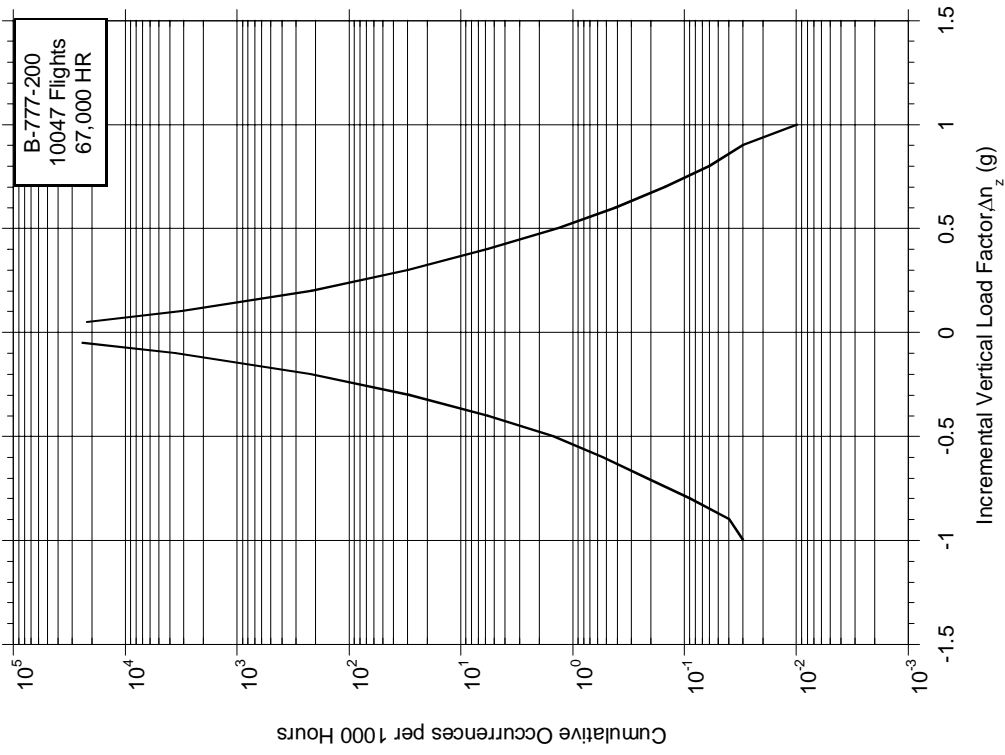


Figure C-42. Cumulative Occurrences of Incremental Vertical Gust Load Factor per 1000 Hours, Combined Flight Phases

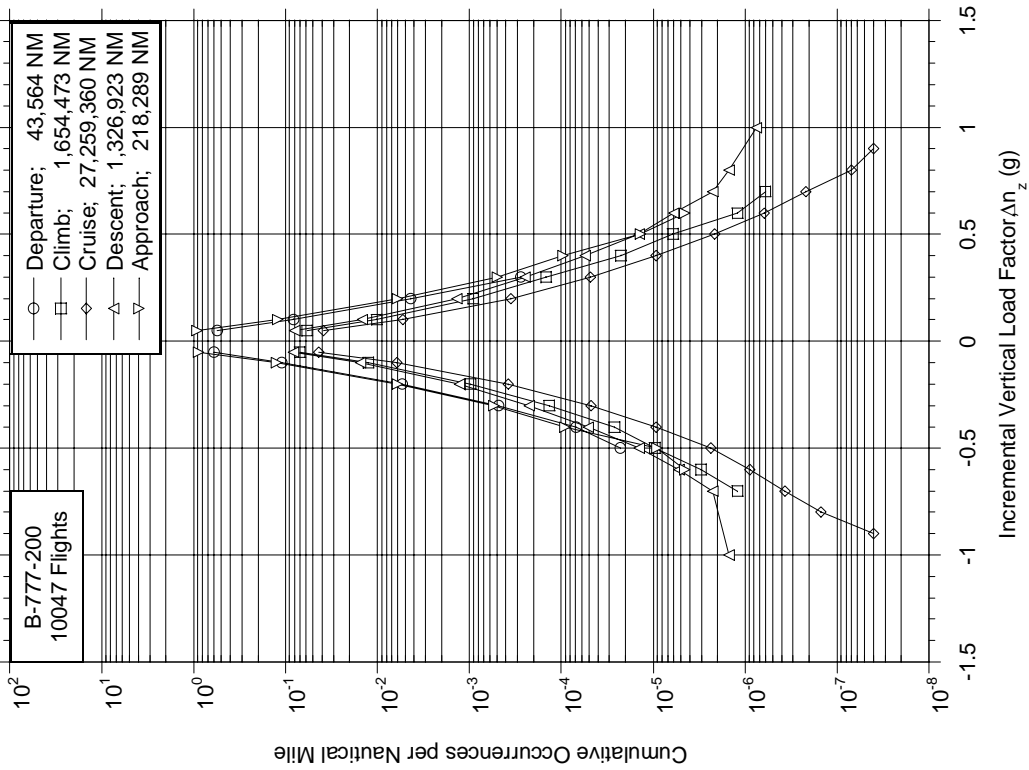


Figure C-43. Cumulative Occurrences of Incremental Vertical Gust Load Factor per Nautical Mile by Flight Phase

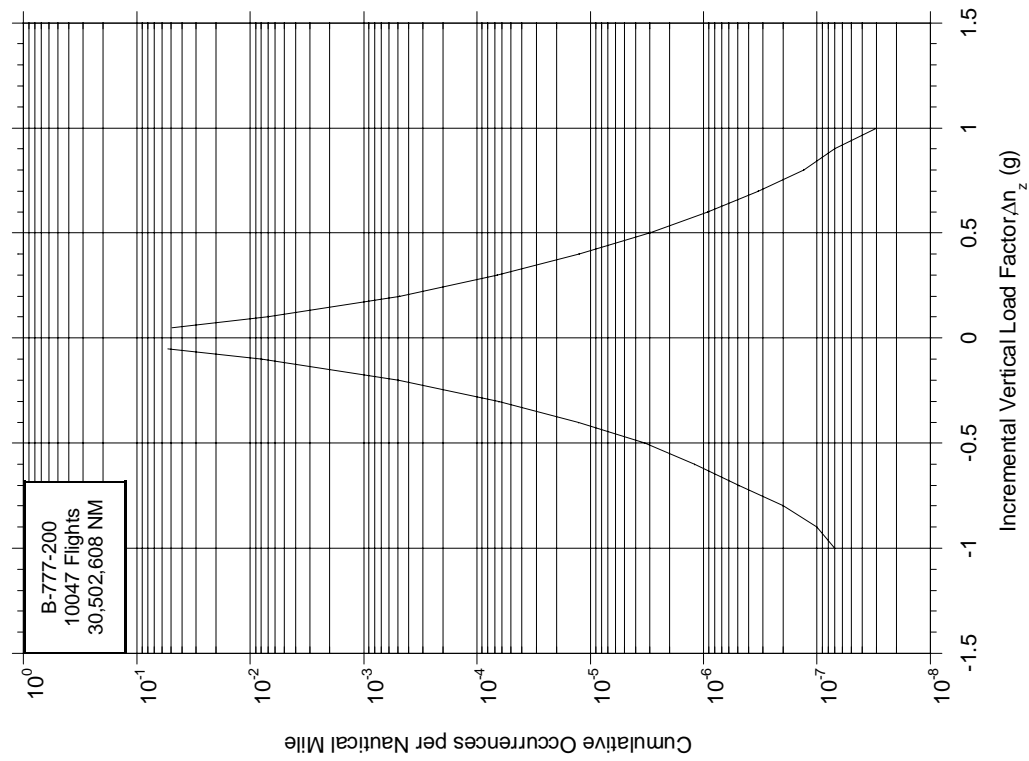


Figure C-44. Cumulative Occurrences of Incremental Vertical Gust Load Factor per Nautical Mile, Combined Flight Phases

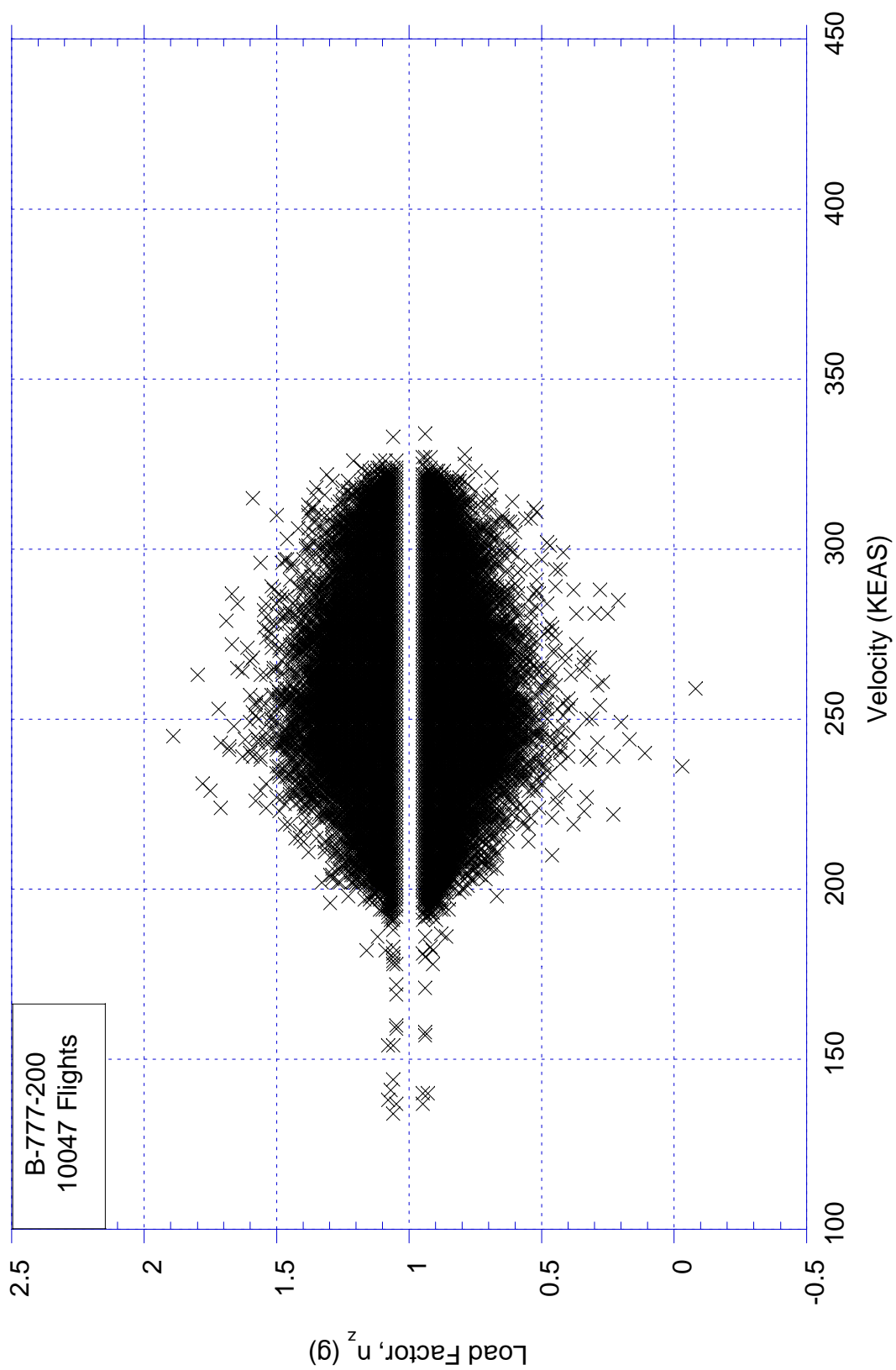


Figure C-45. Gust Load Factor and Coincident Speed for Flaps Retracted

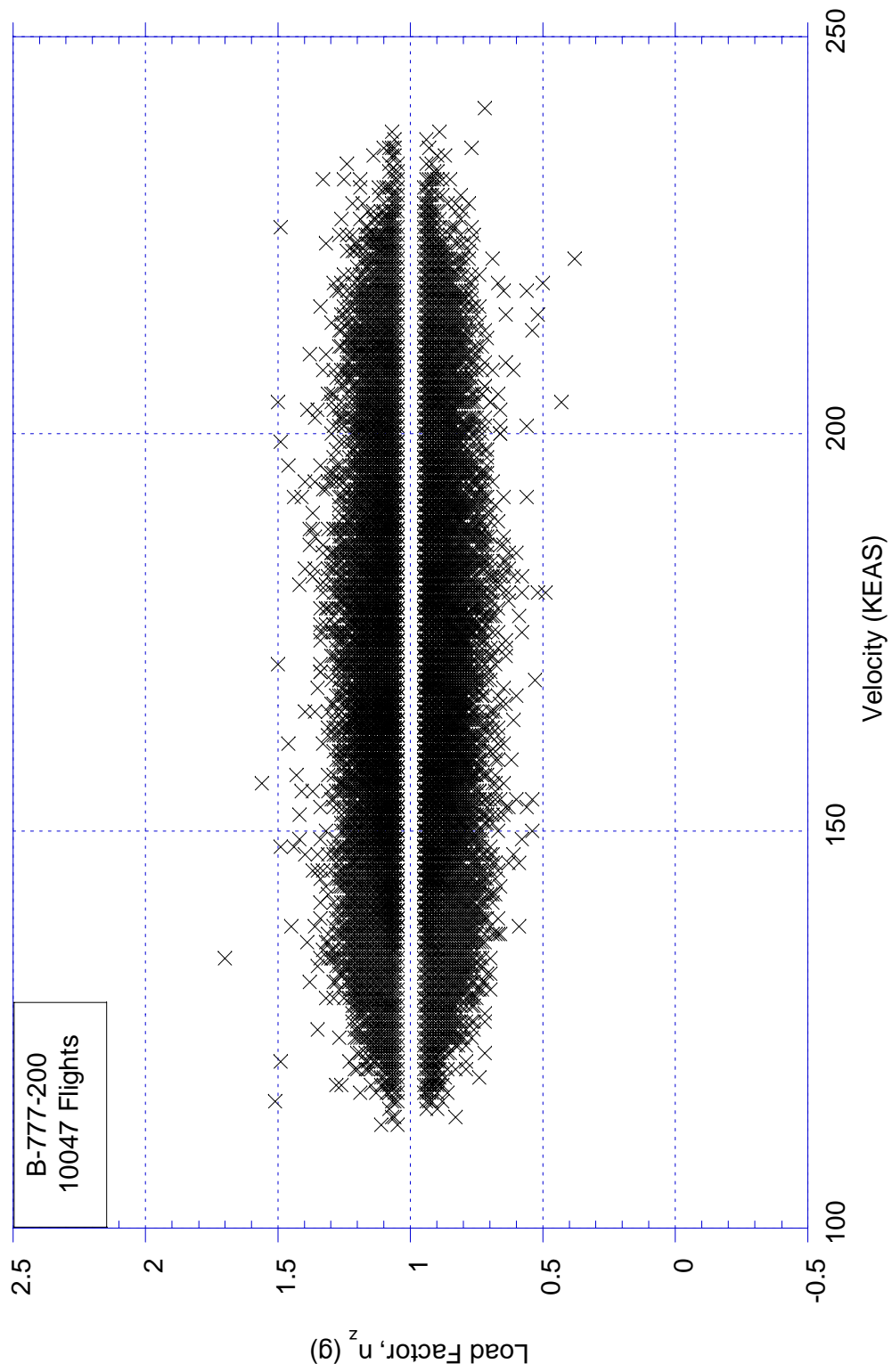


Figure C-46. Gust Load Factor and Coincident Speed for Flaps Extended

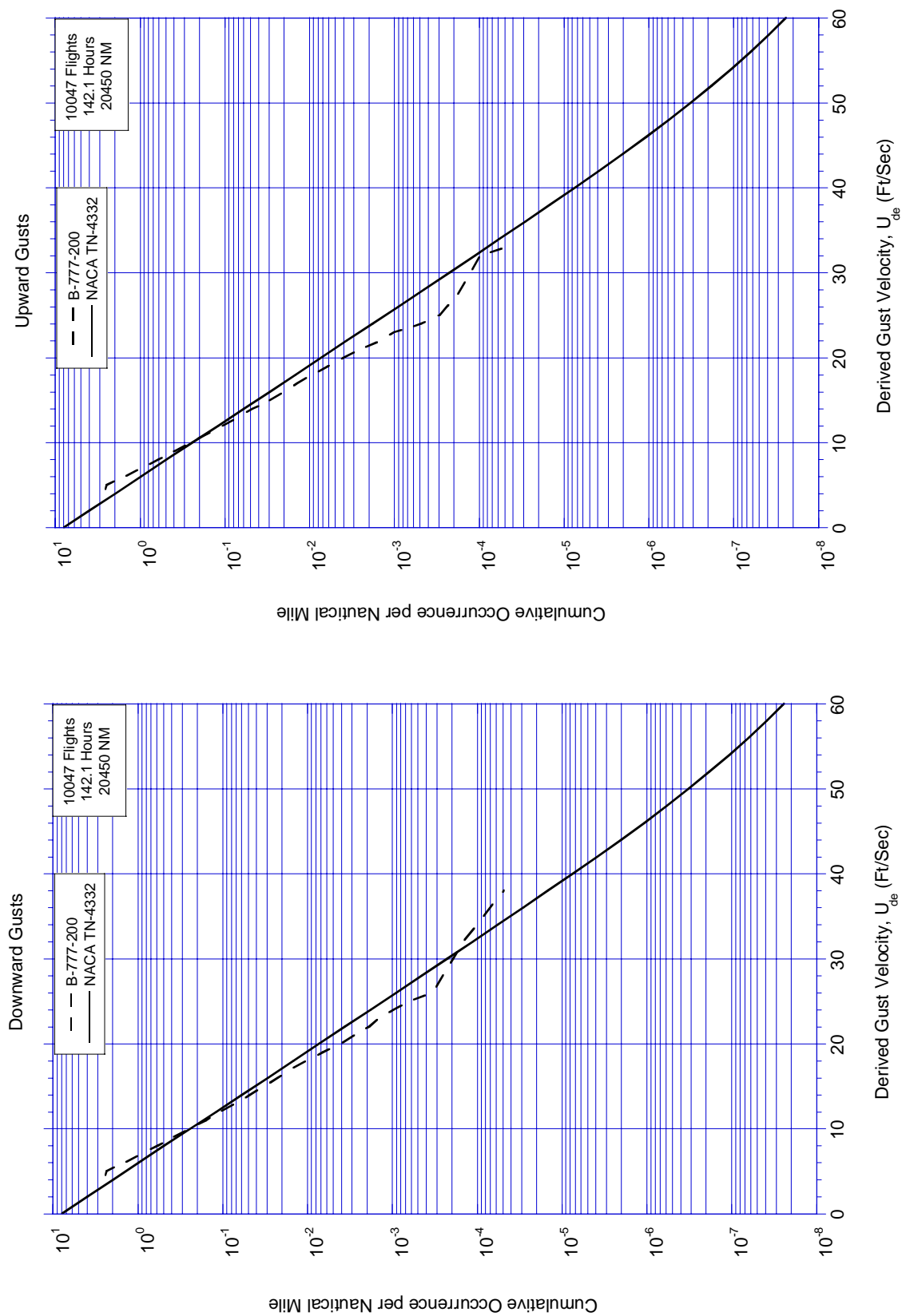


Figure C-47. Cumulative Occurrences of Derived Gust Velocity per Nautical Mile, < 500 Feet

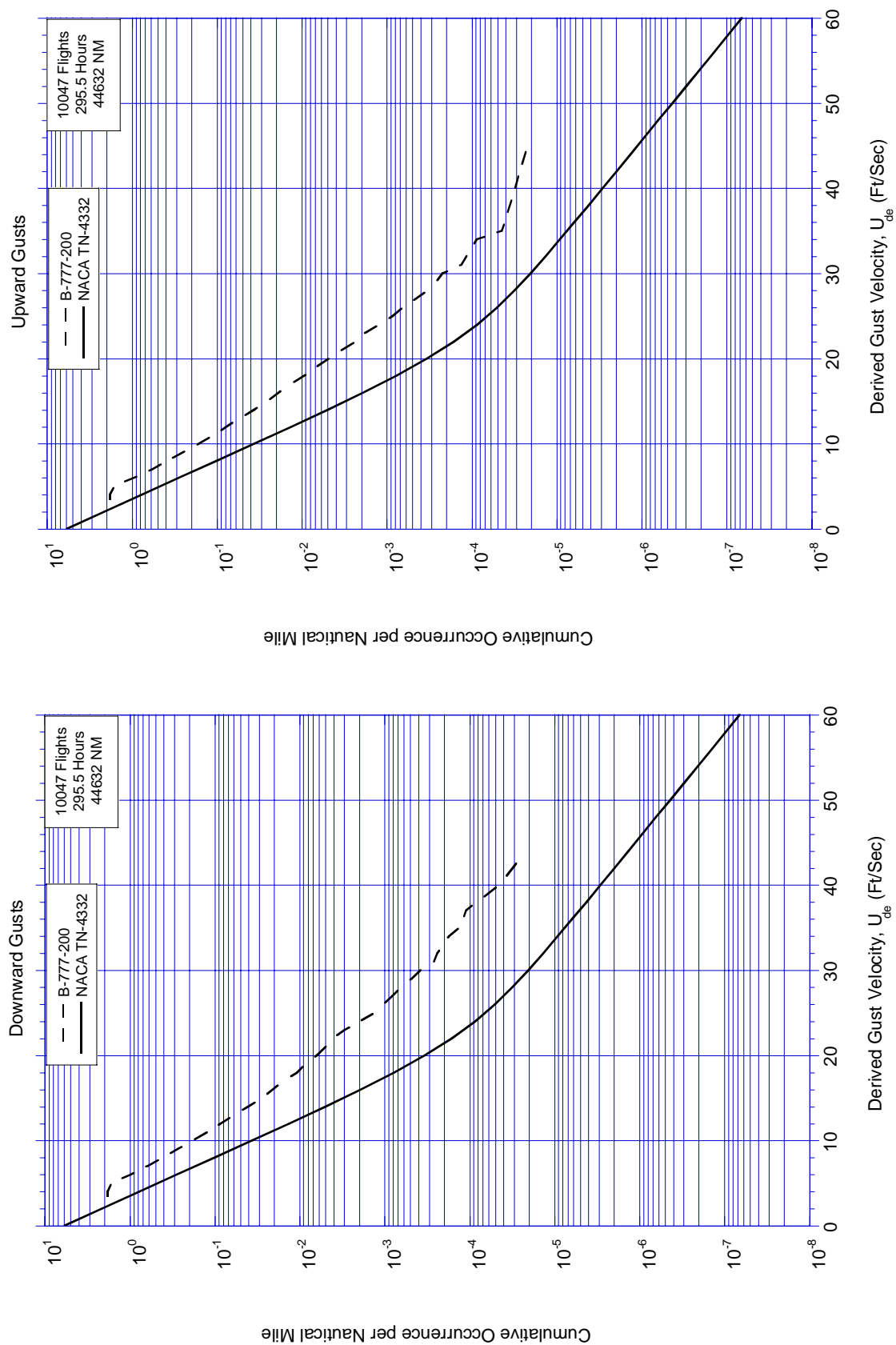


Figure C-48. Cumulative Occurrences of Derived Gust Velocity per Nautical Mile, 500-1500 Feet

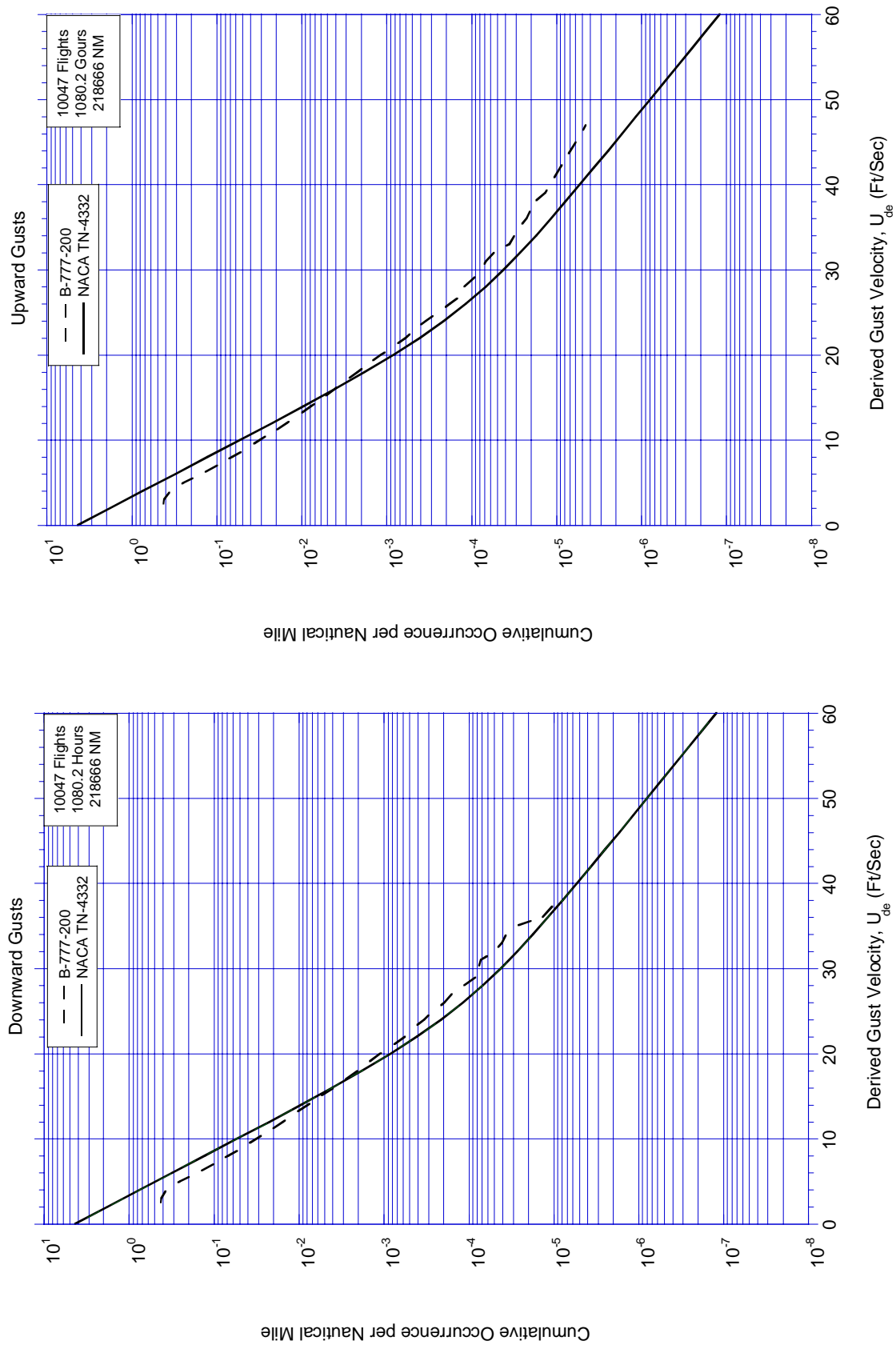


Figure C-49. Cumulative Occurrences of Derived Gust Velocity per Nautical Mile, 1500-4500 Feet

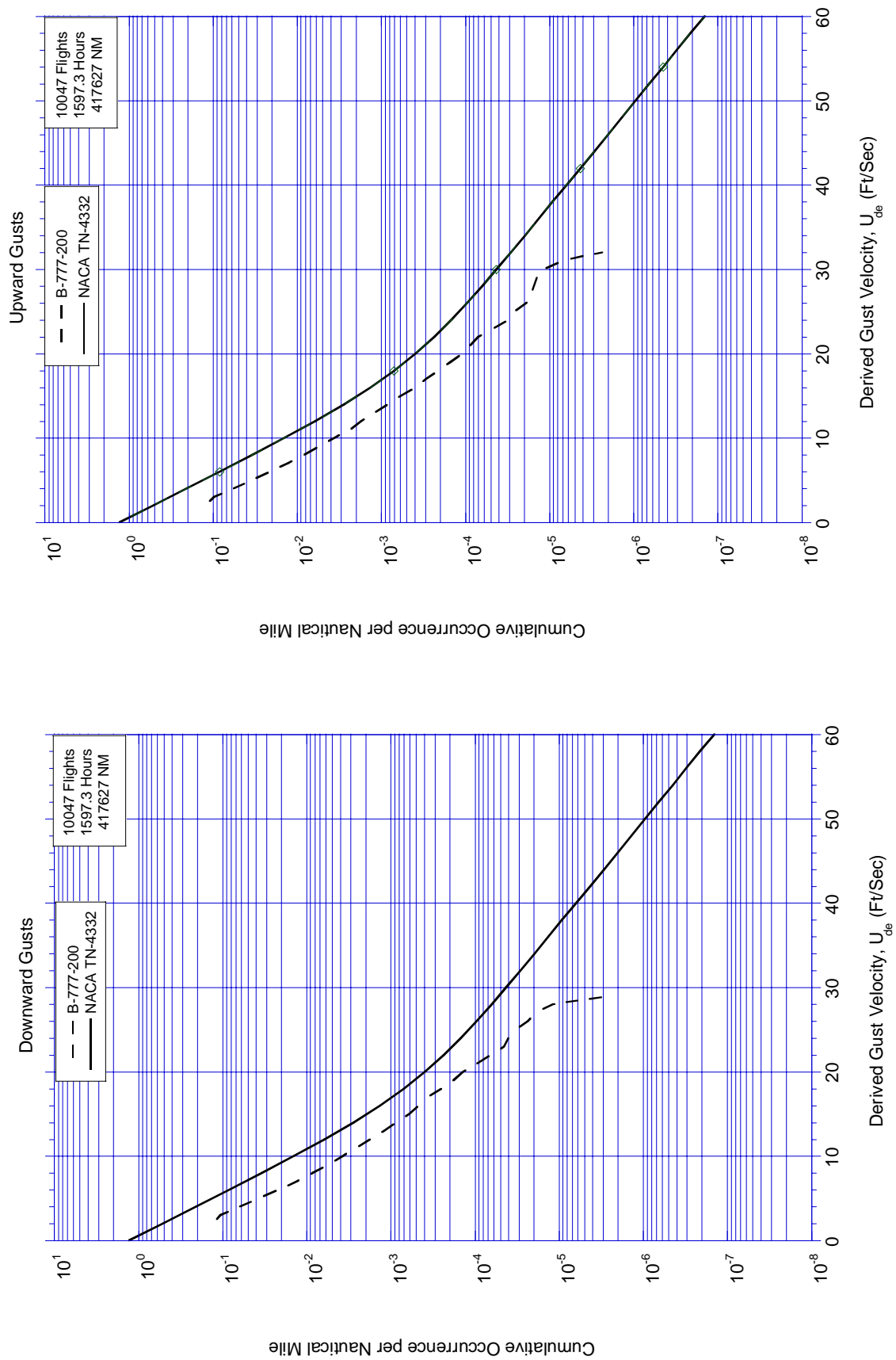


Figure C-50. Cumulative Occurrences of Derived Gust Velocity per Nautical Mile, 4500-9500 Feet

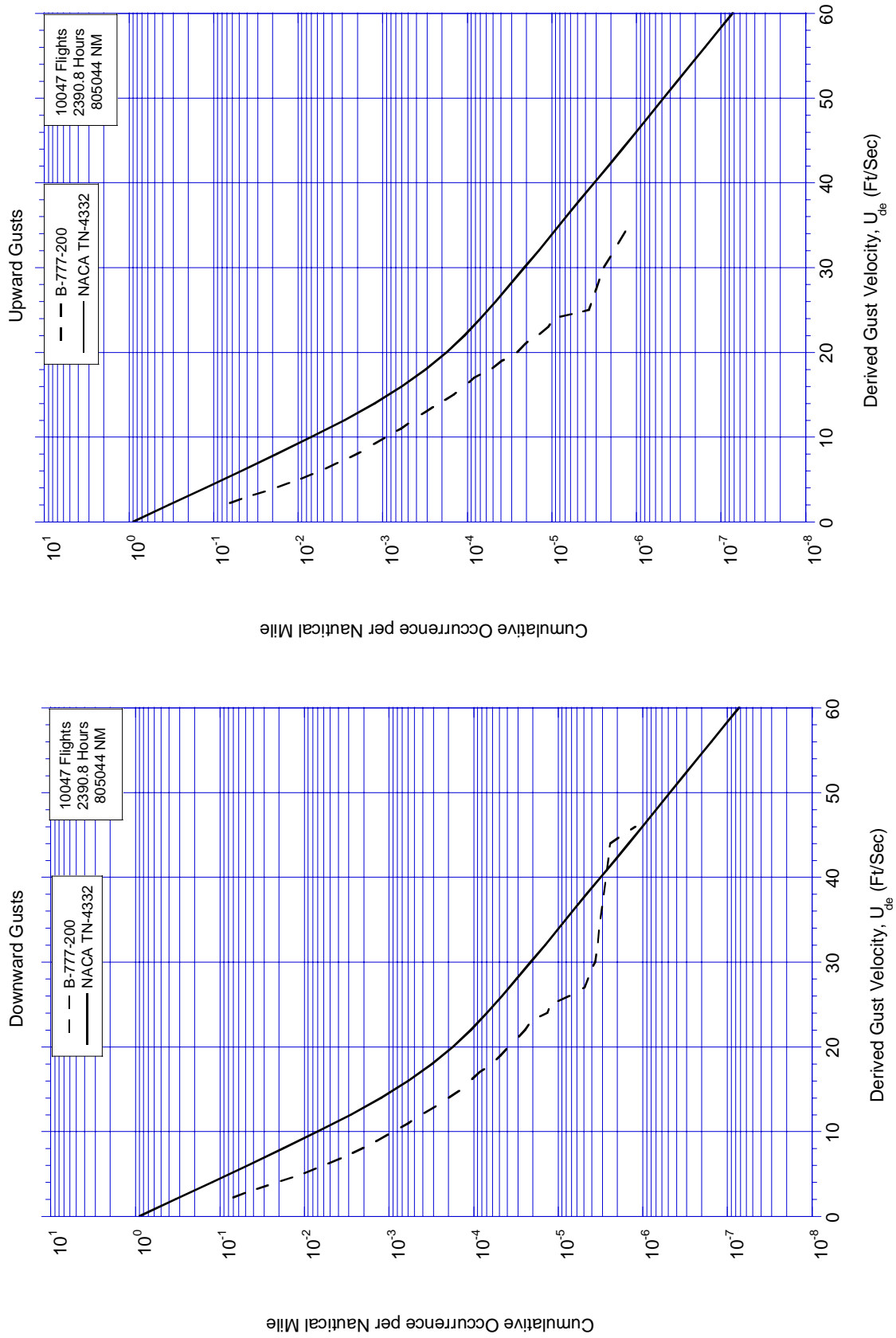


Figure C-51. Cumulative Occurrences of Derived Gust Velocity per Nautical Mile, 9,500-19,500 Feet

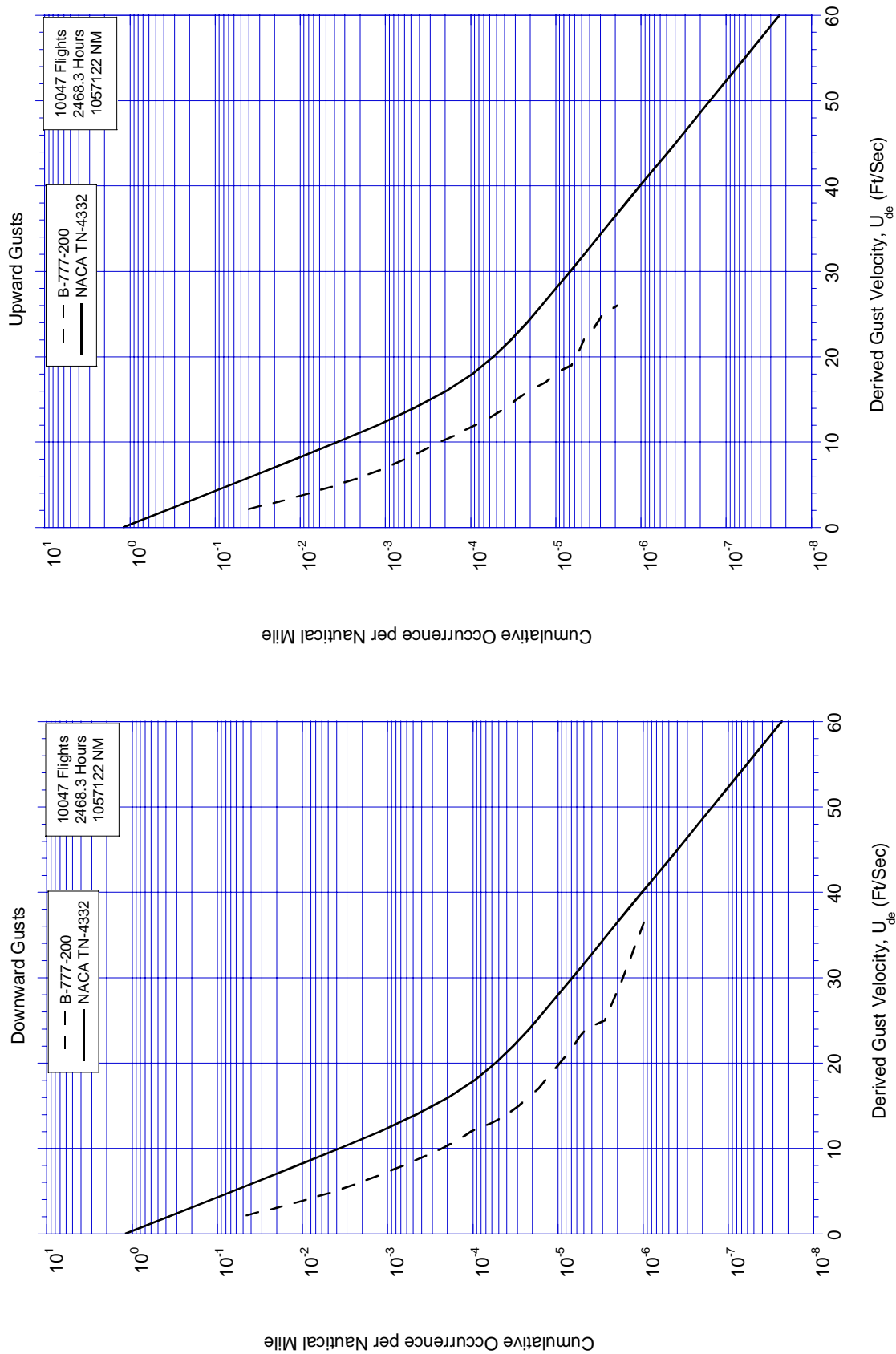


Figure C-52. Cumulative Occurrences of Derived Gust Velocity per Nautical Mile, 19,500-29,500 Feet

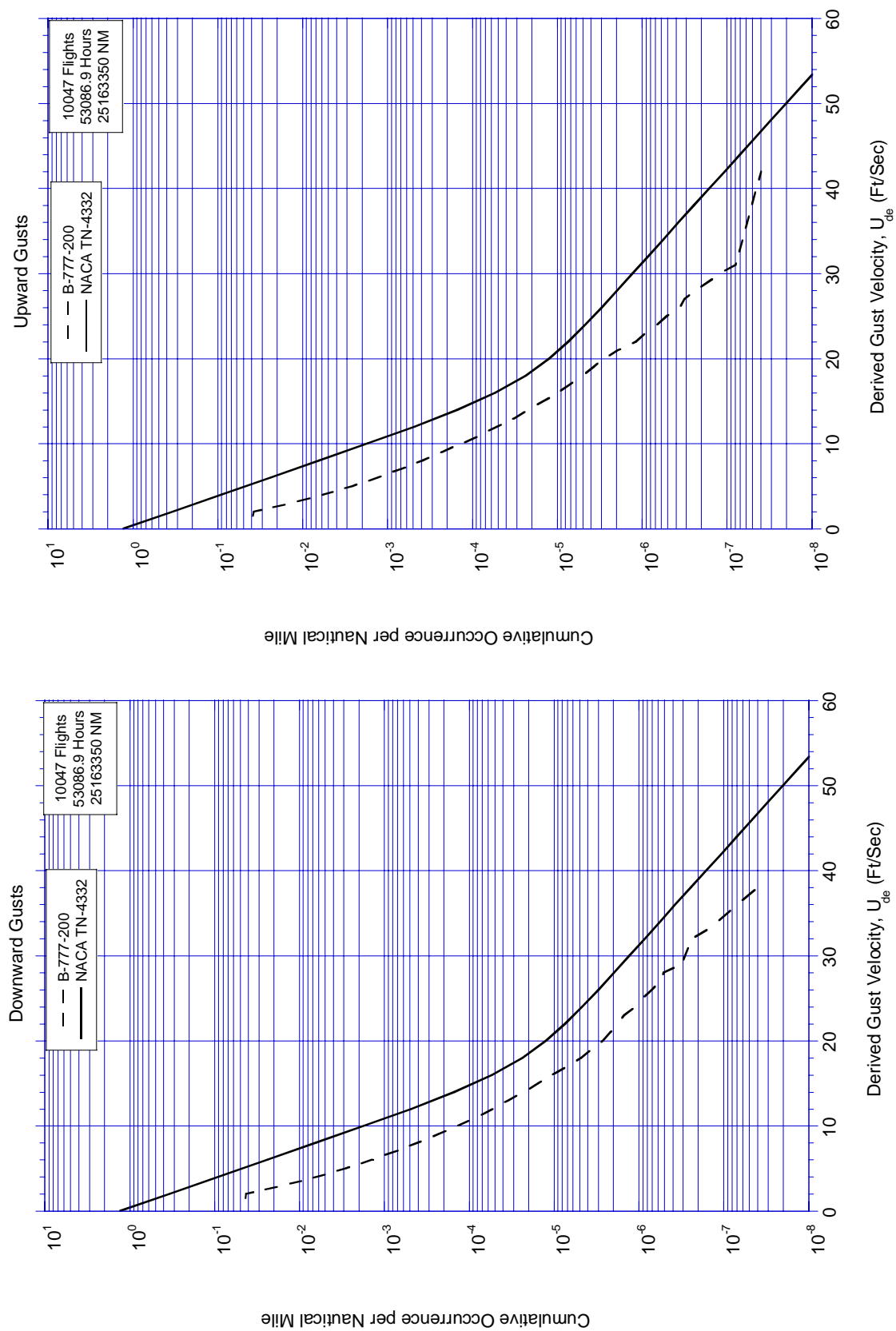


Figure C-53. Cumulative Occurrences of Derived Gust Velocity per Nautical Mile, 29,500-39,500 Feet

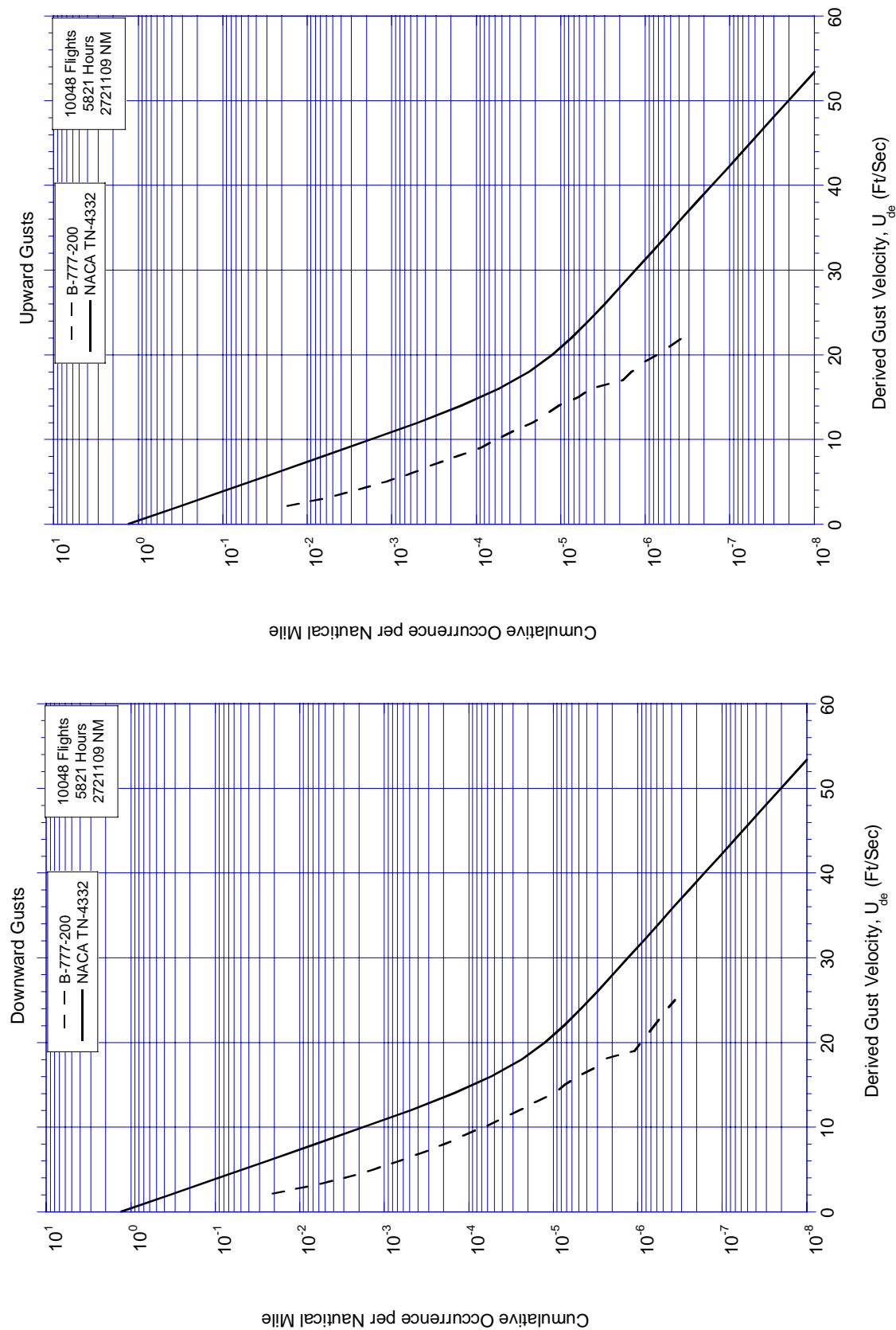


Figure C-54. Cumulative Occurrences of Derived Gust Velocity per Nautical Mile, 39,500-44,500 Feet

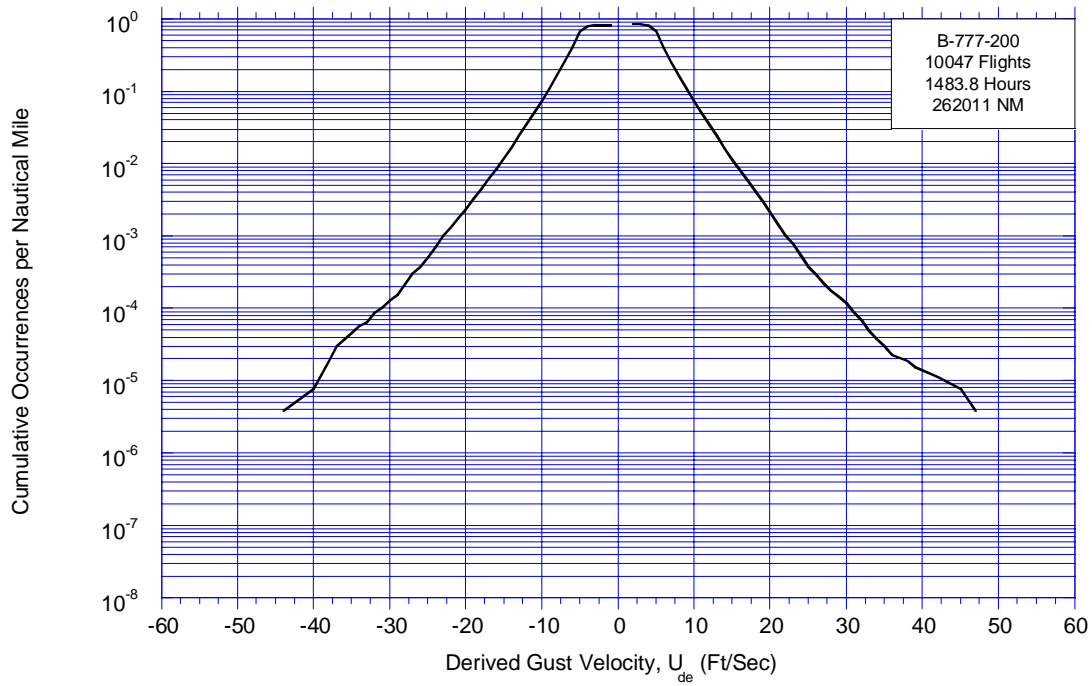


Figure C-55. Cumulative Occurrences of Derived Gust Velocity per Nautical Mile, Flaps Extended

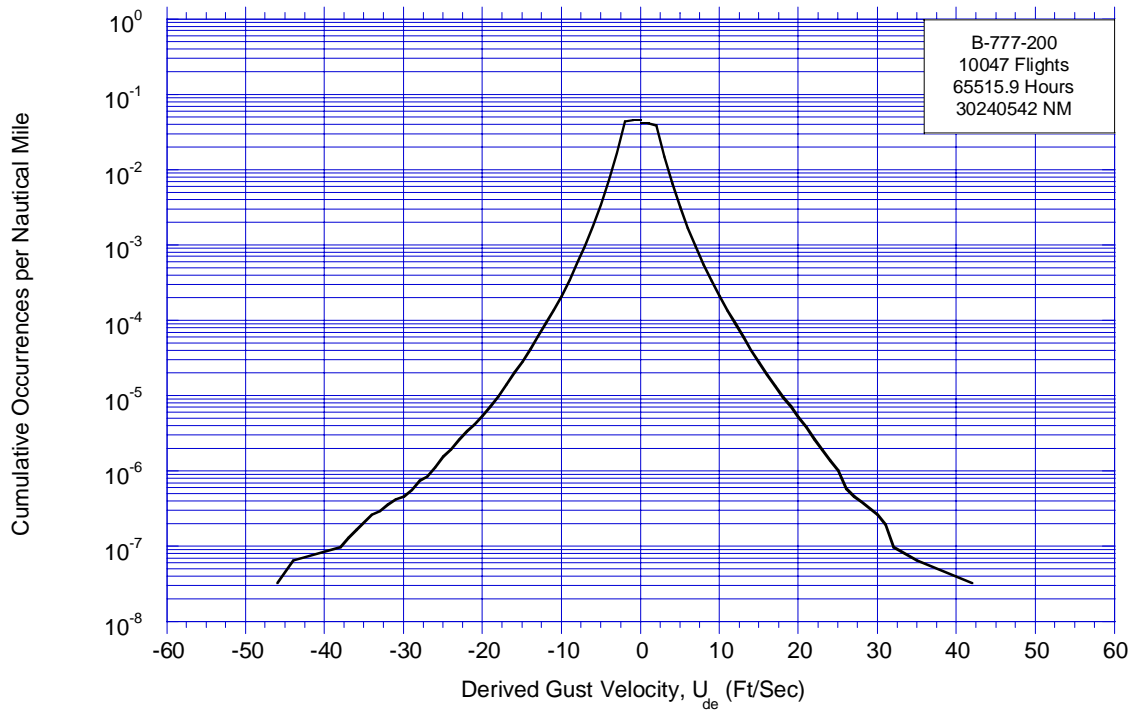


Figure C-56. Cumulative Occurrences of Derived Gust Velocity per Nautical Mile, Flaps Retracted

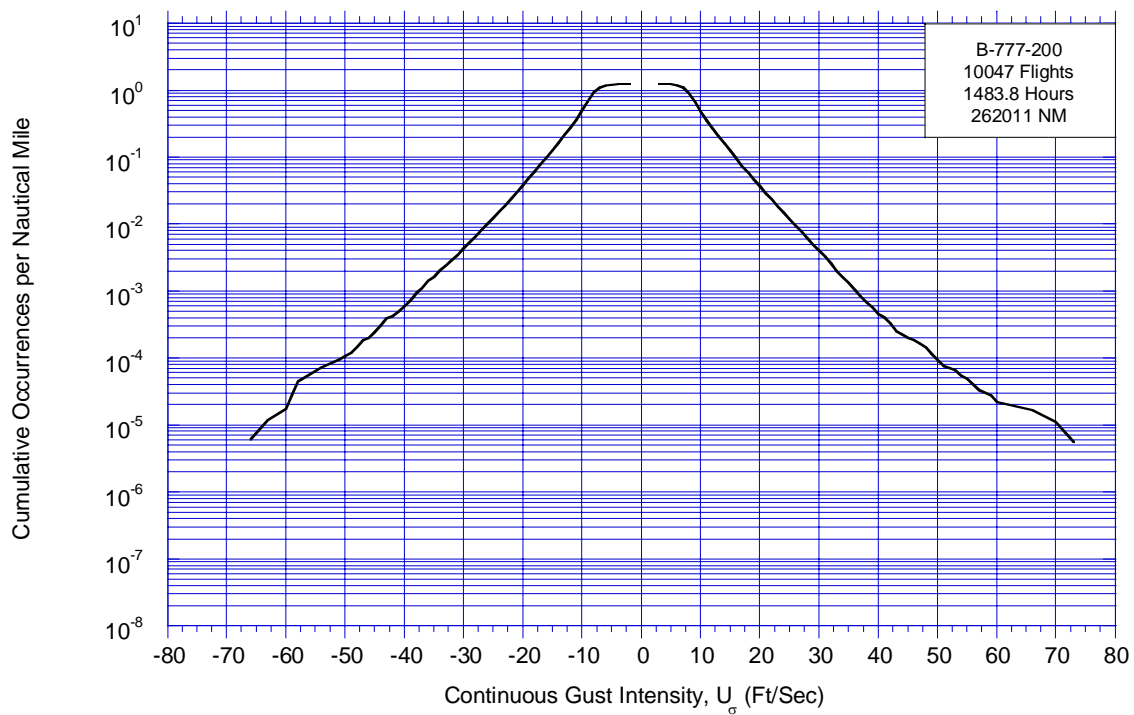


Figure C-57. Cumulative Occurrences of Continuous Gust Intensity per Nautical Mile, Flaps Extended

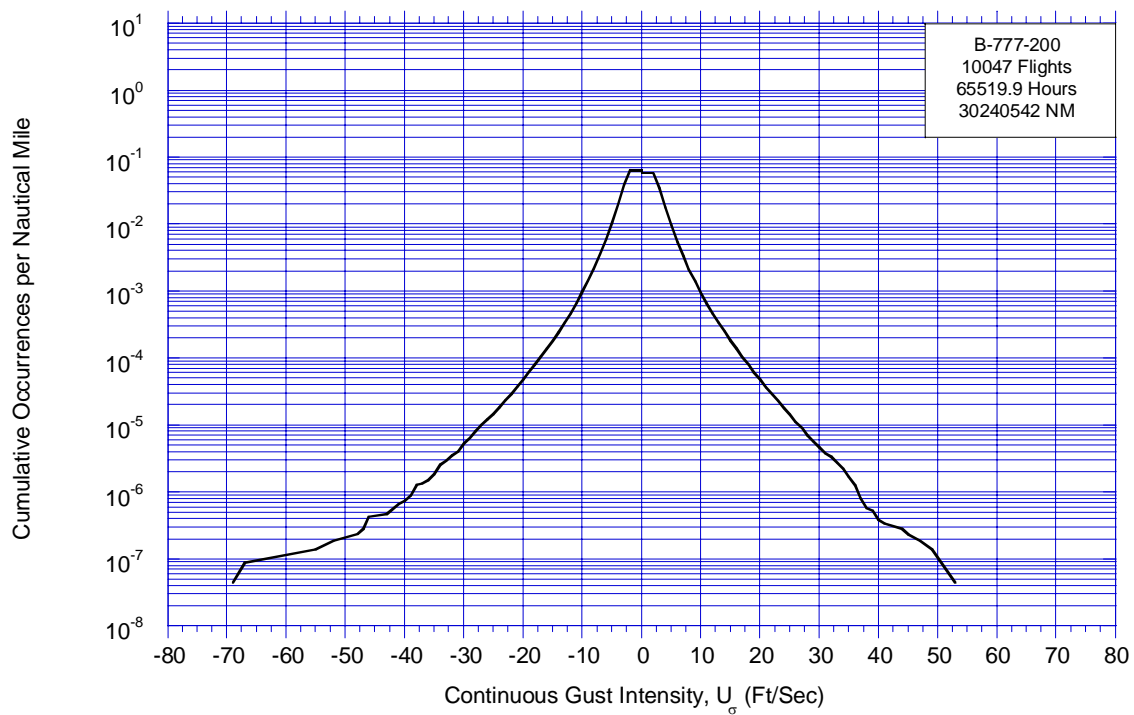


Figure C-58. Cumulative Occurrences of Continuous Gust Intensity per Nautical Mile, Flaps Retracted

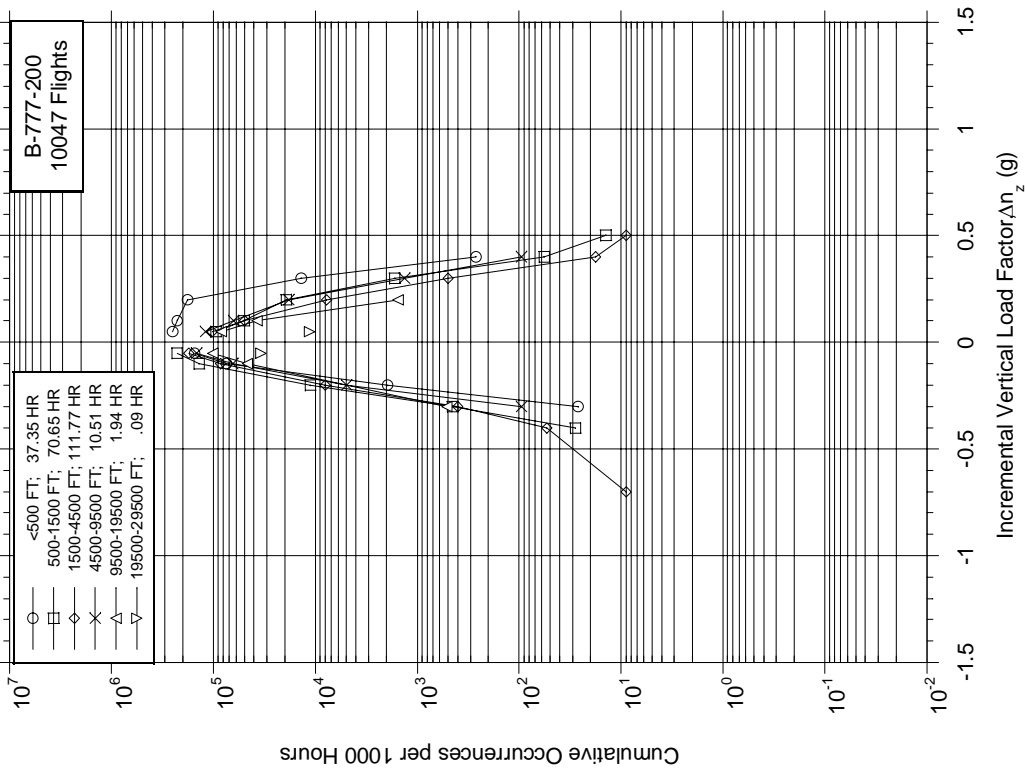


Figure C-59. Cumulative Occurrences of Incremental Vertical Maneuver Load Factor per 1000 Hours During Departure by Altitude

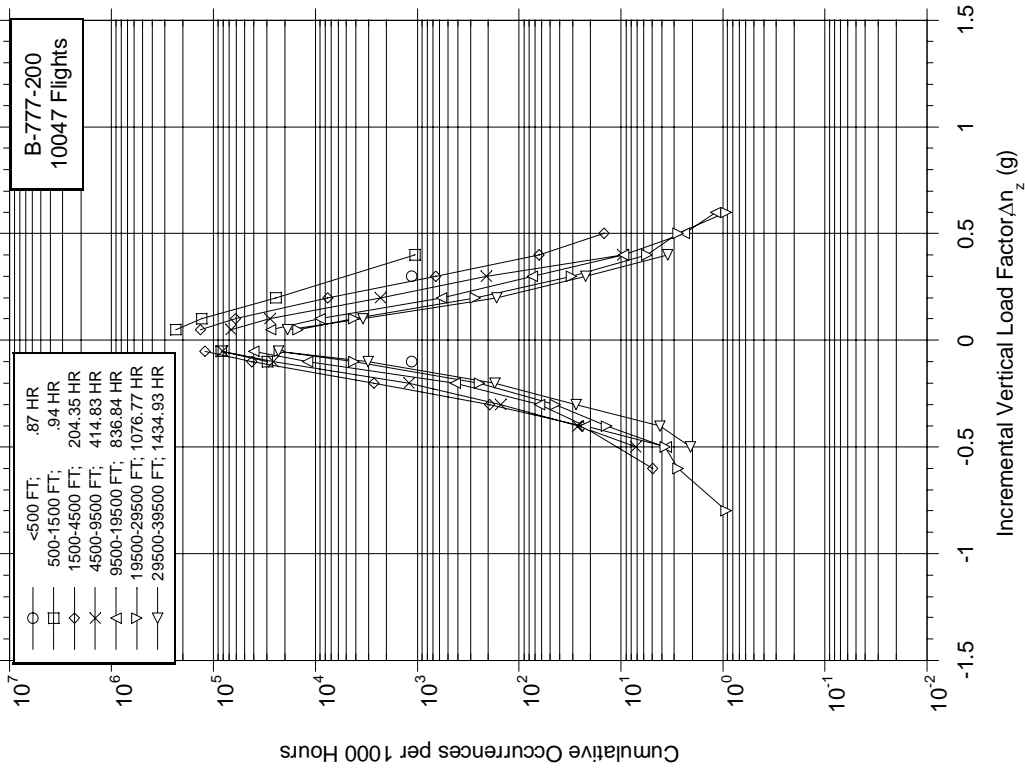


Figure C-60. Cumulative Occurrences of Incremental Vertical Maneuver Load Factor per 1000 Hours During Climb by Altitude

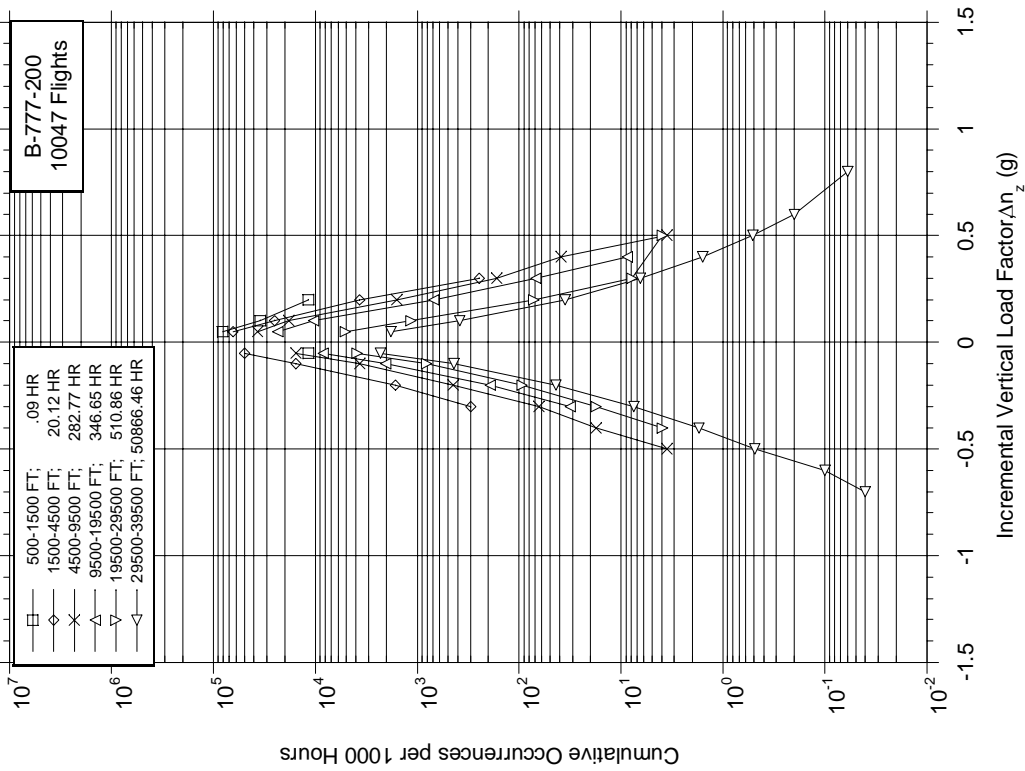


Figure C-61. Cumulative Occurrences of Incremental Vertical Maneuver Load Factor per 1000 Hours During Cruise by Altitude

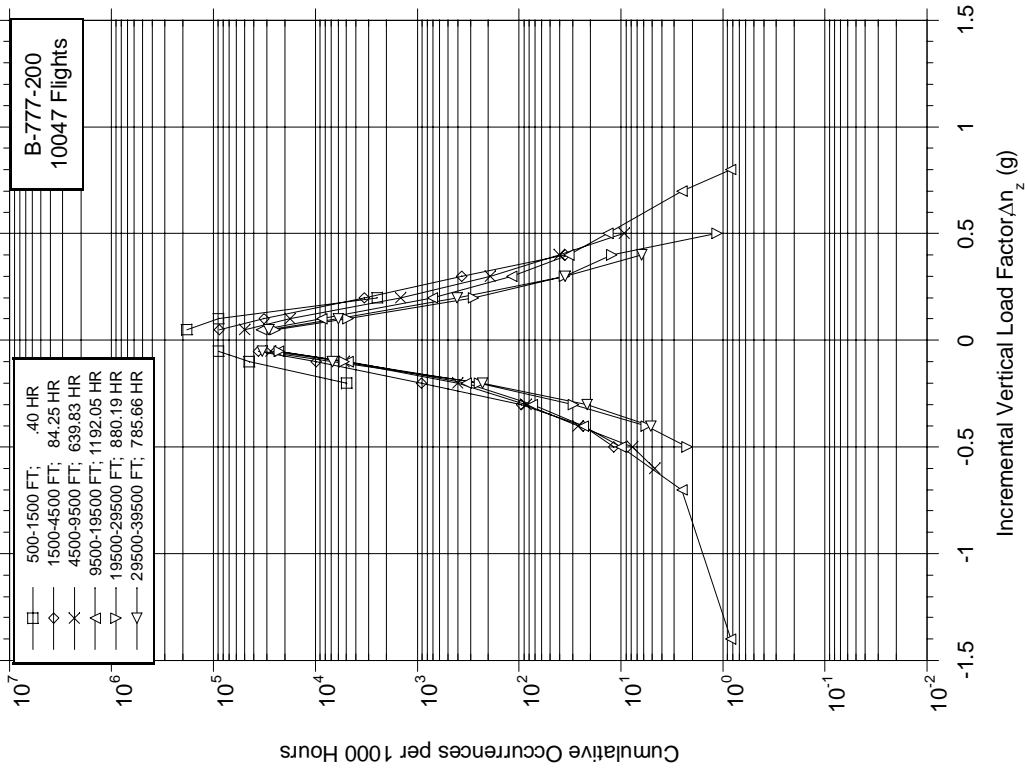


Figure C-62. Cumulative Occurrences of Incremental Vertical Maneuver Load Factor per 1000 Hours During Descent by Altitude

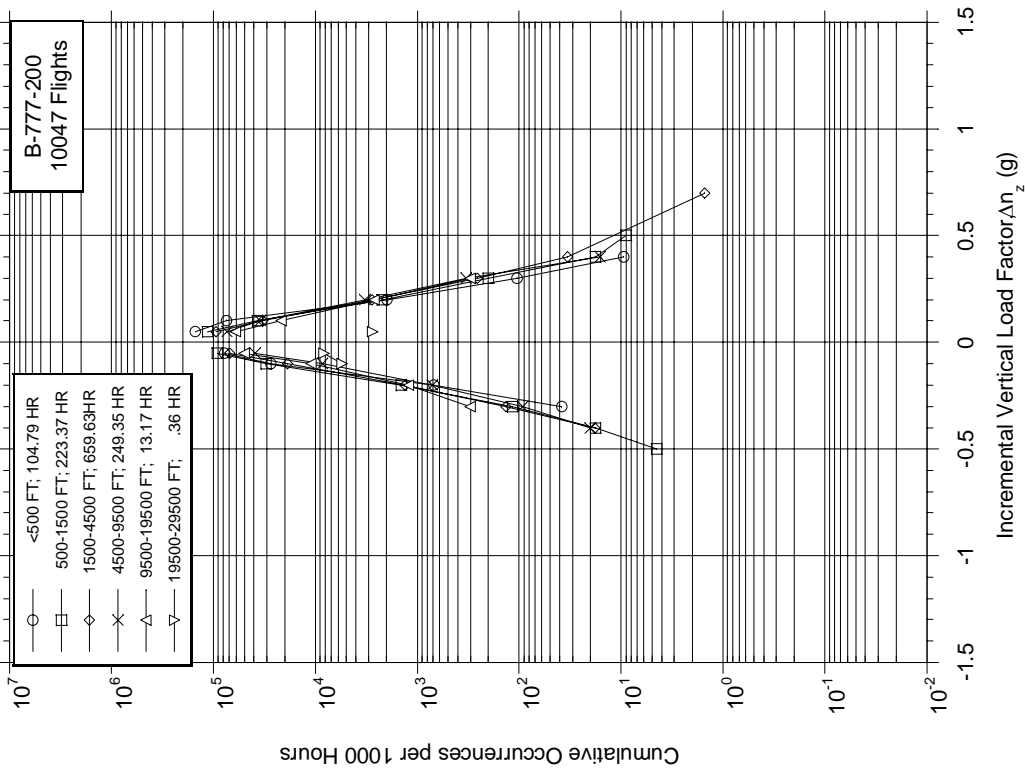


Figure C-63. Cumulative Occurrences of Incremental Vertical Maneuver Load Factor per 1000 Hours During Approach by Altitude

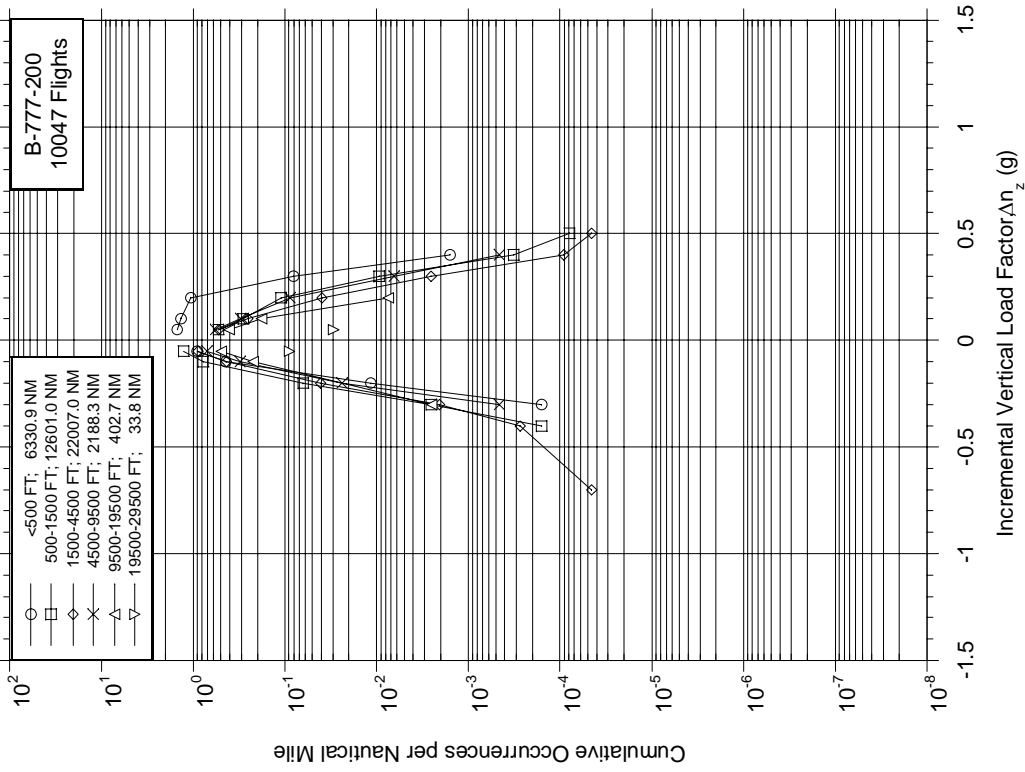


Figure C-64. Cumulative Occurrences of Incremental Vertical Maneuver Load Factor per Nautical Mile During Departure by Altitude

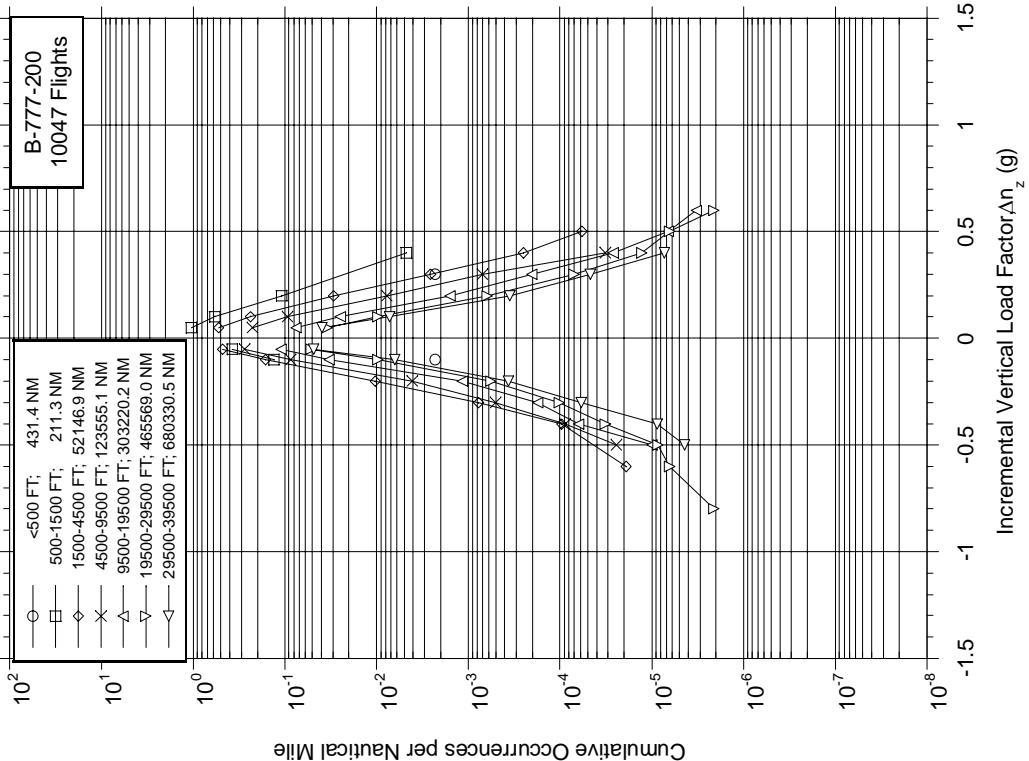


Figure C-65. Cumulative Occurrences of Incremental Vertical Maneuver Load Factor per Nautical Mile During Climb by Altitude

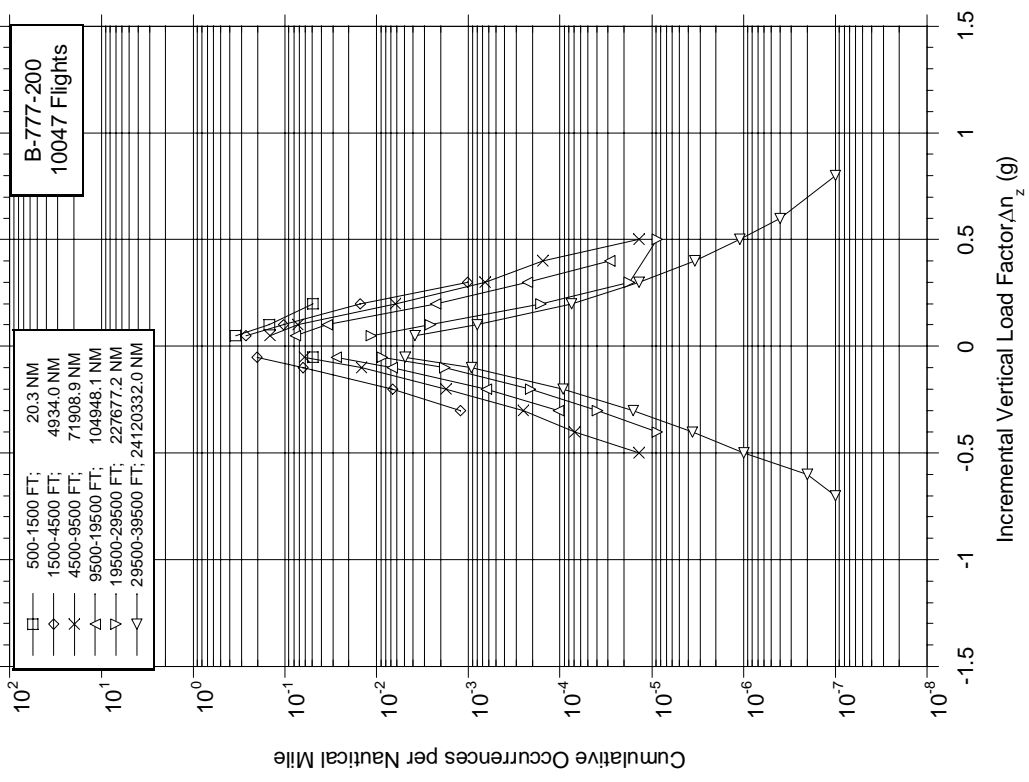


Figure C-66. Cumulative Occurrences of Incremental Vertical Maneuver Load Factor per Nautical Mile During Cruise by Altitude

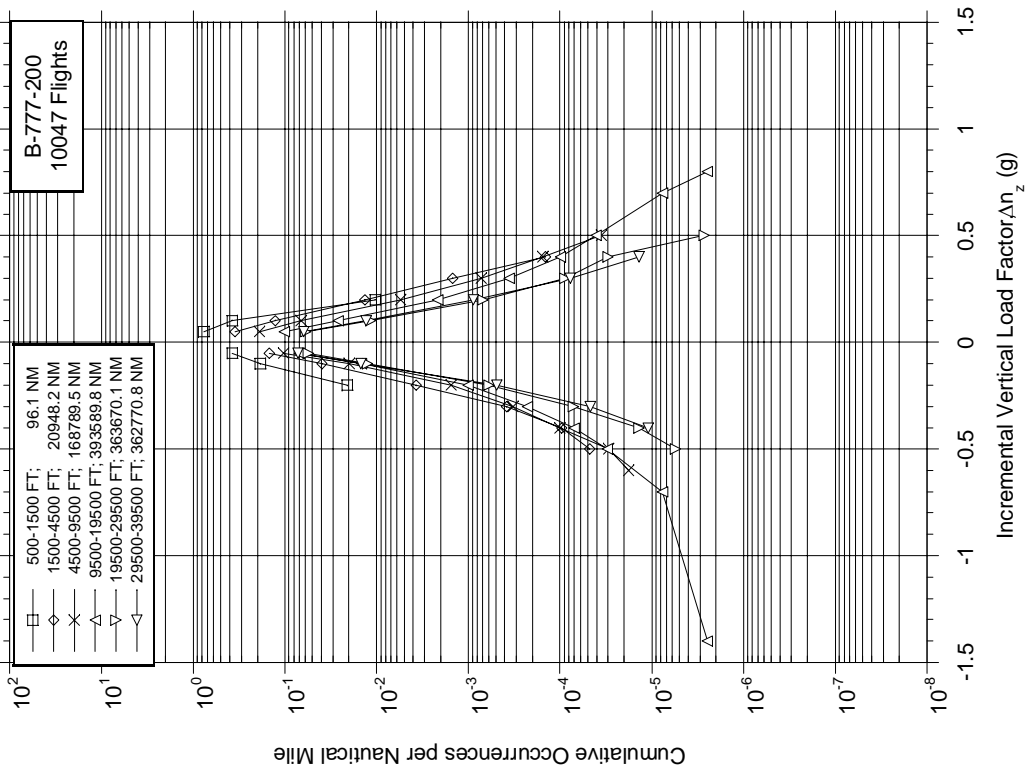


Figure C-67. Cumulative Occurrences of Incremental Vertical Maneuver Load Factor per Nautical Mile During Descent by Altitude

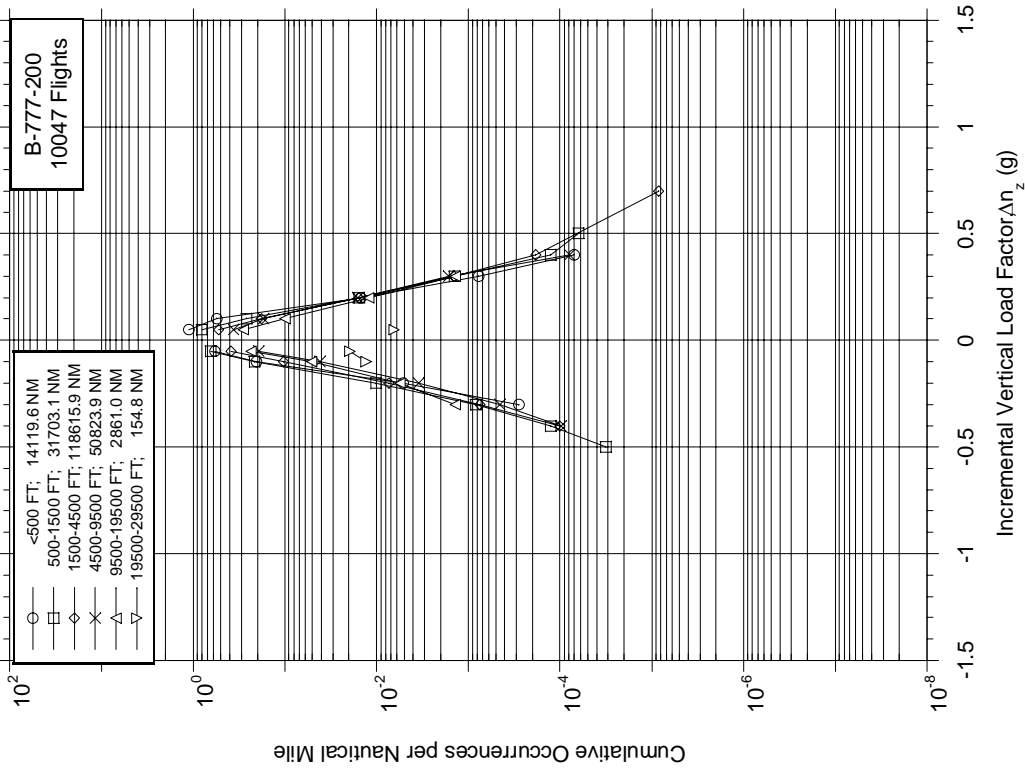


Figure C-68. Cumulative Occurrences of Incremental Vertical Maneuver Load Factor per Nautical Mile During Approach by Altitude

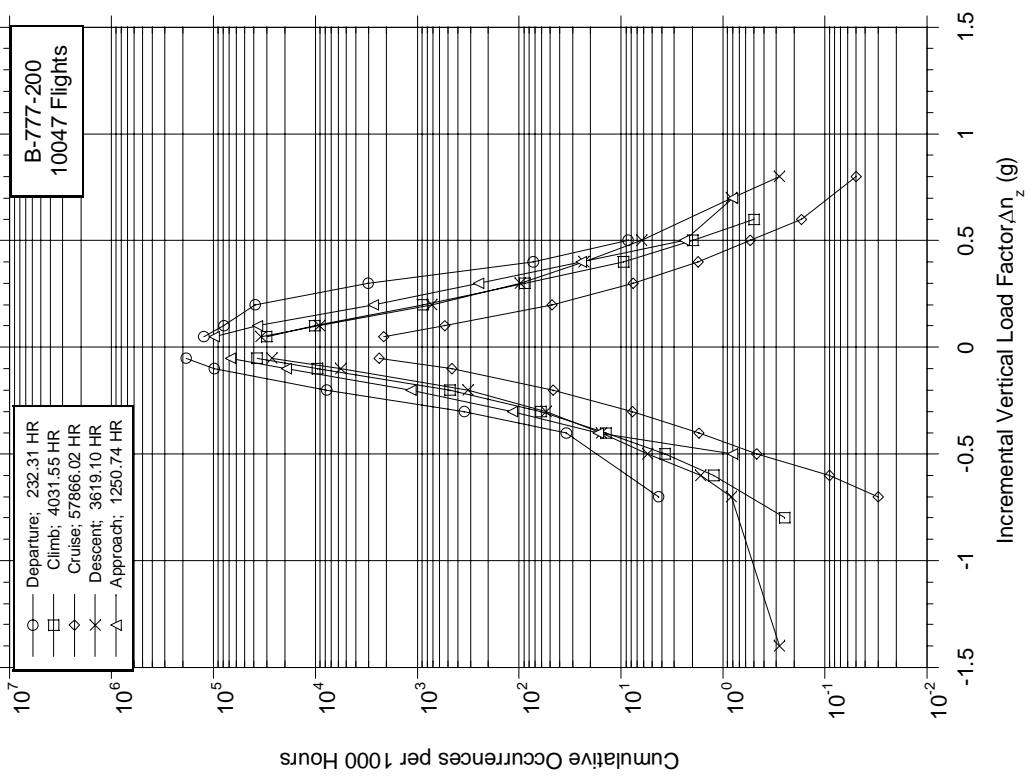


Figure C-69. Cumulative Occurrences of Incremental Vertical Maneuver Load Factor per 1000 Hours by Flight Phase

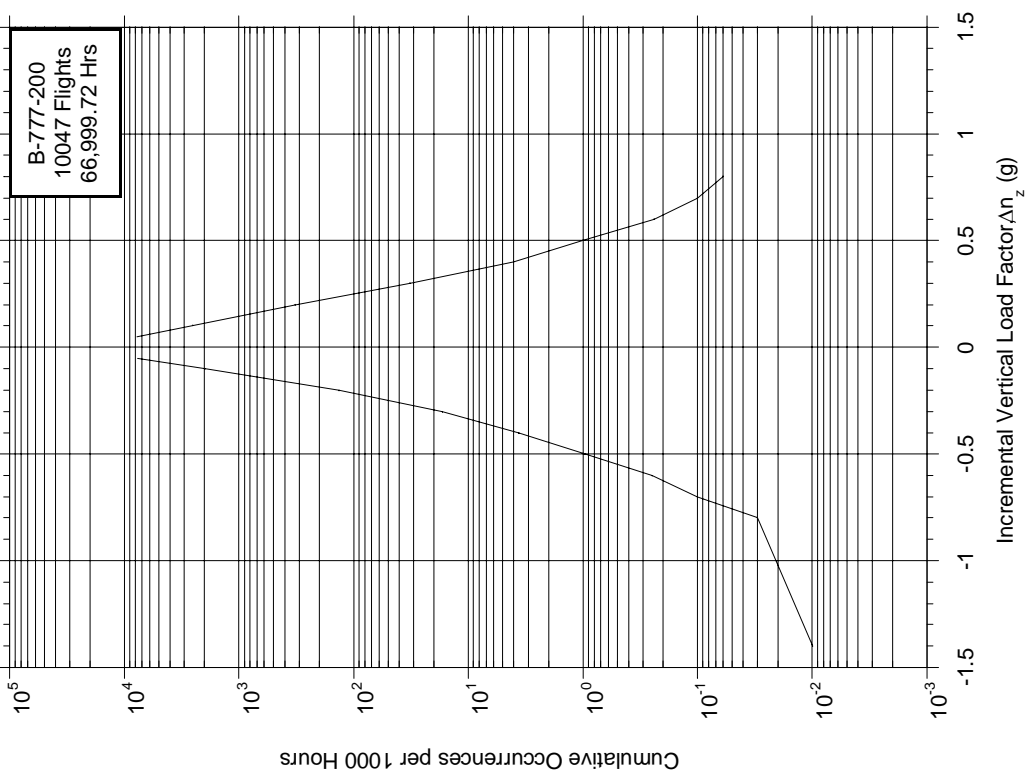


Figure C-70. Cumulative Occurrences of Incremental Vertical Maneuver Load Factor per 1000 Hours, Combined Flight Phases

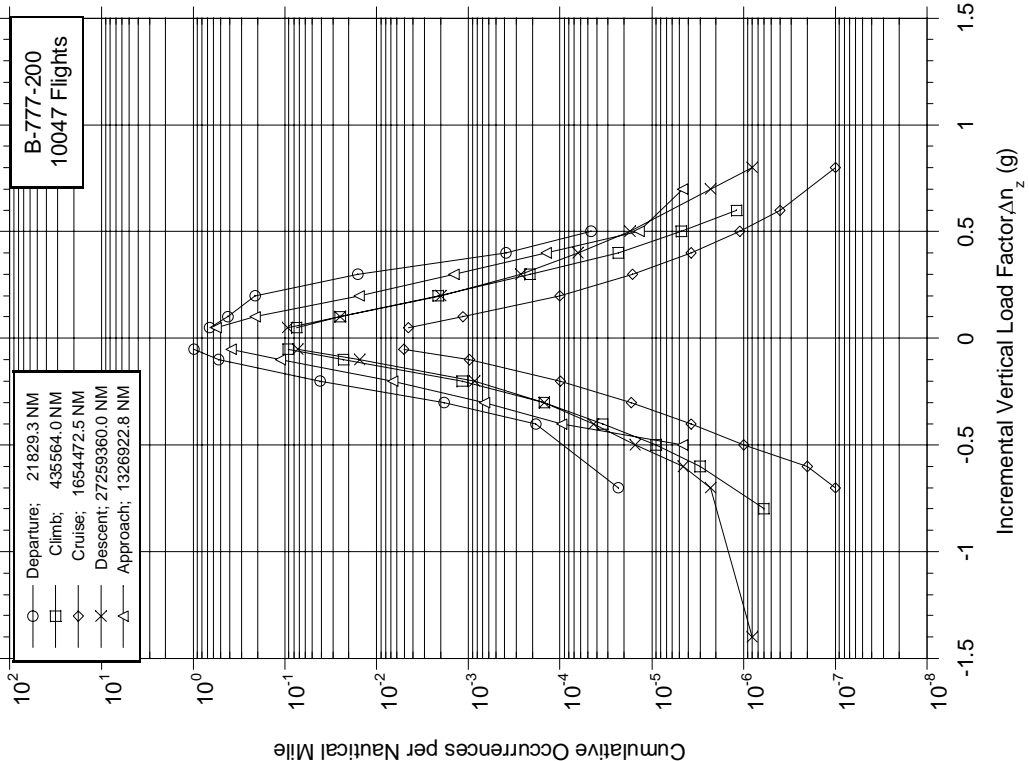


Figure C-71. Cumulative Occurrences of Incremental Vertical Maneuver Load Factor per Nautical Mile by Flight Phase

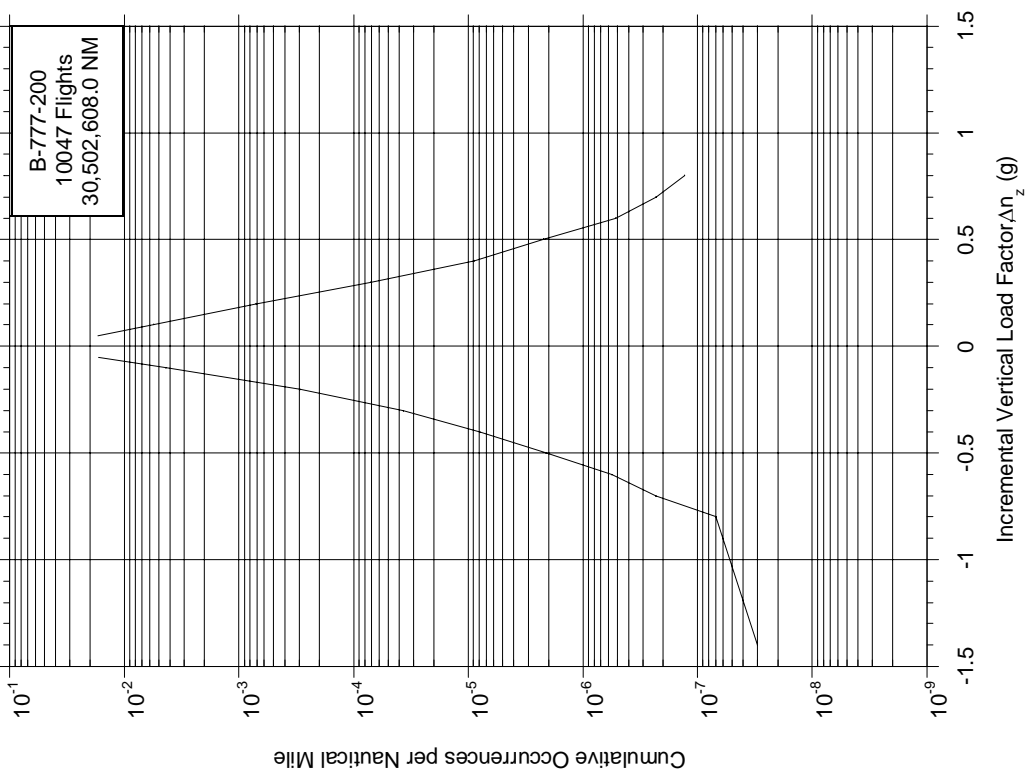


Figure C-72. Cumulative Occurrences of Incremental Vertical Maneuver Load Factor per Nautical Mile, Combined Flight Phases

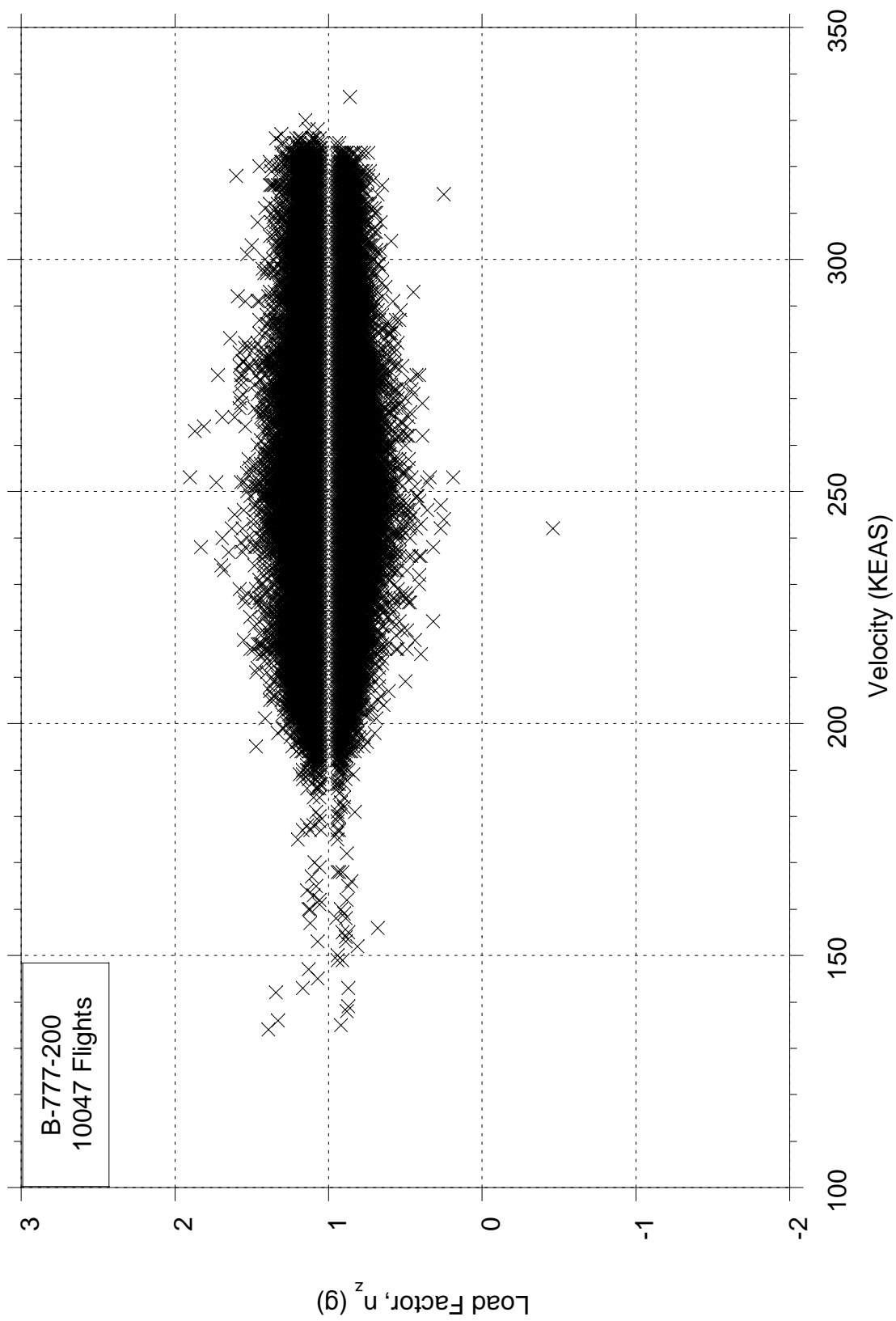


Figure C-73. Maneuver Load Factor and Coincident Speed for Flaps Retracted

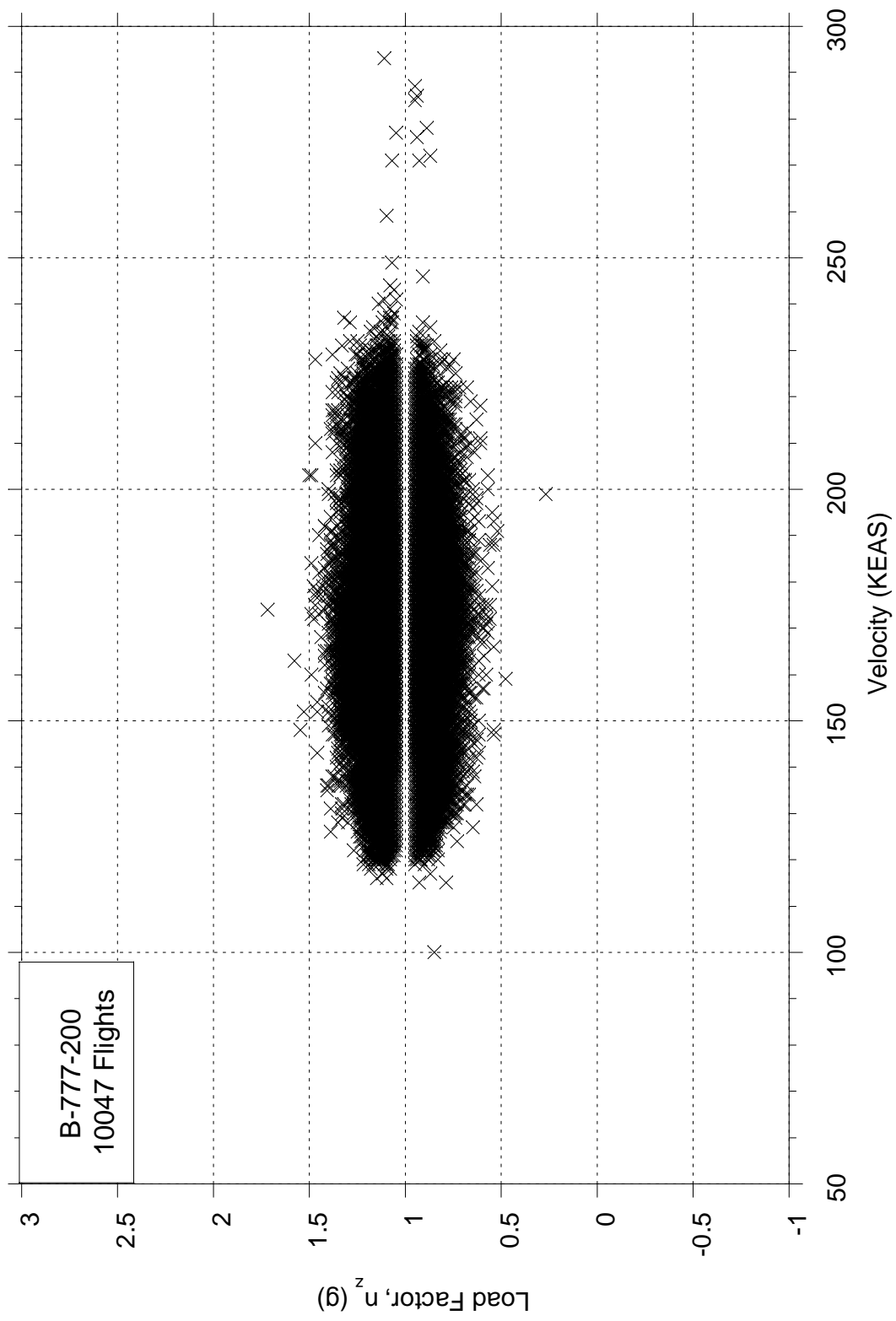


Figure C-74. Maneuver Load Factor and Coincident Speed for Flaps Extended

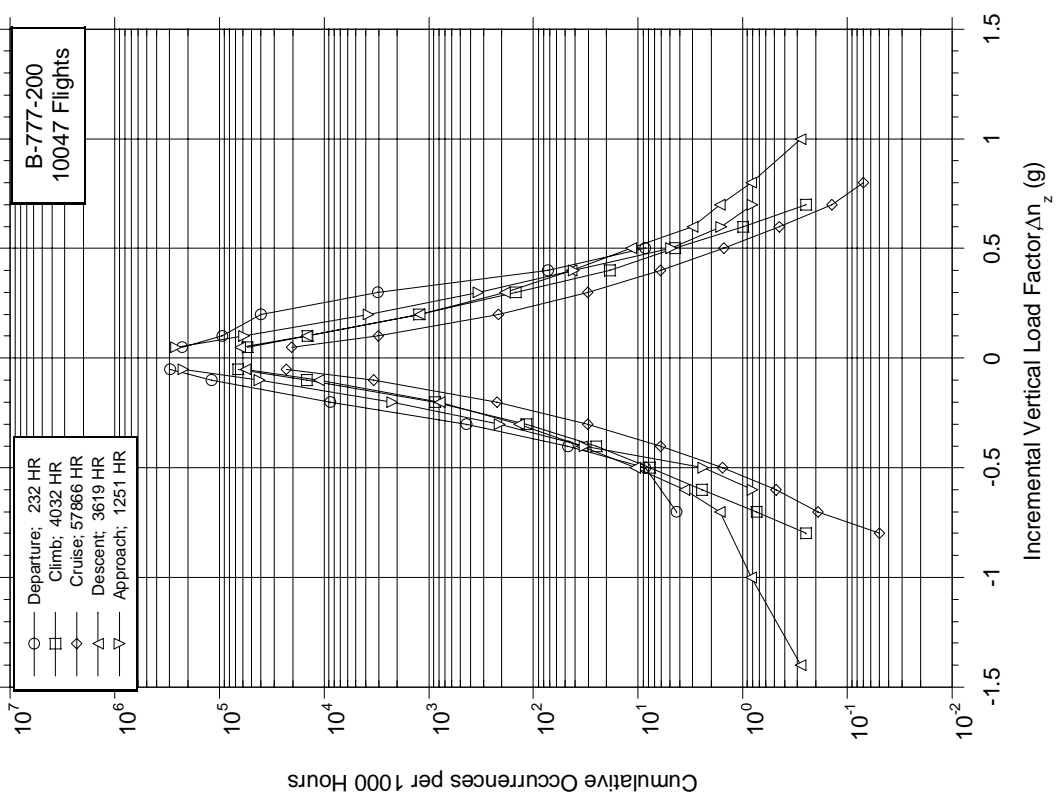


Figure C-75. Cumulative Occurrences of Incremental Vertical Load Factor per 1000 Hours by Flight Phase

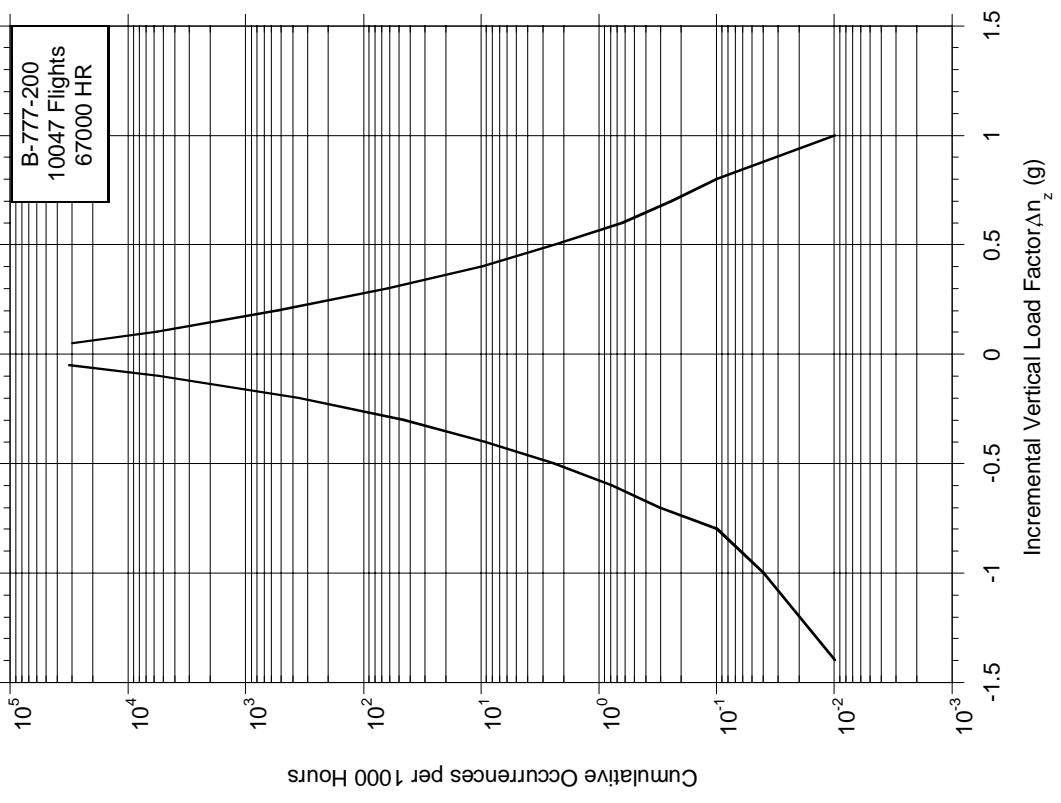


Figure C-76. Cumulative Occurrences of Incremental Vertical Load Factor per 1000 Hours, Combined Flight Phases

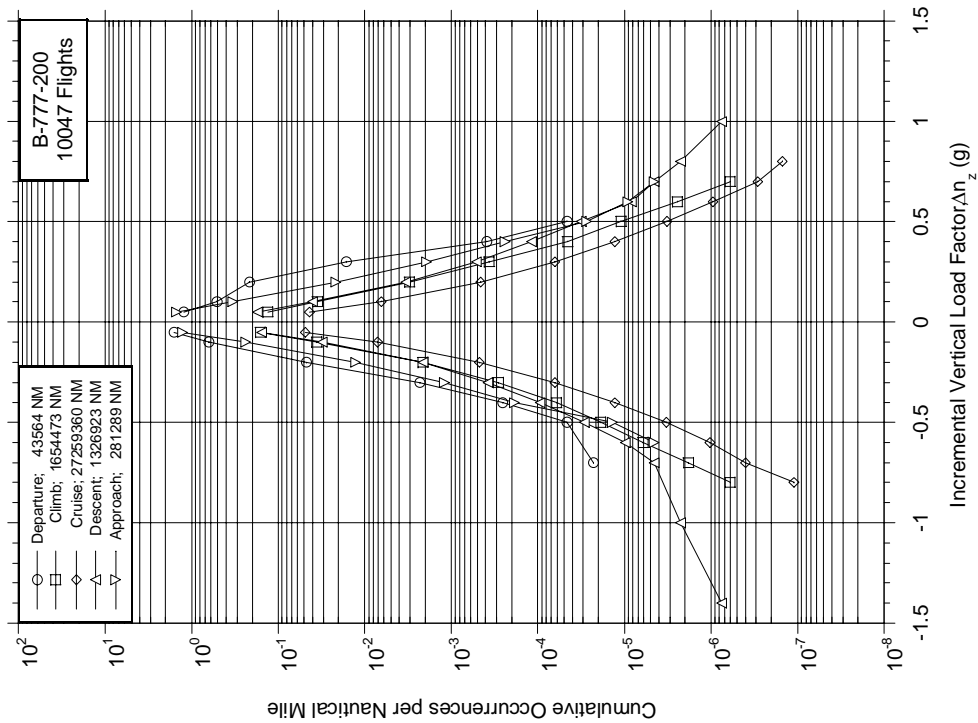


Figure C-77. Cumulative Occurrences of Incremental Vertical Load Factor per Nautical Mile by Flight Phase

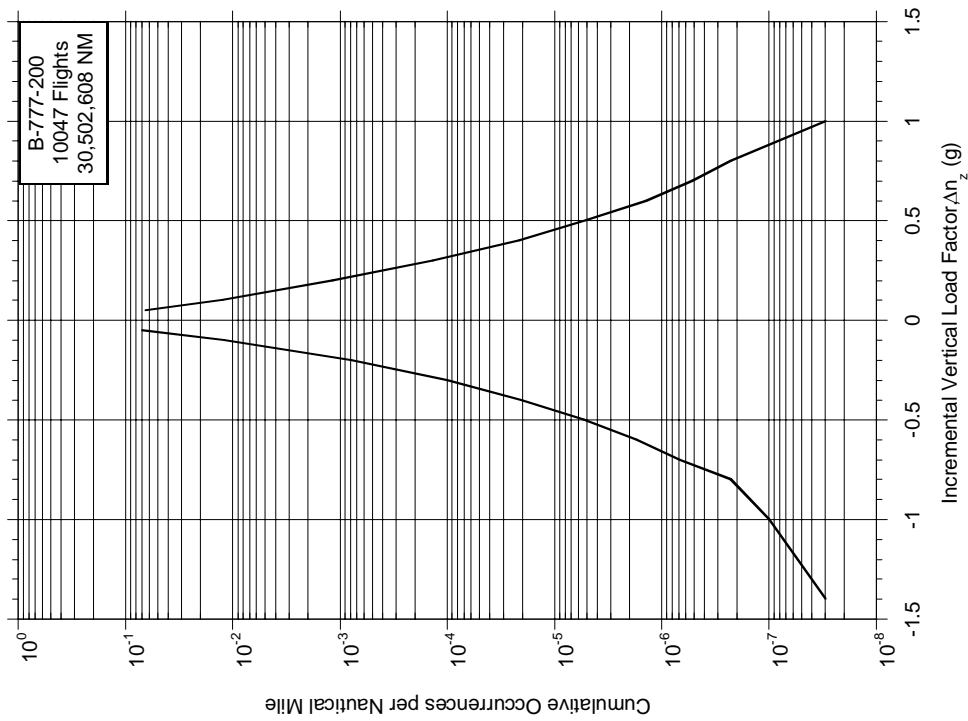


Figure C-78. Cumulative Occurrences of Incremental Vertical Load Factor per Nautical Mile, Combined Flight Phases

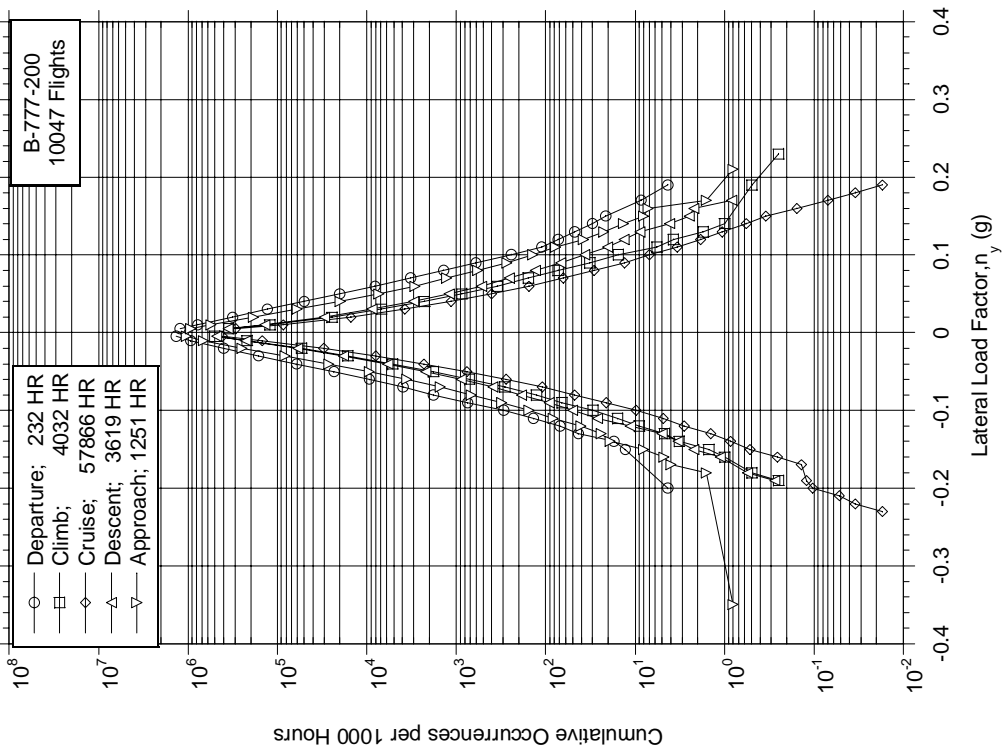


Figure C-79. Cumulative Occurrences of Lateral Load Factor per 1000 Hours by Flight Phase

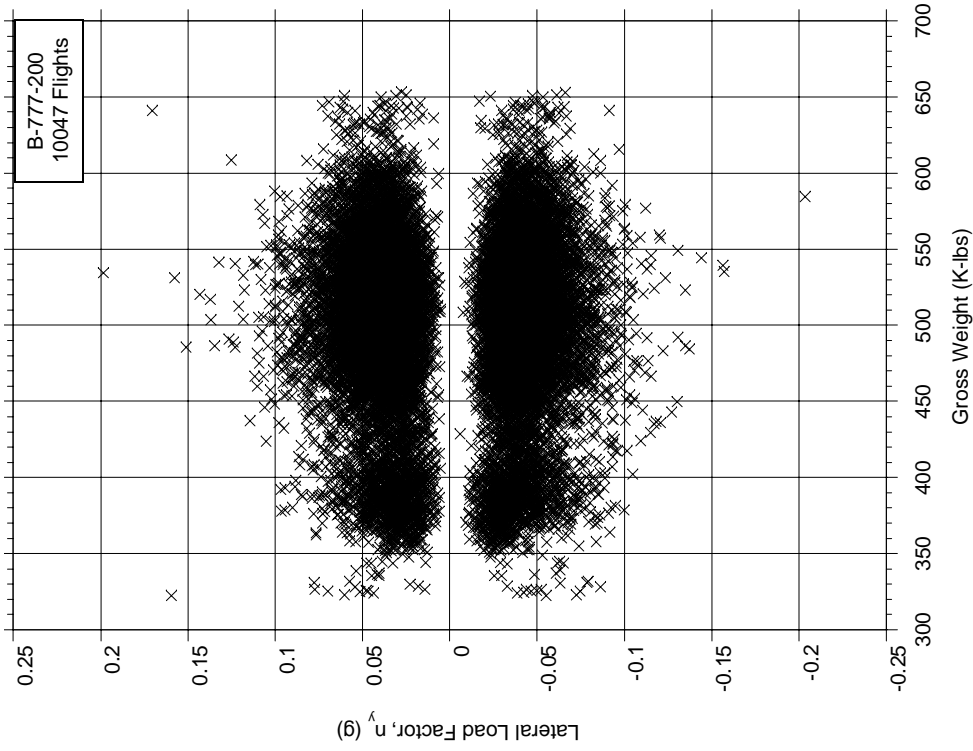


Figure C-80. Maximum Lateral Load Factor vs Coincident Gross Weight During Departure

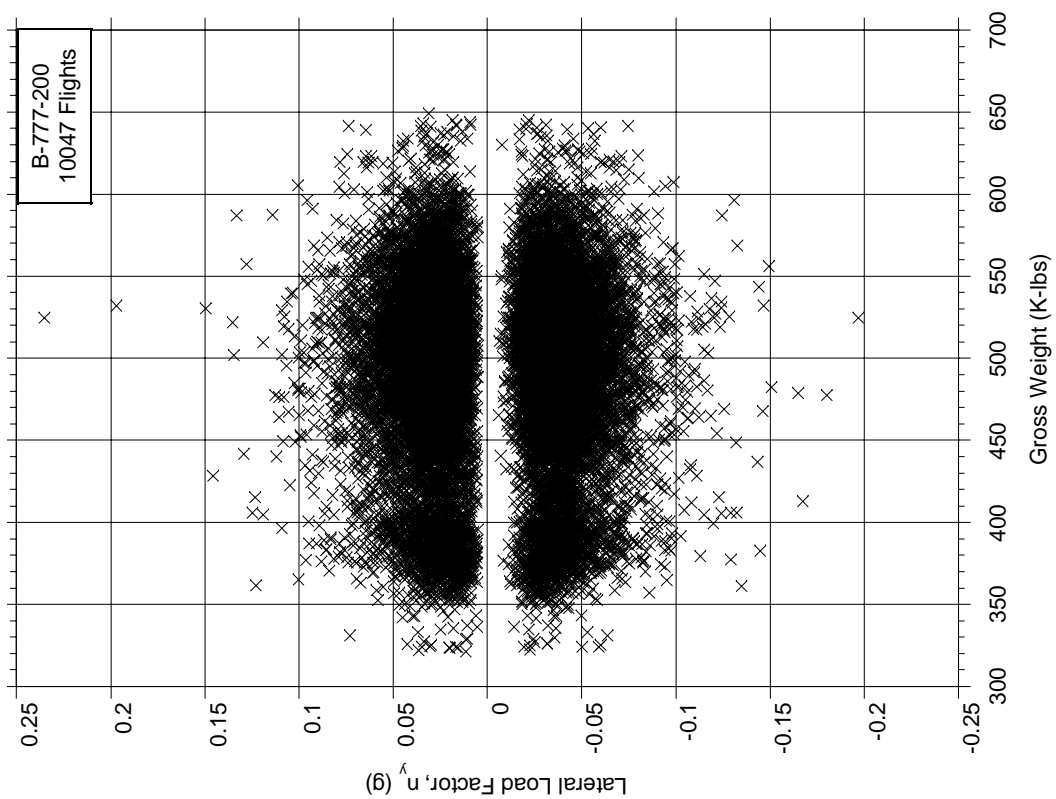


Figure C-81. Maximum Lateral Load Factor vs Coincident Gross Weight During Climb

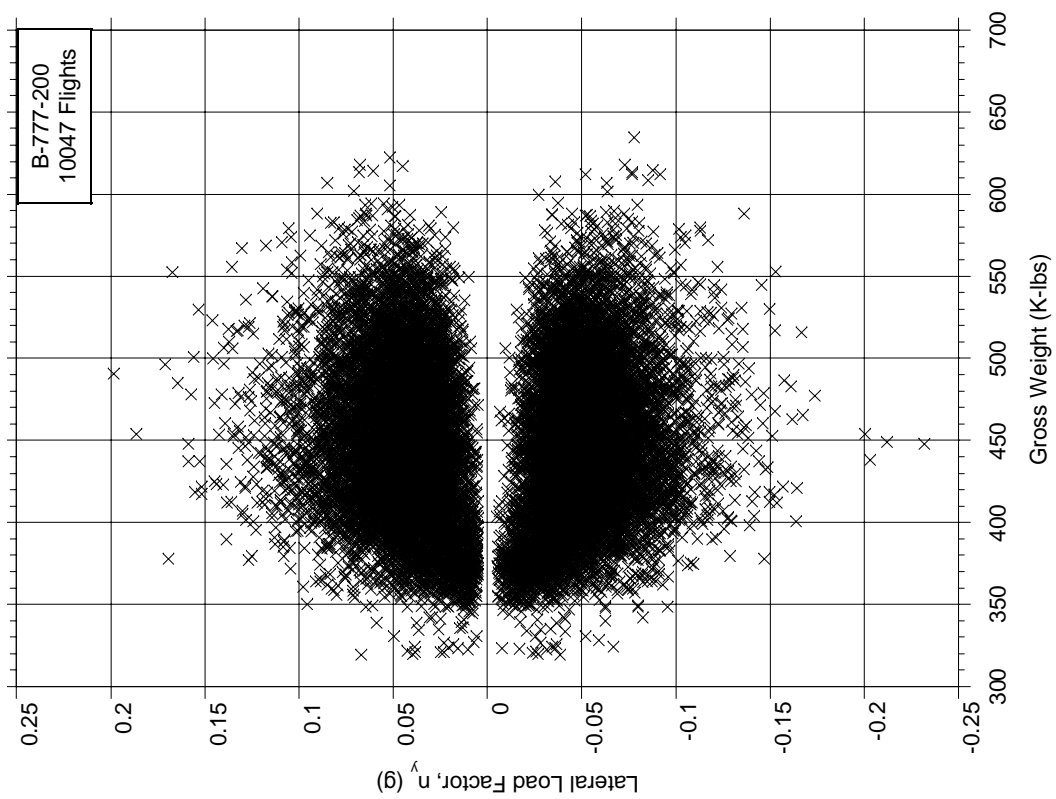


Figure C-82. Maximum Lateral Load Factor vs Coincident Gross Weight During Cruise

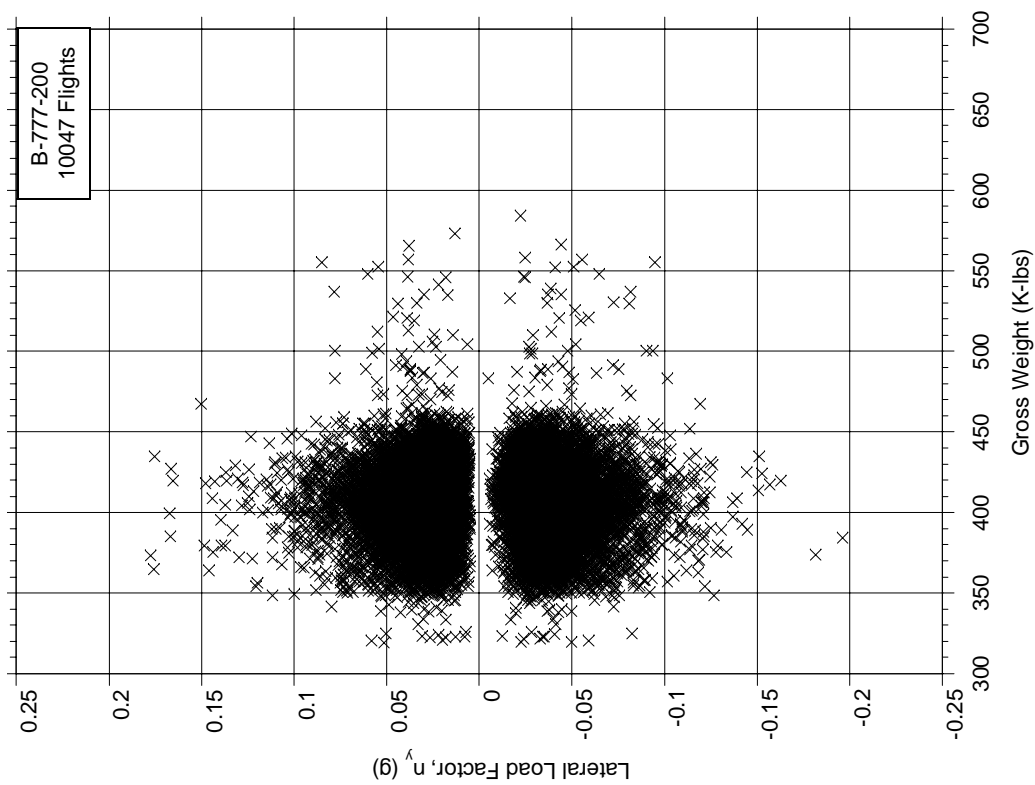


Figure C-83. Maximum Lateral Load Factor vs Coincident Gross Weight During Descent

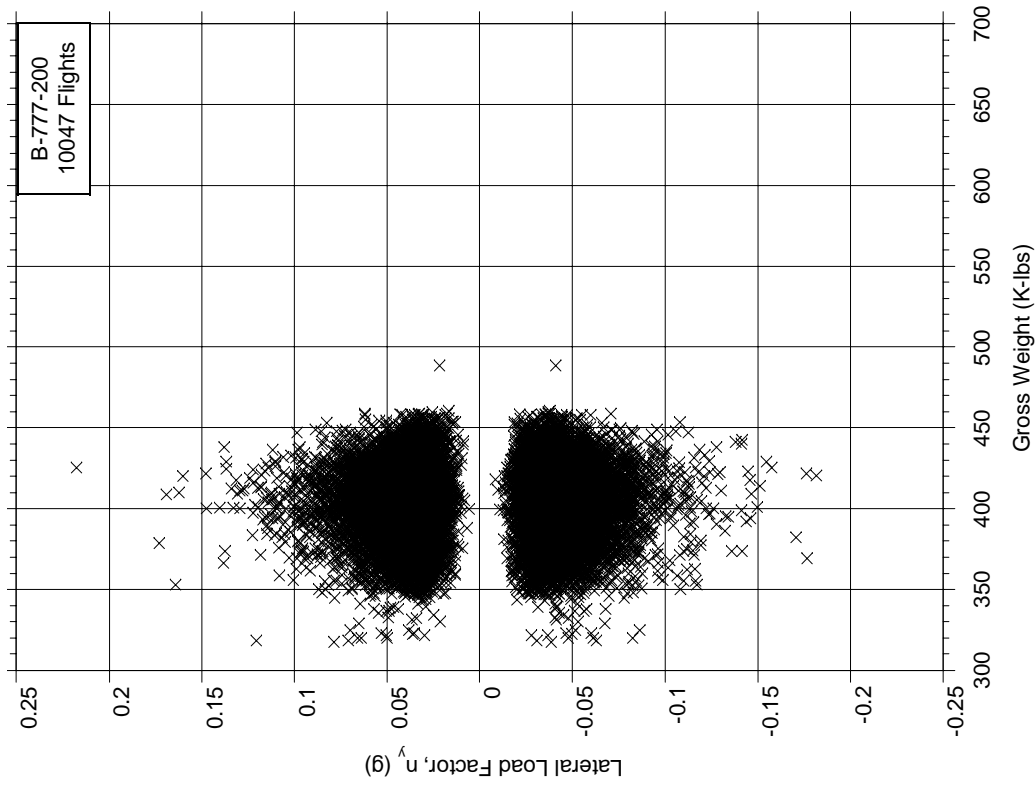


Figure C-84. Maximum Lateral Load Factor vs Coincident Gross Weight During Approach

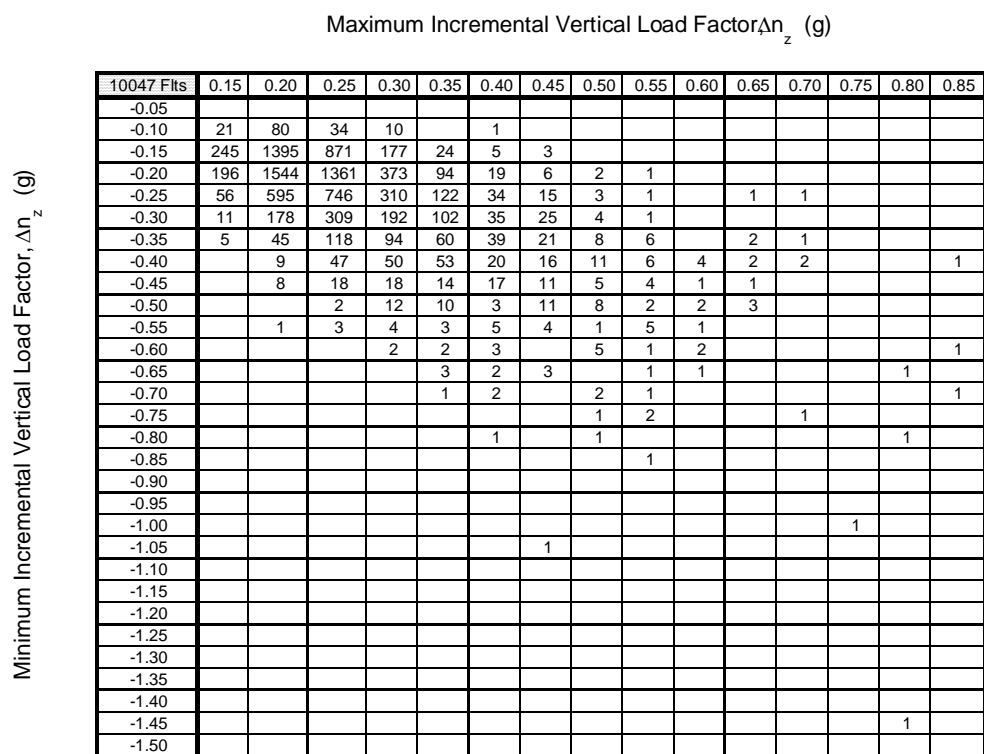


Figure C-85. Ground-Air-Ground Cycle Occurrences of Maximum and Minimum Incremental Vertical Load Factor

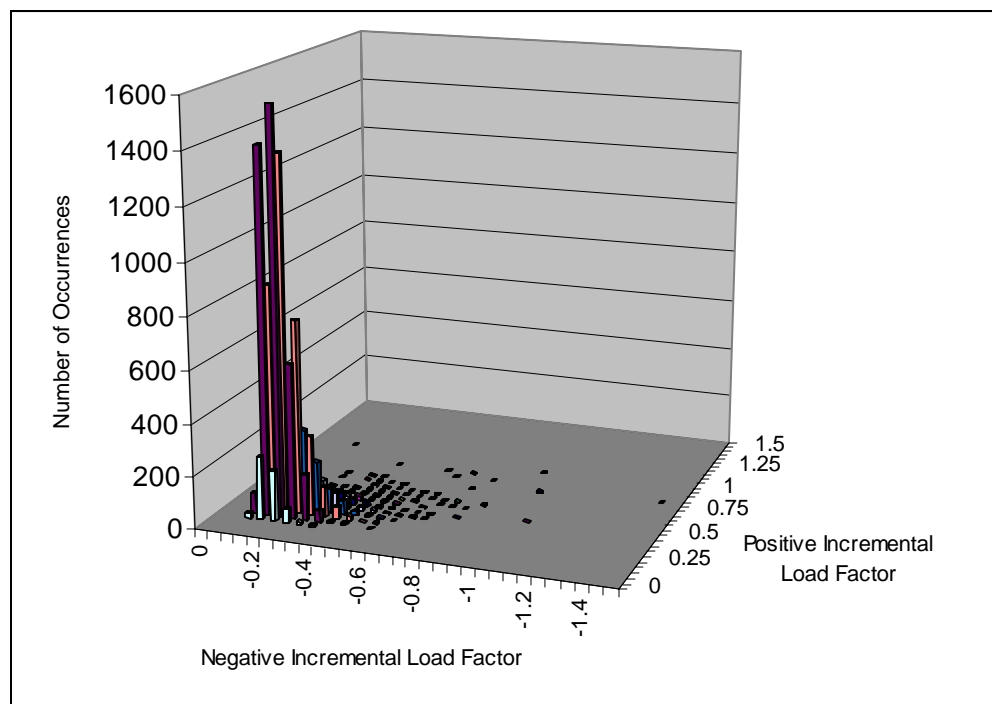


Figure C-86. 3-D Plot of Ground-Air-Ground Cycles

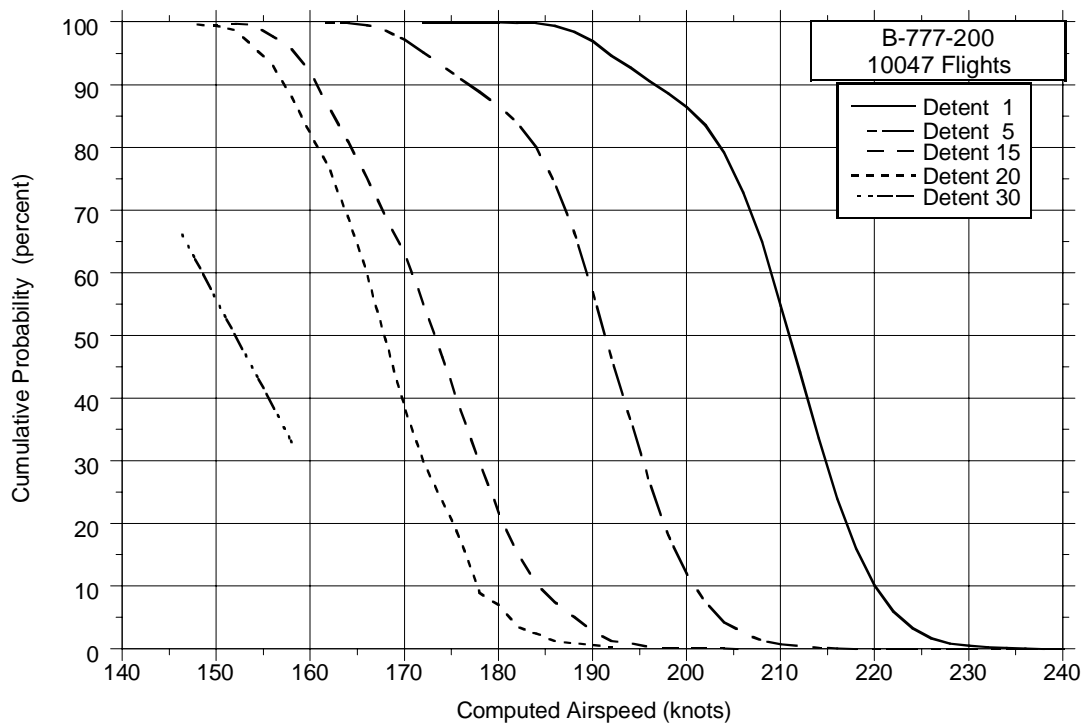


Figure C-87. Cumulative Probability of Maximum Airspeed in Flap Detent During Departure

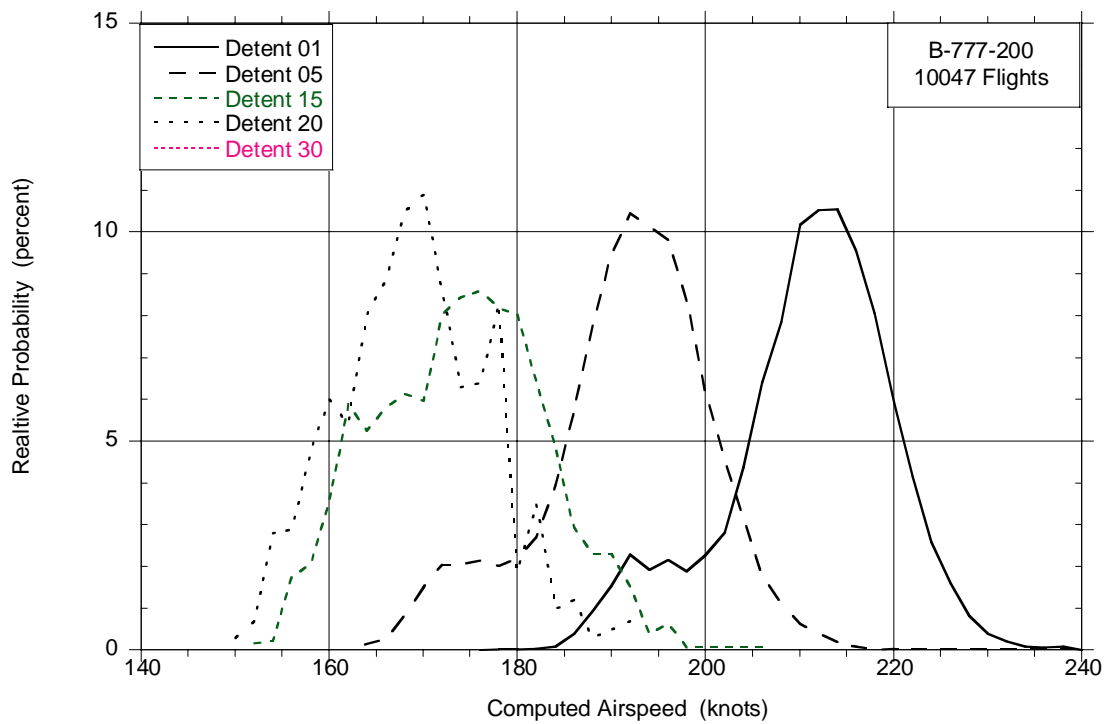


Figure C-88. Relative Probability of Maximum Airspeed in Flap Detent During Departure

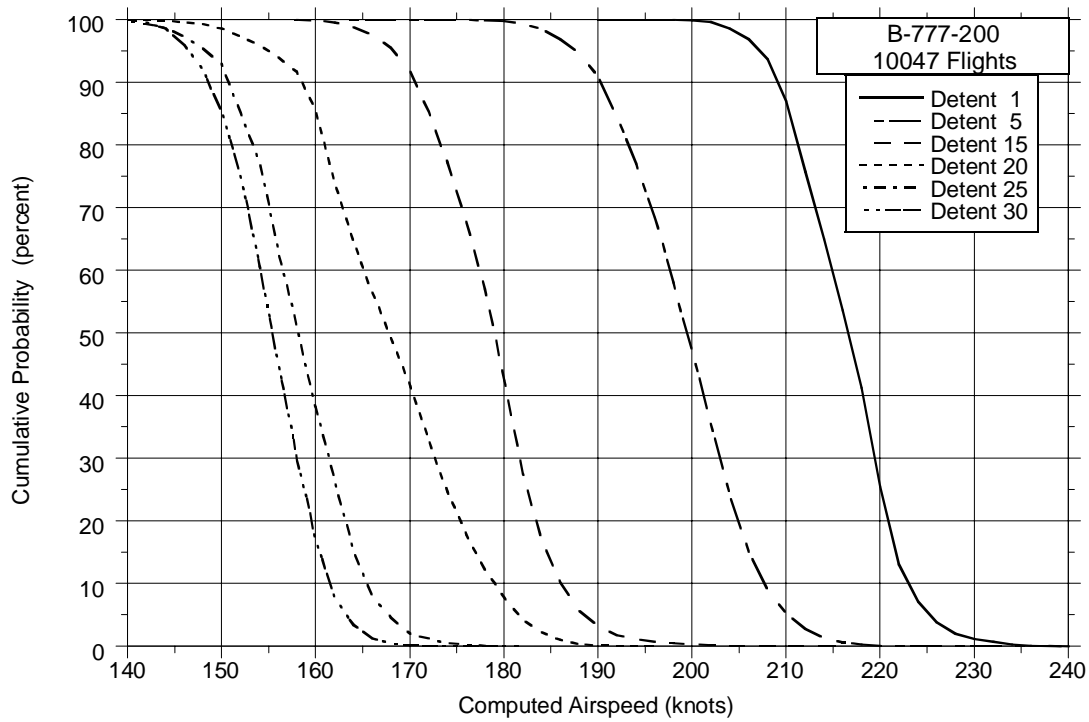


Figure C-89. Cumulative Probability of Maximum Airspeed in Flap Detent During Approach

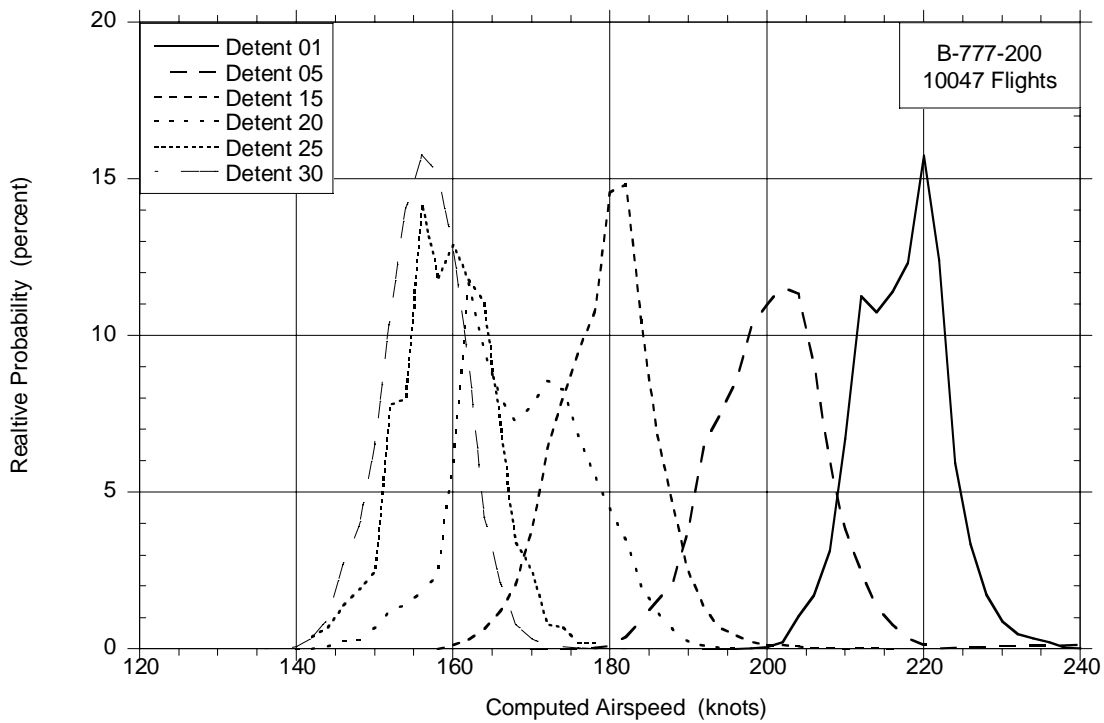


Figure C-90. Relative Probability of Maximum Airspeed in Flap Detent During Approach

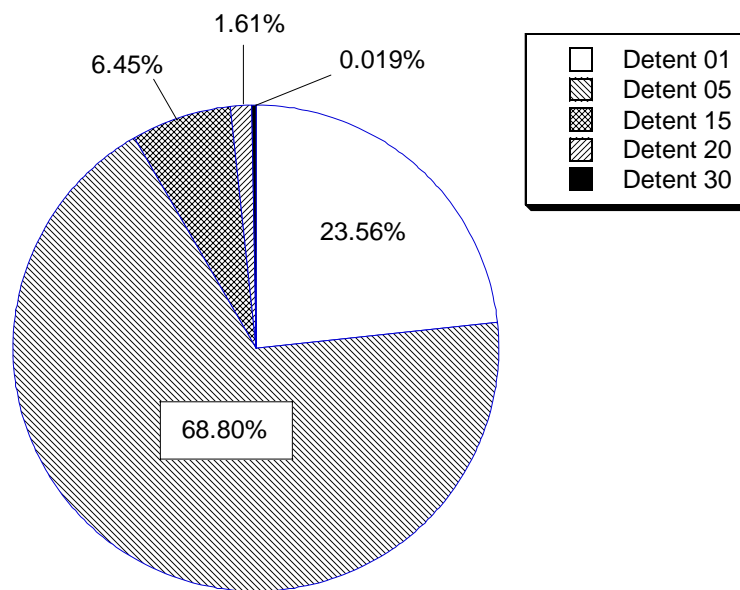


Figure C-91. Percent of Time in Flap Detent During Departure

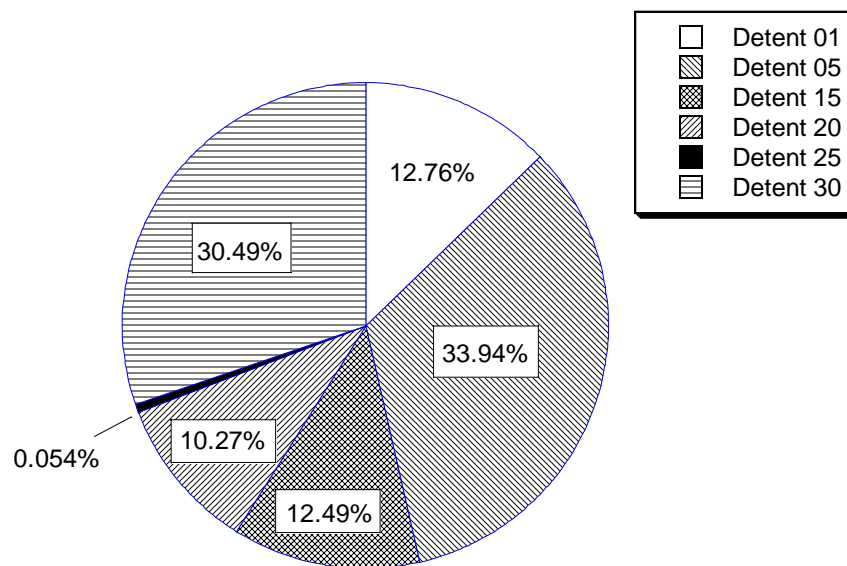


Figure C-92. Percent of Time in Flap Detent During Approach

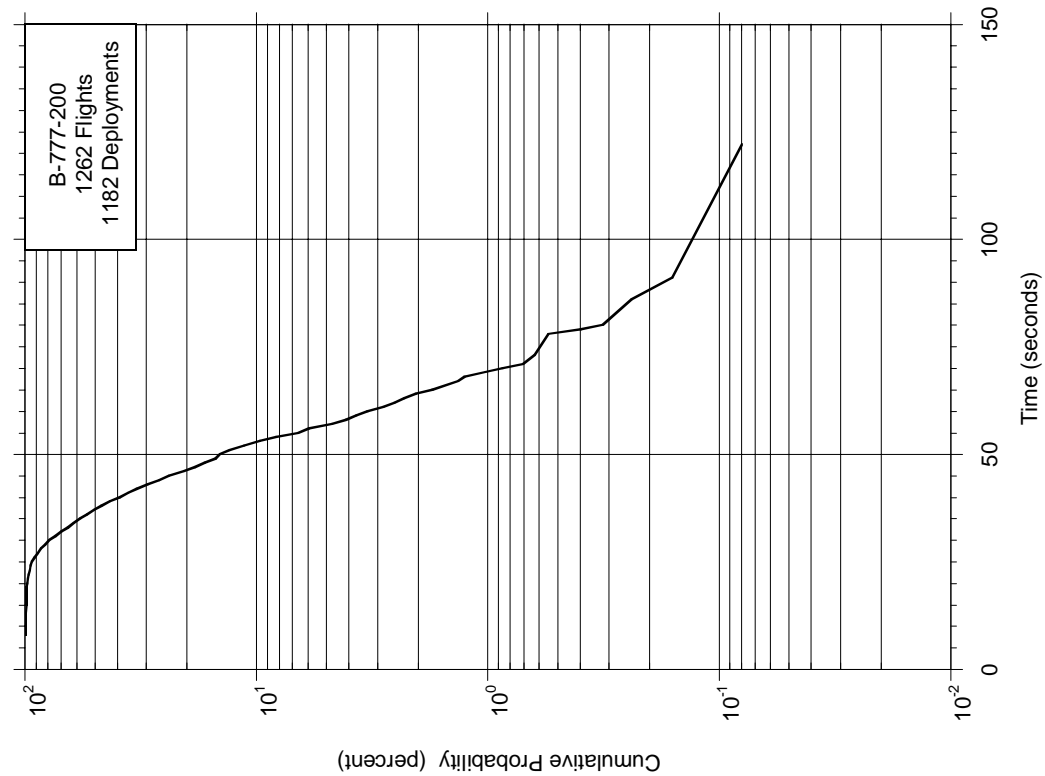


Figure C-93. Cumulative Probability of Time With Thrust Reversers Deployed

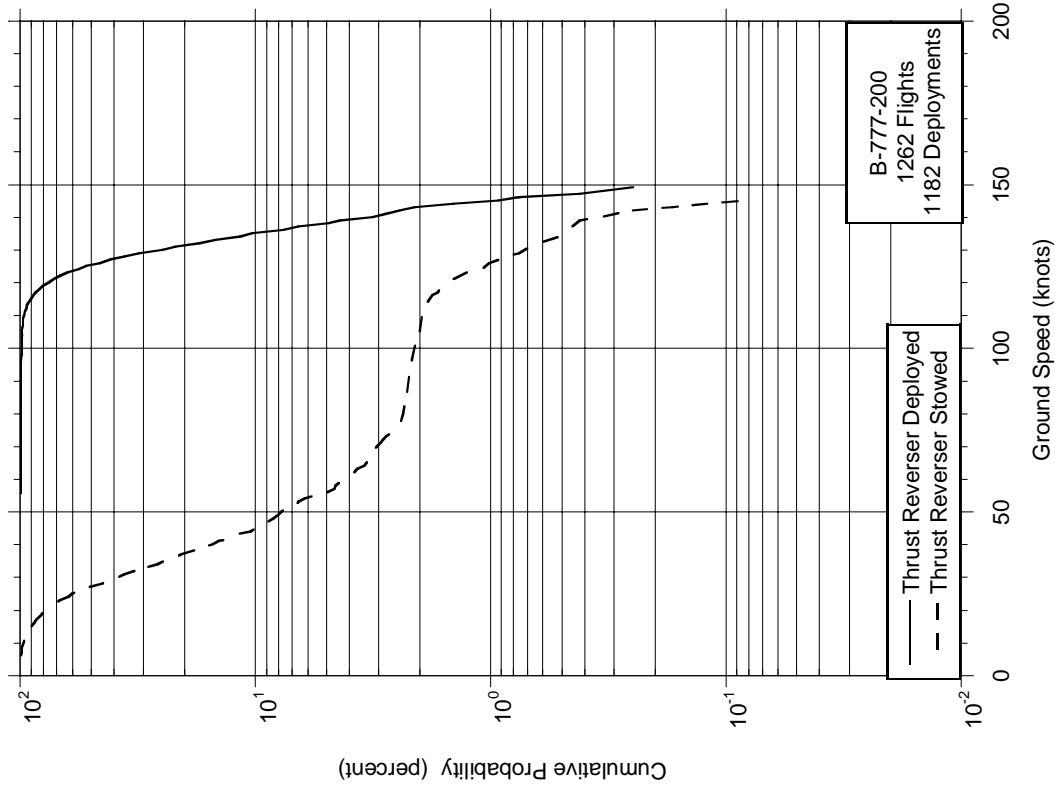


Figure C-94. Cumulative Probability of Speed at Thrust Reverser Deployment and Stowage

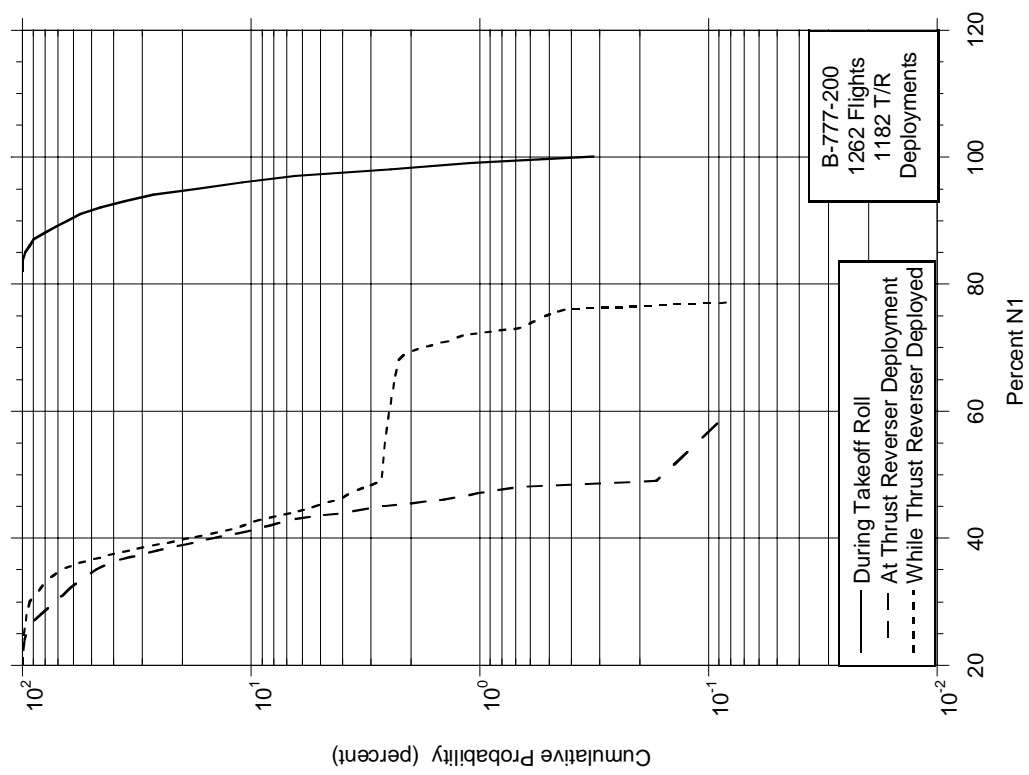


Figure C-95. Cumulative Probability of Percent N₁ During Takeoff, at Thrust Reverser Deployment, and During Thrust Reverser Deployment